The University Of Sheffield.

Access to Electronic Thesis

Author: Xiaofeng Li

Thesis title: Information Processing and Distribution in the Fly Early Visual system

Qualification: PhD

This electronic thesis is protected by the Copyright, Designs and Patents Act 1988. No reproduction is permitted without consent of the author. It is also protected by the Creative Commons Licence allowing Attributions-Non-commercial-No derivatives.

This thesis was embargoed until 16 March 2017.

If this electronic thesis has been edited by the author it will be indicated as such on the title page and in the text.

Information Processing and Distribution in the Fly Early Visual System

Xiaofeng Li

A thesis submitted for the degree of

Doctor of Philosophy

Department of Biomedical Science

The University of Sheffield

Dec 2011

Acknowledgments

感谢国家。最先感谢我的家人一直尊重我的选择，一直给予我支持和鼓励。在你们的爱面前，一切文字都是苍白无力的。感谢你们。

The last three years have been a fantastic time for me. I have really appreciated the opportunity to come to the lovely city of Sheffield, to work on a fascinating project, and also to meet so many amazing people. Firstly, I would like to express my sincere gratitude to Dr.Mikko Juusola, my Ph.D. supervisor and 'science father', who has been a great mentor in science and an inspirational personal friend. This thesis would not have been possible without your encouraging advice and guidance, and your influence on me extends far beyond the bench work.

Many thanks to my colleagues Zhuoyi Song, Uwe Friederich, Sidhartha Dongre, Marie McCulloch, Olivier Lists, Trevor Wardill and Paloma Gonzalez, who have all provided me with great help in my studies and with much laughter as well. Thanks my Ph.D. advisors Louise Robson and Alex Whitworth and people from Biomedical Science Department. Thanks to my co-supervisor Shiming Tang, colleague Fang Liu, Ming Li, now in Beijing University, China; my collaborator, Ahmad N. Abou Tayoun in Dartmouth College, US.

Special thanks to 'Sir'. An Minh Dau, 'the King of Vietnam in Sheffield'. I am grateful for all the 'consulting' you offered during the last two years. I enjoyed all the good times and bad times that we have been through. These memories will never fade and I hope our brotherhood continues.

Thanks to all my housemates, Ed, Chris, Money, Punja, Jules and Tom for all the fun time we shared. Also Rachel, Wang xi, Kong derong, Yang hui, Tian yuan, Chen yaguang, Han Liu, Bai fan and Zhang yan. All of you have been awesome friends and your support has always been a great motivation for me. Thanks to all the people from The Tough Guise Boxing Gym and R.I.P coach Tommy Bradley. Also, thanks to my undergraduate tutors Xue bin and Li Chaojun, now in Nanjing University. Nothing could have happened without you.

This work would not have been possible without the generous financial support from the Overseas Research Students Awards Scheme and the University of Sheffield Studentship. Many thanks to the members of the panels who supported my applications.Clearly, you all have made the right choice.

Abstract

Evolution shapes biological systems to better match their desired functions. Hence, we can assume that sensory systems are adapted to optimize information processing. Nevertheless surprisingly little is known about how sensory systems are optimised, or organised, in relation to the information sampling and processing they perform. In particular, our understanding is limited on certain fundamental issues: (1) what are the roles of individual ion-channels in coding information in specialised neural networks, (2) how does information transfer through synapses, and (3) how are different types of information (motion/colour) routed and processed for higher order visual functions.

Dipteran compound eyes provide highly useful model systems for examining the basic mechanisms involved in visual information processing; in particular, for assessing how graded potentials code visual information. For this thesis, I have performed extracellular and intracellular recordings from photoreceptors and their primary interneurones, large monopolar cells (LMC), in *Calliphora* and *Drosophila*, to investigate the three essential questions mentioned above.

This thesis provides systematic characterisations of: (1) *Drosophila* dSK channels, small conductance calcium-activated potassium channels; (2) Adapting dynamics of postsynaptic quantal bumps in the first visual synapse in *Calliphora*; (3) *in vivo* spectral sensitivities of *Drosophila* R1-R6 photoreceptors and LMCs in wild-type and in selected mutant and transgenic flies.

Together with collaborations inside/outside our laboratory, my study: (1) identified the functional roles and gain control of dSK channels in the first synaptic circuits in the fly eye and also clarified how intrinsic activities of neural network compensates for missing or faulty ion channels; (2) characterised how postsynaptic unitary voltage events (or bumps) adapted dynamically to maximize the rate of information transfer at the fly first visual synapse; 3) provided the first *in vivo* spectral sensitivity functions of *Drosophila* R1-R6 photoreceptors and LMCs, and demonstrated that functional inputs, from photoreceptors that have different spectral sensitivities, improve motion discrimination and robustness of perception.

Contents

List of Abbreviations

AC	Amacrine cell
BG	Background (light intensity)
ERG	Electroretinogram
FFT	Fast Fourier transform
LMC	Large monopolar cells
NS	Naturalistic stimulus
SNR	Signal noise ratio
UV	Ultra violent
V/Log I	Voltage response/light intensity on Log scale
WN	White noise
WT	Wild-type *Drosophila*

List of Symbols

t	In time domain, in millisecond
$N_V(t)_i$	Noise in individual responses
$R_V(t)_i$	Individual voltage responses
$S_V(t)$	Signal, from averaging of the responses
f	Frequency in Hz
$\|\langle\tilde{S}_V(f)\rangle\|^2$	Power spectrum of signal
$\|\langle\tilde{N}_V(f)\rangle\|^2$	Power spectrum of noise
$SNR_V(f)$	Signal-to-noise ratio in the frequency domain
H_R	Total entropy
H_N	Noise entropy
R	Information transfer
H	Information capacity
$T_V(f)$	Frequency response
$k_V(t)$	Linear impulse responses
T	Bump duration
h	Bump amplitude
λ	Bump rate
$\Gamma(t; n, \tau)$	Gamma Distribution
n, τ	Variables for gamma distribution
$B_V(t)$	Bump waveform follows gamma distribution
$D_V(t)$	Bump waveform follows the first derivative of gamma distribution

V_n	Voltage responses in mV
T_t	Time-to-peak of the responses

General Note on Notation

$\tilde{}$	Fourier transform
$\lvert\ \rvert$	Absolute value
$\langle\ \rangle$	Average
*	The complex conjugate

List of Figures

List of Supplement Figures

1 General Introduction

The need to sample and process visual information for successful behaviours has exerted selective pressure on seeing animals, shaping the forms and functions of their visual systems. Yet, our knowledge of the early information processing is limited, in particular regarding certain fundamental issues: (1) what are the roles of individual ion-channel types in coding information in specialised neural networks; (2) how does information transfer through synapses; and (3) how are different types of information (motion/colour) routed and processed for higher order visual functions.

In my thesis, to investigate these questions, I have used two dipteran preparations: *Drosophila Melanogaster* and *Calliphora Vicina*. Their modular eye-structures, each containing networks of identifiable neurons, have long served as models to study fundamental questions of neuroscience. Recent advances in *Drosophila* genetics now enable us to manipulate the functions or connectivity of selected neurones in this system. Furthermore, customised electrophysiological techniques make it possible to study individual neural function *in vivo*, where the network connections remain intact. In this chapter, I will provide an introduction to the early visual system of the Diptera and the relevant literature.

1.1 The structure of dipteran compound eyes and photoreceptors

Diptera, or true flies, have distinctive compound eyes, consisting of hundreds to thousands of repeated units, called the ommatidia (Ready *et al.*, 1976) (**Figure 1-1A**). Each lens-capped ommatidium (**Figure 1-1B**), contains eight photoreceptor cells, R1-R8; six outer photoreceptors: R1-R6 and two inner photoreceptors: R7 and R8. Each photoreceptor has a specialized folded membrane called the rhabdomere, made out of tens of thousands of microvilli (**Figure 1-1B** and **1C**), forming a waveguide structure for light to propagate within. This is where the light sensitive pigment rhodopsin (Hardie & Raghu, 2001a) is expressed to create an opsin-chromophore complex (Briscoe & Chittka, 2001). When excited by photons, rhodopsins activate a complex G-protein cascade. This eventually leads to the opening of light-gated TRP and TRPL-channels ("transient receptor potential"- and "transient respotor potential like"-channels) that are mostly Na^+ and Ca^{2+} permeable (Hardie, 2001), thus, depolarising the cell.

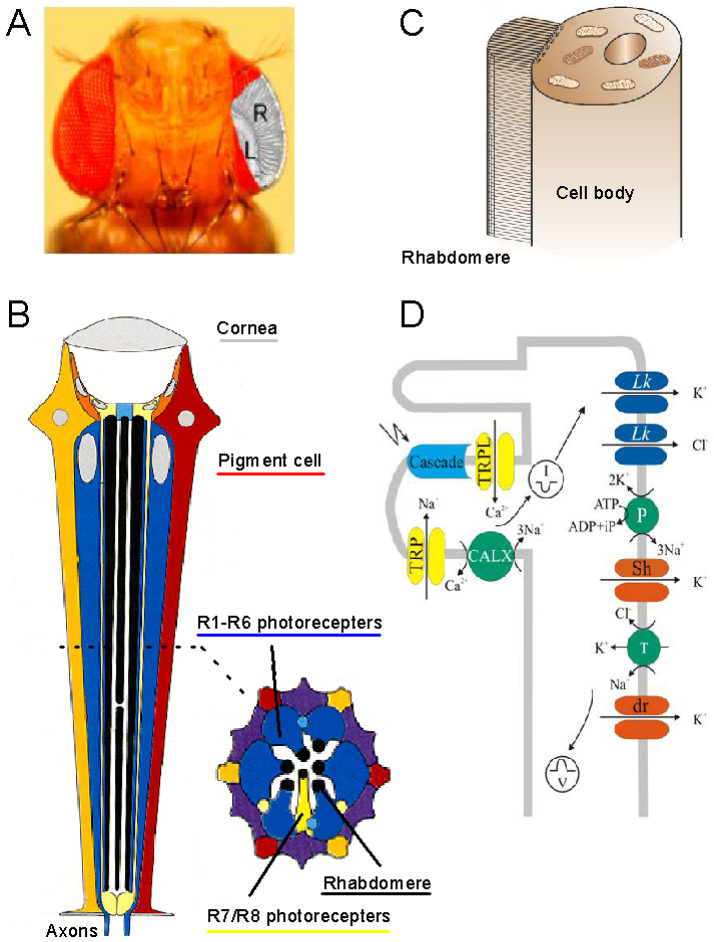

Figure 1-1: *Drosophila* compound eyes and photoreceptors. (**A**) *Drosophila* head with a schematic view of the retina, R, and the next neuropile, the lamina, L. (**B**) Schematic longitudinal and cross section of an ommatidium shows R1-R8 photoreceptors and supporting cells. Dotted line indicates the cut. (**C**) Drawing of one photoreceptor shows the photo-sensitive part, rhabdomere, and photo-insensitive cell body. (**D**) Known membrane conductances and ion-exchangers. Activation of the phototransduction cascade leads to the opening of two light-sensitive cation channels, TRP and TRPL and influx of Ca^{2+} and Na^{+} ions. This light-induced current (I) charges the plasmamembrane, causing the voltage response. The voltage response is further shaped by voltage-sensitive potassium channels, as well as K^{+}, Cl^{-} leak channels and ATP dependent K^{+}/Na^{+} pump (P). Ca^{2+} is extruded out of the cell by CALX, a Ca^{2+}/Na^{+} exchanger, and $Na^{+}/K^{+}/Cl^{-}$ cotransporter (T) restores the resting potential following a response. A is adapted from Zheng and Juusola, 2006; B from Wolff and Ready, 1993; C from Hardie, 2001 and D from Verena Woldram's thesis, 2004.

Like many sensory receptors and second-order neurones, fly photoreceptors encode information by producing graded membrane potentials. Initiated by photosensitising pigment rhodopsin, photoreceptors translate the light energy into selective ion-permeability changes on their cell membrane, through a process called phototransduction. Apart from the photo-sensitive part of the membrane, photoreceptors also have a photo-insensitive part (**Figure 1-1C**), which expresses different voltage- and ligand-gated ion channels

(Hardie, 1991) (**Figure 1-1D**). After the primary light-induced depolarisation in the photo-sensitive membrane, this voltage waveform is further shaped by the membrane capacitance along with the distribution and numbers of ion channels on the photo-insensitive membrane (**Figure 1-1D**). These include voltage-sensitive K^+-channels (Hardie, 1991), Na^+-channels (Hardie & Raghu, 2001a), inward-rectifying (*i.e.* hyperpolarisation-activated) Cl^--channels (Ugarte *et al.*, 2005), ligand-gated neurotransmitter-channels (*i.e.* synaptic feedbacks: Zheng et al., 2006), as well as Na^+/K^+-pumps (Yasuhara *et al.*, 2000), all of which contribute to a photoreceptor's voltage response.

Beneath the photoreceptors lie the first optic neuropile, the lamina, containing a complex web of visual interneurones and glia that process and reroute information, matching the fly's changing visual needs with the changing light conditions. The axons of the interneurones form a neural bundle, called the chiasm, through which the lamina is cross-linked to the second neuropile, the medulla. Visual information is further transmitted to the lobula, the lobula plate and the central brain through a multitude of connections (Borst, 2009) (**Figure 1-2**).

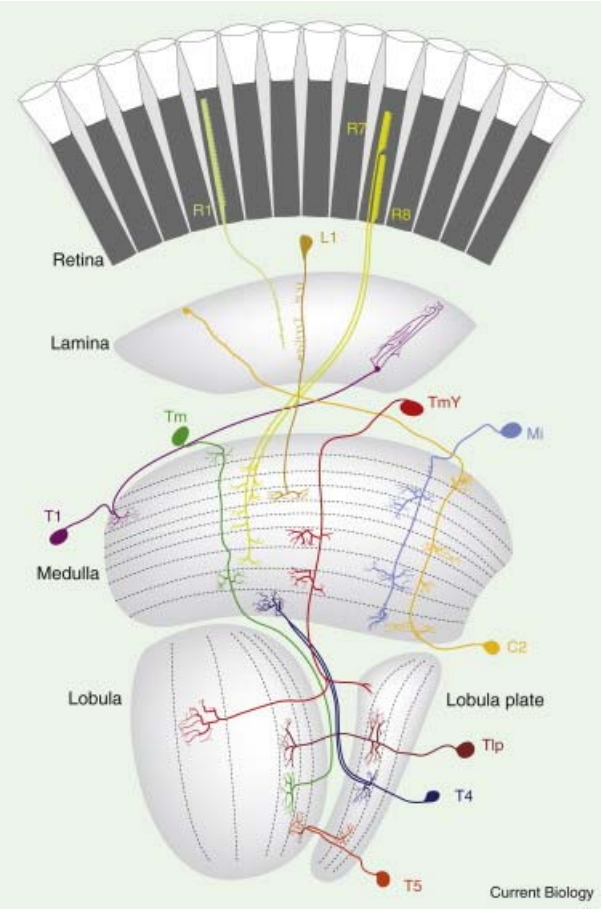

Figure 1-2: Routing and processing of visual information towards the brain. Drawing shows 5 optic neuropiles in the *Drosophila* visual system. After sampling and preprocessing by the photoreceptors in the retina, visual information is relayed to either the lamina or directly to the medulla. From the medulla, information is transferred to the lobula and the lobula plate, finally reaching the central brain. Image adapted from Borst, 2009.

1.2 Voltage-sensitive K+ Channels in photoreceptor information coding

Many ion-channels and ion pumps are involved in processing a photoreceptor's voltage responses. Voltage-sensitive K+ channels, in particular, play key roles in opposing light-induced photoreceptor depolarisation. With an estimated potassium equilibrium potential at -85 mV, opening of K^+-channels extrudes K^+-ions and pulls the membrane potential towards the resting potential. This fundamental tuning process prevents saturation and adjusts the size and speed of the responses to the fly's visual lifestyle (Weckstrom & Laughlin, 1995). *Drosophila* photoreceptors express five voltage-sensitive K^+-channels: *Shaker*, coding a rapid inactivating A-type conductance; two classes of delayed rectifiers, the slow one coded by *Shab* and the fast one possibly coded by *Shaw* (Hardie, 1991; Wicher *et al.*, 2001); and two types of Ca^{2+}-dependent K^+-channel, coded by *Slo* (Becker *et al.*, 1995a; Littleton & Ganetzky, 2000) and *dSK* (Littleton & Ganetzky, 2000; Wolfram, 2001). Although recent evidence suggests that Shab channels might be located near or within the rhabdomere, it is generally believed that most K^+-channels are expressed on the photo-insensitive membrane, the cell body and the axon (Krause *et al.*, 2008).

In fly photoreceptors, Ca^{2+} exerts many effects on visual information processing. For example, it regulates both the gain of phototransduction (Hardie & Raghu, 2001b) and the efficacy of synaptic transmission (Juusola *et al.*, 1996). Accordingly, one would expect high expression levels of Ca^{2+}-dependent K^+-channels in these cells (Stocker, 2004). Indeed, recent evidence suggests that both Slo and dSK are expressed in the *Drosophila* retina, and in other parts of its visual system (Becker *et al.*, 1995b; Hardie, 1995; Brenner & Atkinson, 1996; Brenner *et al.*, 1996; Oberwinkler, 2000; Wolfram, 2001).

Small conductance calcium-activated potassium (SK) channels play a fundamental role in many excitable and non-excitable cells (Stocker, 2004). Although they share the same membrane topology with voltage gated K^+-channels (Kohler et al., 1996), SK channels are voltage-independent and indirectly activated by Ca^{2+} through a constitutively bound calmodulin at the C-terminus of the channel (Xia et al., 1998). In mammals, three genes encode for similar SK1-3 subunits with overlapping expression patterns (Kohler et al., 1996). SK activation causes membrane hyperpolarisation, thus inhibiting cell firing and adjusting the firing frequency of repetitive action potentials (Wolfart *et al.*, 2001; Hallworth *et al.*, 2003). Additionally, SK channels couple to calcium sources at the synapse, forming negative feedback loops, which regulate synaptic transmission and plasticity (Faber et al., 2005; Ngo-

Anh et al., 2005). Consequently, SK channels have been considered as negative regulators within complex cognitive processes, including addiction (Hopf et al., 2010) and learning and memory (Stackman et al., 2002; Stackman et al., 2008), and have been implicated in psychiatric disorders such as schizophrenia (Miller et al., 2001; Tomita et al., 2003). SK channels seem also to play an important role in refining communication and connectivity in sensory systems. In the mammalian retina, SK is expressed in the retinal ganglion cells, in the horizontal and the dopaminergic amacrine cells of the inner nuclear layer, and have been implicated in activity dependent plasticity during development (Shatz, 1990; Wang *et al.*, 1999; Klocker *et al.*, 2001; Clark *et al.*, 2009). However, the contribution of SK channels to neuronal functions in complex circuits underlying sensory processing and behaviours is largely unknown in the absence of suitable animal models.

1.3 First visual synapse

The feedforward transmission in the fly eye is thought to be relatively straightforward: outer photoreceptors (R1-R6) directly transmit information to their postsynaptic interneurones: the large monopolar cells (LMCs: L1-L3) and amacrine cell (AC) (Meinertzhagen & O'Neil, 1991b; Uusitalo *et al.*, 1995c) (**Figure 1-3A**). In these synapses, information in the presynaptic voltage changes is converted to quantal bursts of neurotransmitter, histamine (Hardie, 1987b; 1989a; Gengs *et al.*, 2002a), released from clear core vesicles to a synaptic cleft between the neighbouring neurons. The vesicle fusion involves voltage-driven Ca^{2+}-mediated exocytosis at the active zone of axon terminals (Juusola et al., 1996), followed by different routes of endocytosis and recycling (Richmond & Broadie, 2002). Decades of studies on *Drosophila* neuromuscular junction have identified numerous synaptic proteins, which are involved in the Ca^{2+}-triggered vesicle fusion and recycling (Broadie & Richmond, 2002), with many homologues in mammals (Sudhof, 2004). Recent evidence indicates that the plasma membrane and vesicle lipids are also key regulators of this cycle (Rohrbough & Broadie, 2005).

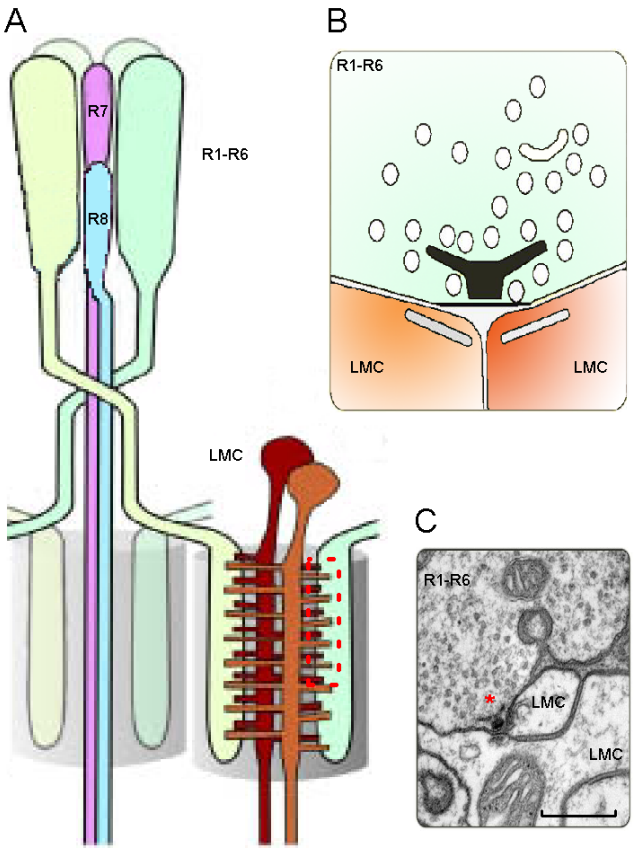

Figure 1-3: The first visual synapses. (**A**) Schematic side view of the photoreceptors with the underlying lamina cartridges, showing the synapses between R1-R6 axon terminal dendrites of LMCs; Axons of R7 and R8 project through the cartridge. (**B**) Outline of T-shaped ribbon structure. Histamine-filled synaptic vesicles concentrate around T-shaped ribbons. (**C**) Cross-section of a graded potential synapse under EM. Scale bar 500nm. A is adapted from Blagburn and Bacon, 2004.

However, there is a continuing debate over the modes of synaptic vesicle cycling (Sudhof, 2004): the classic complete fusion mode, with clathrin-mediated endocytosis, and the more controversial 'kiss and run' mode, transient formation of a vesicle fusion pore and retrieval (Rohrbough & Broadie, 2005). Numbers of studies have found molecular, functional and ultrastructural suggestions for kiss-and-run mode in different animals (Pyle *et al.*, 2000; Richards *et al.*, 2000; Wang *et al.*, 2003), while recent work showed two types of fusion pores (He *et al.*, 2006) and activity-dependent compound fusion in the Calyx of Held (He *et al.*, 2009), forming of large vesicles to increased quantal size. In *Drosophila*, evidence supports two forms of vesicle retrieval in motor neurons (Verstreken *et al.*, 2002) and photoreceptor terminals (Koenig & Ikeda, 1996), suggesting a potential kiss-and-run fusion release mode. It is also worth mentioning that the R1-R6-LMC synapse, like those in mammalian photoreceptors and hair cells (Schmitz, 2009), exhibits tonic transmitter release even in

darkness (Uusitalo *et al.*, 1995a; Uusitalo & Weckstrom, 2000). However, the fusion dynamic in the R1-R6-LMC synapse is still largely unknown.

After vesicle fusion, changes in the histamine concentration are then picked up by specific receptors on the post-synaptic membrane (Skingsley et al., 1995), thereby channelling information back into voltage changes. Histamine-activated chloride channels have been identified in LMCs of the large flies (Skingsley et al., 1995), while two types are found in *Drosophila*: hclA (also known as ort), expressing in LMCs and hclB (also known as hisCl1) in the lamina glia (Pantazis *et al.*, 2008b). Meanwhile, two classes of potassium channels are expressed in different LMCs in blowfly *Calliphora Vicina*, generating A-type K^+ current (Ka) and a delayed-rectifier-like K^+ current (Kd) (Hardie & Weckstrom, 1990). Together with the transmitter induced inward Cl^- current, these outward currents shape up the voltage responses of postsynaptic LMCs.

In comparison to conventional synapses that convey pulsatile information in action potential patterns, graded potential synapses of many sensory systems communicate with much higher information transfer rates (Van Steveninck & Laughlin, 1996), having adapted structures for high-fidelity signalling (Prokop & Meinertzhagen, 2006). The synapses between photoreceptors and LMCs belong to the ribbon synapse family; synapses with large, electron-dense structures at presynaptic terminals (Schmitz, 2009). These so-called 'T-bar ribbon' synapses share a pronounced T-shaped dense body, which immobilise numerous synaptic vesicles next to presynaptic release sites (**Figure 1-3B, C**) (Koenig & Ikeda, 1996).

This structural and functional specialisation is normally accompanied with high transmitter release rates (Schmitz, 2009). In mammals, receptor neurons, or their second-order targets, possess ribbon synapses (Sterling & Matthews, 2005). In contrast, ribbon synapses are widely found in *Drosophila*: at photoreceptor terminals, neuromuscular junctions and other central synapses (Prokop & Meinertzhagen, 2006). Vesicle exocytosis occurs at the presynaptic active zone beneath the T-bar (**Figure 1-3C**) (Saintmarie & Carlson, 1982; Verstreken *et al.*, 2002), with expected co-localisation of calcium channels (Kawasaki *et al.*, 2004). Despite the detailed morphological studies of this presynaptic organelle, its function is still unclear. Studies in mammalian systems provide evidence that the ribbon either acts as a conveyor belt (Parsons & Sterling, 2003) or tethers vesicles for release as multi-unit packages (Singer *et al.*, 2004); thus, it may adjust vesicle release for the different conditions that the sensory neurons encounter (Dieck & Brandstatter, 2006). Nonetheless, the T-bar's function in R1-R6-LMC synaptic transmission remains an enigma.

1.4 Dipteran lamina: the neural network

The previous simplified view of R1-R6-LMC synapses fails to appreciate the complexity of wiring in the lamina neural network. The insect lamina and the vertebrate retina share the same design principle of massively parallel processing, implemented through rich networks of interconnected microcircuits with multiple-contact synapses (**Figure 1-4**) (Meinertzhagen & Sorra, 2001; Sanes & Zipursky, 2010). In return to the feedforward from R1-R6 photoreceptors, L2 and AC feedback onto R1-R6 photoreceptor terminals via excitatory ligand-gated synapses (Sinakevitch & Strausfeld, 2004; Zheng *et al.*, 2006a; Kolodziejczyk *et al.*, 2008). Upon light stimulation, photoreceptors depolarize while LMCs/ACs hyperpolarize, which thereby reduces excitatory feedback onto the photoreceptors (Shaw, 1984b; Zheng *et al.*, 2006a). Accordingly, voltage responses in the photoreceptor-LMC-photoreceptor network appear shaped, and adapt together (network adaptation), presumably to optimize the encoding and routing of light information (Nikolaev *et al.*, 2009b; Zheng *et al.*, 2009).

Furthermore, other interneurones receive indirect R1–R6 input in the lamina network (**Figure 1-4**): C2–C3 fibers, L4–L5, T1 and Tan cells, some of which form feedback synapses to R1-R6 axon terminals (Meinertzhagen & O'Neil, 1991b) (Rivera-Alba *et al.*, 2011). Glia cells, which receive R1–R6 input through a different histamine-receptor (Pantazis *et al.*, 2008b), and gap-junctions between the lamina cells (Shaw, 1984a) take part in regulating lamina network activity as well. How these connections and glia cells participate in information processing is still unclear, but it is reasonable to assume that they too could influence the neuronal functions of photoreceptors and/or LMCs through network functions.

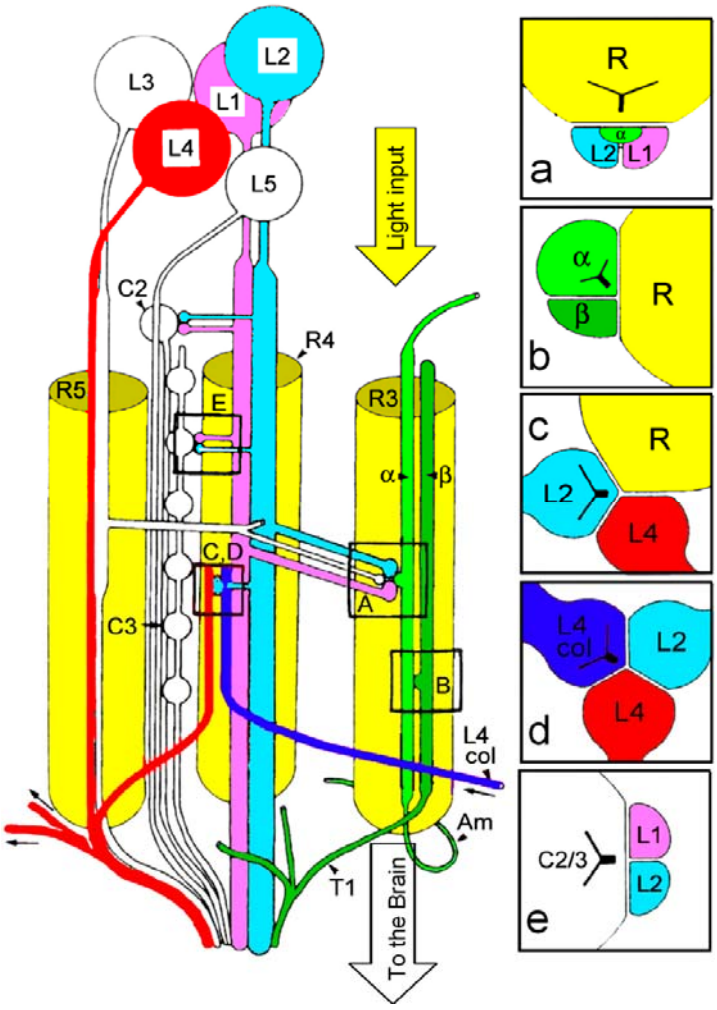

Figure 1-4: A greatly simplified schematic of synaptic lamina connections. Photoreceptor axon terminals, R1–R6 (three are showed) form output synapses with three large monopolar cells (LMCs), L1–L3, and an amacrine cell (AC), α. Inset **a**, tetrad synapse, a photoreceptor terminal connects to two LMCs and an AC. Insets **b** and **c**, feedback synapses from AC and L2 cell to a photoreceptor, respectively. Insets **d**, connections between LMCs, and **e**, C2/C3, from the next neuropile medulla, feedback on to L1 and L2. Figure adapted from Meinertzhagen & O'Neil, 1991b.

1.5 Colour and motion information in early vision system

In the visual system, colour and motion information is thought to be channelled through specific subsystems to higher-order processing centres (Livingstone & Hubel, 1988). In higher vertebrates, colour, motion and shape information are at least partially segregated into different channels, at the level of the retina (Livingstone & Hubel, 1988). Similarly, dipterans flies have characteristic sets of photoreceptors, which are widely believed to process motion and colour information separately (Bausenwein *et al.*, 1992; Rister *et al.*, 2007; Joesch *et al.*, 2010). In *Drosophila* eyes: R1-R6 photoreceptors are believed to subserve achromatic motion detection channels, while R7 and R8 photoreceptors should form two chromatic channels (Chi-Hon Lee, 2008) (**Figure 1-1B** and **1-5**). R1-R6 photoreceptors, expressing blue-green Rh1-opsin (O'Tousa *et al.*, 1985) and UV-sensitizing pigment (Kirschfeld & Franceschini, 1977) feed to the motion pathway (Heisenberg & Buchner, 1977a) by innervating histaminergic (Hardie, 1989a) large monopolar cells (LMCs: L1 and L2) (Rister *et al.*, 2007; Joesch *et al.*, 2010) in the 1st optic neuropile, the lamina (**Figure 1-2** and **1-5B**). These neurons, which should form separate on- and off-channels (Joesch et al., 2010) project to the medulla (Takemura et al., 2008) (**Figure 1-2**). After unknown processing, the signals transmit from the medulla output layers to lobula neurons and motion-sensitive tangential cells of the lobula plate (LPTCs) (Bausenwein et al., 1986) (**Figure 1-2**).

Meanwhile, central photoreceptors, R7 and R8, initiate two colour channels (**Figure 1-5**). R7s are UV-sensitive; expressing short (R7p:Rh3) or long (R7y:Rh4) wavelength opsins, whereas R8 are blue (R8p:Rh5) or green-yellow sensitive (R8y:Rh6), having 30:70 retinal distributions, respectively (Hardie, 1979b; Chou *et al.*, 1996). R7s/R8s, bypassing the lamina, innervate different medulla layers (**Figure 1-2**) (Takemura *et al.*, 2008), where some contribution to their processing comes from R1-R6 via L3 monopolar neurons (Gao *et al.*, 2008). Thus all photoreceptors feed putative inputs to the colour pathway.

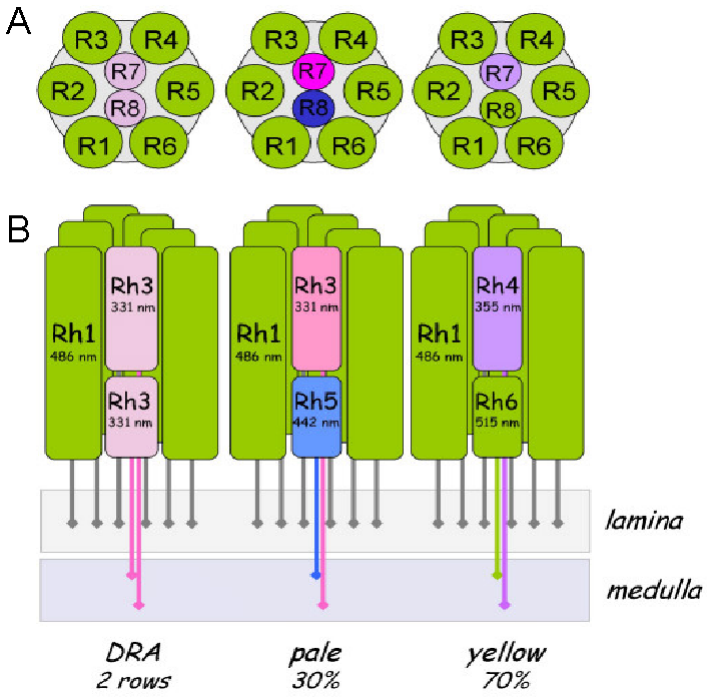

Figure 1-5: Three types of photoreceptors initiate motion and colour pathways. (**A**) Three subtypes of ommatidia showing different photoreceptors: DRA ommatidia (two dorsal rows) express Rh3 in both R7 and R8, 30% ommatidia (called pale) express Rh3 and Rh5 in R7 and R8, respectively, and 70% ommatidia (called yellow) express Rh4 and Rh6 in R7 and R8, respectively. (**B**) Side view of **A**, indicates the different projection of R1-R6 and R7/R8. Figure adapted from Markus and Friedrich 2007.

Independency of colour and motion pathways is still under debate (Derrington, 2000; Cropper & Wuerger, 2005). In the human visual system, colour and motion information is often thought to be processed by segregated pathways, as concluded from neurophysiological and anatomical studies (Livingstone & Hubel, 1988). However, recent evidence casts doubts on this dogma, as movement of two equiluminant colour patterns can still be detected by human observers (Takeuchi *et al.*, 2003; Nishida *et al.*, 2007). In *Drosophila*, unlike in the debated human vision, it is widely believed that motion detection is mediated exclusively by one spectral class of photoreceptors (R1-6) (Kaiser & Liske, 1974; Heisenberg & Buchner, 1977b). Recent behavioural study supported the view that motion vision is independent of colour (Yamaguchi *et al.*, 2008), while many other studies exclude the possible colour pathway input to the motion detection system (Joesch *et al.*, 2010; Reiff *et al.*, 2010) (Rister *et al.*, 2007). Nonetheless, since linking colour to motion can improve perceptual discrimination (Barlow, 2001), one would assume that these channels somehow interact. Ultrastructural studies have implied interactions between the two pathways in the medulla, where R7/R8 photoreceptors form synapses onto LMCs (Takemura *et al.*, 2008). Moreover,

gap-junctions between R1-R6 and R7/R8 in the lamina (Shaw, 1984b; Shaw *et al.*, 1989a) and in the medulla (Gao et al., 2008) suggest that colour and motion pathways could form sophisticated local processing networks (Meinertzhagen & O'Neil, 1991a) (**Figure 1-4**). It remains an open question whether and how colour and motion channels interact in the *Drosophila* early visual system.

1.6 Outline of the Thesis

Motivated by the three fundamental questions of neural information processing, my thesis covers three independent topics as outlined in the following:

1) What are individual ion-channels' role in information coding in neural network?

For this question, I studied the small conductance calcium-activated potassium (dSK) channels in *Drosophila* photoreceptor function and early visual processing.

In Chapter 2, I investigated the role of dSK channels in photoreceptors and LMCs by using *in vivo* intracellular recordings in wild-type and mutant flies. My data are consistent with a model where dSK contributes to photoreceptor performance by mediating sensitivity control at the lamina network. Compared to wild-type, loss of dSK led to faster, oscillatory responses in both photoreceptors and LMCs. Although mutant photoreceptors exhibited a slightly broader frequency bandwidth, they had a surprisingly normal encoding capacity, highlighting the robustness of the network adaptation for maintaining appropriate information processing in the circuits.

This work has been published in the *Journal of Neuroscience* (Li, Abou Tayoun *et al*., 2011). (See Appendix).

2) How does information transfer through synapses?

For this question, I studied post-synaptic quanta (or bump) dynamics; the unitary voltage responses likely evoked by bursts of histamine, released from single vesicles at the synapse between R1-R6 photoreceptors and LMC.

In Chapter 3, I exploit the *in vivo* blowfly preparation (*Calliphora Vicina*). By analyzing the voltage noise of LMCs under different stimulus conditions, I could estimate changes in the corresponding average unitary postsynaptic events (bumps). My data showed that the bump waveforms change with mean light intensity. By dynamically adjusting the shape of

the transmitted quanta, the photoreceptor-LMC synapse seems to help to maximise the flow of visual information into the lamina network.

3) How is different information (motion/colour) routed and processed before reaching higher order neurons?

For this question, I studied *Drosophila* motion and colour vision pathways. By combining molecular biology, genetics and electrophysiology, I tried to examine whether these pathways crosstalk in the early visual system.

In Chapter 4, I presented the first characterisation of *in vivo* spectral sensitivity of R1-R6 photoreceptors and LMCs in wild-type *Drosophila*, and in mutants with genetically deactivated colour channels. My results show that *Drosophila* R1-R6 photoreceptors and postsynaptic LMCs have dual peaked spectral sensitivity, which correlates with *in vitro* pigment studies and matches the spectral sensitivity of those in larger dipteran flies. I also discovered that light-adaptation induced a pupil effect in *Drosophila* R1-R6 photoreceptors. However, I found no significant difference in the spectral sensitivity of R1-R6 photoreceptors and LMCs in the mutant, which lacked light-sensitive R7s and R8s.

In Chapter 5, to overcome the experimental complication that the spectral sensitivities of the colour and motion channels overlap, I used variants of UV-sensitive flies, which enabled activation of one pathway without activating the other. I tested the spectral sensitivity and visual information processing of R1-R6 photoreceptors and LMCs in different UV-flies. My results indicate that the motion pathway receives inputs from the colour pathway in the early visual system of *Drosophila*. Together with the results from the behavioural and optical imaging experiments in our laboratory, this study clarified how the retinal wiring and its circuit computations improve visual perception and the robustness of behaviour.

This work has been nominally accepted for publication in *Science* (Wardill, *et al.*, 2011). Pending requested changes.

2 The Drosophila SK channel (dSK) contributes to photoreceptor performance by mediating sensitivity control at the first visual network

2.1 Introduction

Small conductance calcium-activated potassium (SK) channels play a fundamental role in excitable and non-excitable cells, linking changes in intracellular Ca^{2+} to membrane potential (Stocker, 2004). Although they share the same membrane topology with voltage gated K^+ channels (Kohler *et al.*, 1996), SK channels are voltage-independent and are indirectly activated by Ca^{2+} through a constitutively bound calmodulin at the C-terminus of the channel (Xia *et al.*, 1998).

In mammals, SK activation causes membrane hyperpolarisation, thus inhibiting cell firing and shaping the firing frequency of repetitive action potentials (Wolfart *et al.*, 2001; Hallworth *et al.*, 2003). SK channels also couple to calcium sources at the synapse, forming negative feedback loops, which regulate synaptic transmission and plasticity (Faber *et al.*, 2005; Ngo-Anh *et al.*, 2005). In addition, SK channels seem also to play an important role in refining communication and connectivity in sensory systems, as it is expressed in the mammalian retinal ganglion cells, in the horizontal and the dopaminergic amacrine cells of the inner nuclear layer, and have been implicated in activity dependent plasticity during development (Shatz, 1990; Wang *et al.*, 1999; Klocker *et al.*, 2001; Clark *et al.*, 2009).

However, the contribution of SK channel to neuronal functions in complex circuits underlying sensory processing and behaviour is largely unknown in absence of suitable animal models. Recently, a *Drosophila* line is generated that lacks the single highly conserved SK gene in its genome (*dSK*) (Abou Tayoun *et al.*, 2011). Immunostaining for dSK in the adult fly brain showed that dSK is highly enriched at the lamina synaptic network where it localizes to photoreceptor axons and a group of non-glutamatergic monopolar cells; including L4s, which receive indirect input from R1-R6 photoreceptors through the lamina network but form feedback synapses both to L2 monopolar cells and R1-R6 terminals (Meinertzhagen and O'Neil, 1991) (Rivera-Alba *et al.*, 2011). Whole-cell voltage clamp of R1-R6 photoreceptors, from dissociated ommatidia, showed that *dSK* encodes a slow Ca^{2+}-activated K^+ cur-

rent similar to its mammalian counterparts, pointing towards conserved role(s) for this conductance in neurons.

Here I investigate the role of dSK channels in photoreceptor function and early visual processing in intact lamina network with *in vivo* intracellular recordings. My data are consistent with a model where dSK contributes to photoreceptor performance by mediating sensitivity control at the lamina network. Compared to wild-type, loss of dSK led to faster, oscillatory responses in both photoreceptors and LMCs. Since *dSK*$^{-}$ photoreceptors also adapted faster but less efficiently to light transitions, having lower input resistance and higher resting potential in the dark, these findings suggested that *dSK*$^{-}$ photoreceptors entertained larger depolarizing conductances at photoreceptor axons from extrinsic inputs; as supported by their normal phototransduction machinery and high dSK expression in the lamina circuits. I further show that the fast responses are attributed to absence of dSK R1-R6 photoreceptors, while oscillations are likely to reflect suboptimal compensation of the missing dSK-channels by the lamina feed-forward and feedback synapses. Although mutant photoreceptors exhibited a slightly broader frequency bandwidth, they had a surprisingly normal encoding capacity, highlighting the robustness of the network adaptation for maintaining appropriate information processing in the circuits.

2.2 Experimental Procedures

2.2.1 Fly stocks

Canton-S (wild-type) flies were acquired from the Bloomington Stock Center. Other stocks in this chapter were generated by Ahmad N. Abou Tayoun from Dartmouth College, USA. In short, d*SK* fly was generated by using the FRT-FLP mediated recombination in a deletion in the d*SK* gene. UAS/GAL4 system was used to inactivate dSK in R1-R6 cells using the eye-specific *longGMR-GAL4* driver. While dominant negative dSK was created by changing the subunit (*UAS-SKDNmyc*), in which the K^{+} pore "GYG" was mutated into "AAA" (Abou Tayoun *et al.*, 2011).

2.2.2 *In vivo* Electrophysiology

Intracellular recordings of R1-R6 photoreceptors and LMCs and their analysis were carried out as described before (Juusola & Hardie, 2001a; Juusola & de Polavieja, 2003; Zheng *et al.*, 2006a). Briefly, flies were immobilized in a conical fly holder with beeswax, as explained previously (Juusola & Hardie, 2001a; Zheng *et al.*, 2006a). To allow the recording microelectrode to enter the retina/lamina, a small hole with the size of few ommatidia was cut in the

dorsal cornea and sealed with Vaseline to prevent the eye from drying. Intracellular voltage responses were recorded through sharp quartz and borosilicate microelectrodes (Sutter Instruments), having 120–200 MΩ resistance. Recordings from R1-R6 photoreceptors and large monopolar cells (LMCs) were performed separately, using 3 M KCl intra-electrode solution (photoreceptors) and 3 M potassium acetate with 0.5 mM KCl (LMC; to minimize reduction in the chloride battery). A blunt reference electrode was inserted into the fly head capsule close to the ocelli. The head temperature of the flies was kept at 19 ± 1°C by a feedback-controlled Peltier device (Juusola & Hardie, 2001a), to keep in accordance with our collaborater's experimental conditions.

To preclude poor data biasing our analysis, only high quality stable recordings were used. Such photoreceptors had resting potentials in the dark <−50 mV and maximum responses to saturating bright pulses >40 mV (WT Canton-S, all mutants and controls). For the used LMCs, the resting potentials were <−30 mV and maximum responses >15 mV (WT Canton-S, all mutants and controls). In *Calliphora* lamina, L1 and L2 generate similar responses, while the responses of L3 are more hyperpolarized, showing the largest off-transients (Uusitalo *et al.*, 1995a). In *Drosophila*, I have not identified different LMC subtypes, but as L1 and L2 occupy the largest volume most recordings were probably in them. It is also possible that I occasionally record from processes of amacrine cells that share histaminergic input with L2 and L1 cells (Shaw, 1984b; Zheng *et al.*, 2006a; Zheng *et al.*, 2009). However, because the selected recordings to the given stimuli in *Drosophila* lamina had rather similar hyperpolarizing characteristics, all LMC data were analysed together. Moreover, attributable to the smaller dimensions of L4 monopolar cell and their non-histaminergic inputs (Kolodziejczyk *et al.*, 2008), it is unlikely that any of the stable recordings (used in this study) would be from them.

Cells were stimulated at the centre of their receptive fields with a high-intensity green LED (Marl Optosource, with peak emission at 525 nm). The light stimulus was delivered through a fiber optic bundle, mounted on a rotatable Cardan arm, subtending 5° as seen by the fly. Its Luminance was controlled by neutral density filters (Kodak), covering a 4 log unit range up to 6 x 10^6 photons/s (Juusola and Hardie, 2001). Figures show results for dim (6,000 photons/s), medium (6 × 10^5 photons/s), and bright luminance (6 × 10^6 photons/s), corresponding to log -3, log -1 and log 0. The responsiveness of the cells was tested by repeated presentations of light pulses or naturalistic light intensity series (10,000 points/s). Naturalistic stimulus patterns were selected from the Van Hateren natural-stimulus-collection (van

Hateren, 1997). Since their luminance was adjusted by placing neutral density filters on the light source, the stimulus sequence retained its contrast constant (c = ΔI/I).

Voltage responses were amplified by an SEC-10L single-electrode amplifier (NPI Electronic) in current-clamp mode using 15 kHz switching rate. The stimuli and responses were low-pass filtered at 500 Hz (KemoVBF8), and sampled at 1 or 10 kHz. The data were often re-sampled/processed off-line at 1-2 kHz for the analysis. Stimulus generation and data acquisition were performed by custom-written Matlab (MathWorks, Natick, MA) programs: BIOSYST (Juusola & Hardie, 2001a; Juusola & de Polavieja, 2003), with an interface package for National Instruments (Austin, TX) boards (MATDAQ; H. P. C. Robinson, 1997–2005).

2.2.3 Data Analysis

Signal and noise components of photoreceptor and LMC voltage responses were estimated both in the time and frequency domains.

2.2.3.1 Processing of Voltage Responses to Naturalistic pattern in Time Domain

Identical repeated 1,000 ms long light contrast patterns (naturalistic stimulation, NS) were presented to the flies (60–90 times). Only steady-state adapted responses were analyzed; first 10-20 responses were omitted because of their adaptive trends. Individual voltage responses, $R_V(t)_i$, vary slightly due to recording noise and the stochastic nature of the underlying biological processes (Juusola & Hardie, 2001a). Averaging of the responses to the given light contrast stimulus gave the virtually noise-free voltage signal, $S_V(t)$. The noise components in individual responses can be estimated by subtracting of the signal, $S_V(t)$, from the individual responses, $R_V(t)_i$:

$$N_V(t)_i = R_V(t)_i - S_V(t) \tag{2.1}$$

Therefore, for an experiment using n trials (with n = 40–90), there was one signal trace and n noise traces.

2.2.3.2 Signal and Noise in Frequency Domain

The power spectrum of signal,$|\langle \tilde{S}_V(f) \rangle|^2$, and noise, $|\langle \widetilde{N}_V(f) \rangle|^2$, was calculated using Matlab's Fast Fourier Transform (FFT) algorithm like in the last chapter, where $\tilde{}$ indicates the Fourier transform, $|\ |$ denotes the absolute value and $\langle\ \ \rangle$ denotes the spectral average. In detail, both signal, $S_V(t)$, and noise data, $N_V(t)$, chunks were divided into 50% overlapping stretches and windowed with a Blackman-Harris-term window, each giving seven 250-point-long samples. Thus, I obtained 280–630 spectral samples for the noise and seven

spectral samples for the signal. These were averaged, respectively, to improve the estimates. Same method was used for noise during static adaptations.

2.2.3.3 Information Transfer Rate

A triple extrapolation method (Juusola & de Polavieja, 2003) was used to estimate the rate of information transfer, R, of steady-state-adapted photoreceptor voltage responses to naturalistic stimulus, NS. This method, unlike SNR analysis (details in the next chapter's method part), requires no assumptions about the signal and noise distributions or their additivity (Juusola & de Polavieja, 2003).

Photoreceptor voltage responses were digitized by sectioning them into time intervals, *T*, that were subdivided into smaller intervals *t* = 1 ms. (Only dim luminance data was downsampled to 125 Hz, giving *t* = 8 ms, which better represented their slow dynamics). This approach captures 'words' of length *T* with *T*/*t* 'letters'. The mutual information between the response, *r*, and the stimulus is then the difference between the total entropy:

$$H_R = -\sum_i P_R(r_i) log_2 P_R(r_i) \tag{2.2}$$

and the noise entropy:

$$H_N = -\langle \sum_{i=1} P_r(\tau) log_2 P_i(\tau) \rangle_\tau \tag{2.3}$$

Where $P_i(\tau)$ is the probability of finding the *i*-th word at a time *t* from the onset of the trial. This probability $P_r(\tau)$ was calculated across trials to the repeated NS. The values of the digitized entropies depend on the length of the 'words' *T*, the number of voltage levels *v* and the *size* of the data file, $H^{T,v,size}$.

The estimates for the entropy rate, R_R, and noise entropy rate, R_N, were then extrapolated from the values of the experimentally obtained entropies to their successive limits, as in (Gonzalez-Bellido *et al.*, 2011).

$$R = R_R - R_N = \lim_{T\to\infty} \frac{1}{T} \lim_{v\to\infty} \lim_{size\to\infty} \left(H_R^{T,v,size} - H_N^{T,v,size} \right) \tag{2.4}$$

The difference between the entropy and noise entropy rates gives then the rate of information transfer (Shannon, 1948; Juusola & de Polavieja, 2003).

2.3 Results

2.3.1 dSK is required for normal photoreceptor light response

To test the contribution of dSK channel to the photoreceptor voltage output *in vivo*, I performed intracellular recordings from *dSK*⁻ null photoreceptors and their wild-type counterparts (**Figure 2-1A**) to light flashes (**Figures 2-1B and 2-3C**). Both sets of photoreceptors responded with graded transient depolarisations, covering similar ranges (**Figures 2-1B** and **2-3C**). However, *dSK*⁻ photoreceptors showed accelerated kinetics; their responses reached peak amplitudes faster and recovered to resting potential earlier (**Figures 2-1B** and **2-3C**). Here, I recall that the voltage output of fly photoreceptors constitutes a complex convolution of light current (Hardie & Raghu, 2001b), light-insensitive membrane filtering and feedbacks from their neuronal neighbours (Shaw, 1984b; Weckström & Laughlin, 1995; Juusola & Hardie, 2001a; Zheng *et al.*, 2006a).The *dSK* mutation could, therefore, affect any or all of these mechanisms, leading to the observed fast responses.

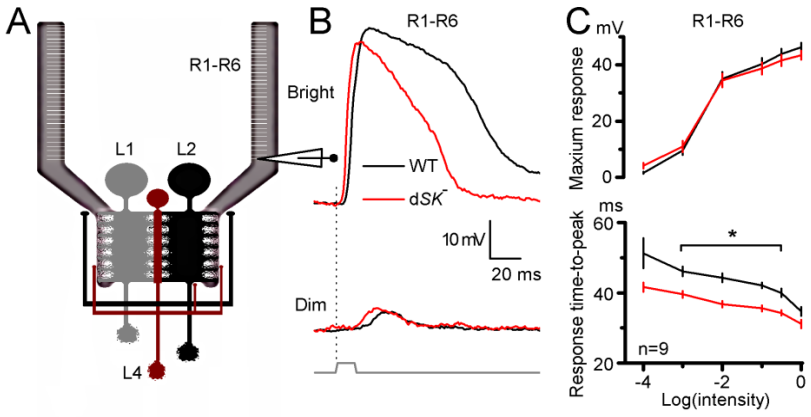

Figure 2-1: *dSK*⁻ photoreceptors have faster responses and intact phototransduction. (**A**) In vivo recordings from R1-R6 photoreceptors, connected to the lamina network; schematic highlights feedback connections (L2/AC and L4) to R1-R6 axon terminals. (**B**) Voltage responses of WT and dSK-photoreceptors to a bright and a dim 10 ms pulse in the dark. *dSK*⁻ responses rise and decay faster. (**C**) Voltage ranges of WT and *dSK*⁻ are similar, but response time-to-peak is faster in dSK-. ($p < 0.020$, t-test).

To exclude the possibility that dSK deletion could alter the photoreceptor morphology, our collaborators Brain Chu and Roger Hardie in Cambridge University examined eye sections of dark-reared flies. Both wild-type and *dSK*⁻ eyes consisted of highly ordered units or ommatidia, which had normal photoreceptors with intact rhabdomeres (**Figure S1A**). To test whether the dSK deletion could potentially affect the properties of the phototransduction machinery leading to altered light-induced currents, they assessed quantum bumps (ele-

mentary responses to single-photon absorptions) and impulse responses to light flashes using whole-cell recordings from R1-R6 photoreceptors (**Figure S1B**) in dissociated ommatidia (Hardie *et al.*, 1991). In this preparation, the dissociated photoreceptors lack axonal terminals and thus any synaptic feedback. Bump waveforms in *dSK*$^-$ photoreceptors were indistinguishable from those of the wild-type photoreceptors (**Figures S1C** and **S1D**). Furthermore, macroscopic responses to increasing light intensities were similar in wild-type and mutant photoreceptors and shared the same kinetics (**Figures S1E** and **S1F**). These data suggest that neither photoreceptor morphology nor the phototransduction machinery is affected by the dSK deletion.

The faster responses in *dSK*$^-$ photoreceptors could be caused by faster charging through the photo-insensitive membrane, if the membrane bandwidth is limiting. In the Diptera, species with fast or slow responding photoreceptors exploit different combinations of K^+ conductances to tune the photoreceptor membrane to match the fly's visual ecology (Weckström & Laughlin, 1995). In the absence of dSK, an increase in compensatory K^+ conductances could, for example, lower the membrane input resistance, and thus its time constant, helping to explain the observed fast responses in *dSK*$^-$ photoreceptors. However, the whole-cell recordings of photoreceptors showed that, compared to wild-type, mutant cells had ~25% reduction in *Shaker* (I_A) current but normal slow delayed rectifier (I_{KS}, or *Shab*) current. In addition to the absence of dSK current, the observed decrease in I_A current should, all things being equal, lead to higher membrane resistance and slower responses. Consequently, the photo-insensitive membrane properties together with the normal phototransduction machinery suggest that the observed faster intracellular responses in mutant photoreceptors reflect a role for dSK in later membrane processes at the photoreceptor axon/synapse.

Nonetheless, since dSK is absent from the major AC feedback interneurones, and also from L2 monopolar cells, the direct synaptic feedbacks to R1-R6 photoreceptors axons should be less affected. dSK expression pattern, therefore, provides an additional evidence that dSK contributes to photoreceptor voltage response by fine-tuning feed-forward output and/or feedback input at photoreceptor axons.

2.3.2 dSK contributes to the photoreceptor axon membrane potential in the dark

Given this high expression at the layer of the first visual synapse, dSK channels may play a role in facilitating sensitivity regulation by counteracting Ca^{2+} influx in this network where

the feed-forward and feedback crosstalk tightly adjusts the potentials of the cells (Zheng *et al.*, 2006a). In the dark, LMCs and AC receive less feed-forward inputs and therefore are more depolarized. This, in return, will adjust the photoreceptor's potential to more positive values (compared to dissociated photoreceptors) due to increased feedback inputs from the interneurones. Consequently, dSK removal from synapses in this network would disrupt its intricate balance in the dark, altering electrical properties of photoreceptors. To test this hypothesis, I performed *in vivo* intracellular recordings from dark-adapted wild-type and *dSK*$^-$ photoreceptors (**Figures 2-2 A-C)**. Strikingly, voltage responses evoked by negative current steps revealed that input resistance of the *dSK*$^-$ photoreceptors was significantly decreased relative to the wild-type cells (**Figures 2-2B** and **2-2C**). The decrease in input resistance was also accompanied with a more depolarized resting potential in the dark (**Figure 2-2C**).

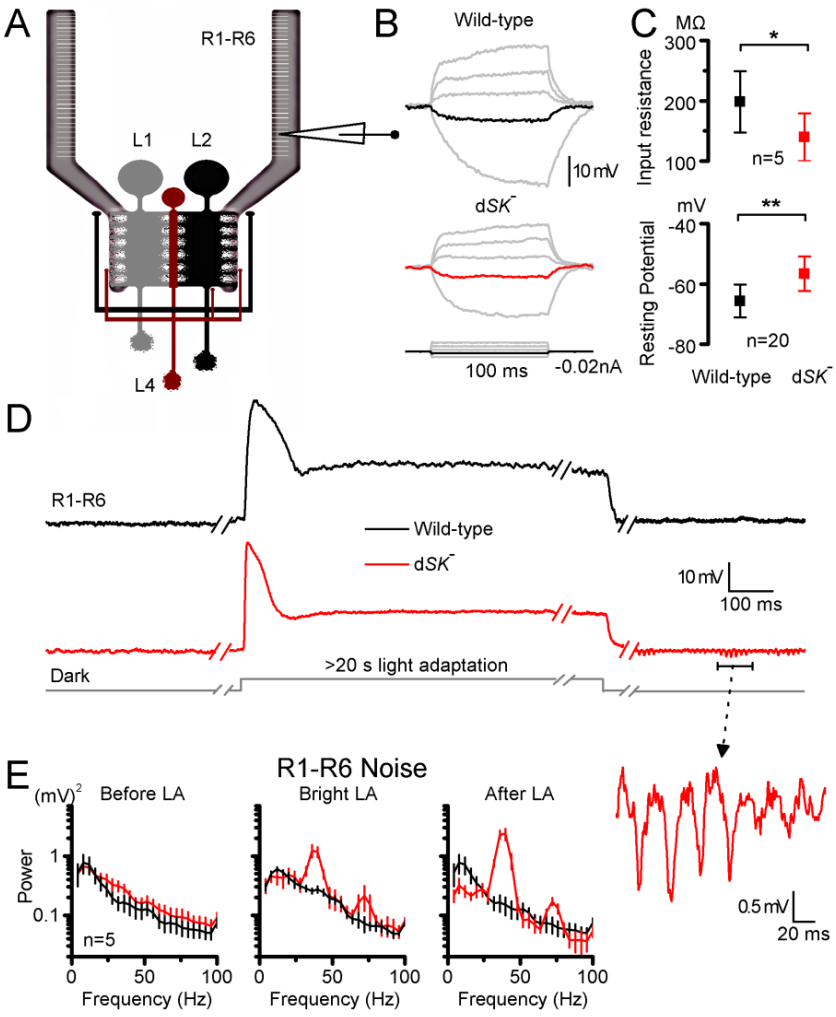

Figure 2-2: *dSK*$^-$ photoreceptors have reduced input resistance, elevated resting potential and slow oscillating responses in vivo. (**A**) Recordings from R1-R6 photoreceptors, connected to the lamina network; feedback connections (L2/AC and L4) to R1-R6 terminals highlighted. (**B**) Volt-

age responses of dark-adapted WT and *dSK⁻* photoreceptors to small current pulses. Responses to a -0.02 nA shown in black (WT) and red (*dSK⁻*) in the respective figures. (**C**) Input resistance to -0.02 nA pulses ($p < 0.017$, t-test), and their resting potentials in the dark ($p < 0.0002$, t-test). (**D**) Oscillations in *dSK⁻* photoreceptors depend on light exposure. Representative responses of WT and *dSK⁻* before, during and after bright light adaptation. Notice the discontinuous time scale. Insert: an oscillating response on a larger scale. (**E**) Noise power spectra of corresponding epochs in **D**. Dark noise are larger in *dSK⁻* photoreceptors in respect to WT (left), revealing strong oscillations at 40 and 70 Hz during and after light adaptation. Oscillations are augmented after light adaptation. Mean ± SD shown.

These findings strongly suggest an increase in depolarizing conductances in *dSK⁻* photoreceptor axons. While it is likely to contribute to the more positive value of the *dSK⁻* photoreceptor resting potential, the reduced *Shaker* conductance, together with removal of dSK conductance, would be expected to result in higher resistance at rest. I, therefore, conclude that the observed lowered input resistance is likely to result from increased axonal conductance that cannot be a pure K^+ (which would hyperpolarize the membrane appreciably relative to wild-type).

Overall, this data support a role for dSK in fine-tuning photoreceptor resting potential and its input resistance. Additionally, the decrease in photoreceptor's input resistance explains, at least partially, the faster responses seen in the intracellular recordings from the mutant photoreceptors (**Figures 2-1B** and **2-1C**). Furthermore, the expression profile, the normal light-induced current, and the photo-insensitive membrane dynamics strongly suggest that this lowered input resistance and the consequent fast *dSK⁻* photoreceptor responses are attributable to a change in photoreceptor's axonal inputs and/or output in the dark.

2.3.3 dSK mediates light-dependent sensitivity regulation at the lamina network

Blocking mammalian SK channels has been shown to enhance activity-dependent synaptic transmission and plasticity, suggesting a role for SK in coupling to and negatively regulating synaptic Ca^{2+} sources (Faber *et al.*, 2005; Ngo-Anh *et al.*, 2005). To test the effect of dSK removal on light-dependent activity in the lamina network, I first recorded intracellular voltage responses of photoreceptors in wild-type and *dSK⁻* flies to prolonged light pulses. I discovered that in most recordings the responses of mutant photoreceptors oscillated distinctively at 40 Hz and 70 Hz during and after prolonged light adaptation (LA) (**Figures 2-2D** and **2-2E**). Notably, the oscillations depended on light history (*cf*. before and after LA) and were boosted at lower potentials (*cf*. during and after LA) that should drive stronger LMC/AC feedbacks into photoreceptors (Zheng *et al.*, 2006a). Furthermore, in the dark, when their output showed no oscillations, *dSK⁻* photoreceptors were noisier than their wild-

type counterparts (**Figure 2-2E**, before LA); probably due to a barrage of depolarizing synaptic inputs into their axons, leading to the observed low input resistance (**Figure 2-2C**). Nonetheless, since these recordings were performed at the level of photoreceptor somata, the observed dynamics were likely to underestimate the processing taking place at the axon terminals.

I next recorded intracellularly from postsynaptic LMCs *in vivo* (**Figure 2-3A**). Although both wild-type and *dSK*¯ LMCs responded to light flashes with graded hyperpolarisations of similar sizes, the responses of mutant LMCs were significantly faster; thus the LMCs encoded faster presynaptic kinetics (**Figures 2-3B** and **2-6C**). Interestingly, ~40% (3/7) of *dSK*¯ LMCs showed oscillating responses. The oscillations were exacerbated at dim conditions (**Figure 2-3B**), where the gain of both the photoreceptor output synapses and synaptic feedbacks is the highest (Juusola *et al.*, 1995a; Zheng *et al.*, 2006a), thereby leaving the lamina network most perturbable to intrinsic activity. Longer recordings indicated that the oscillations in mutant LMCs carried different frequencies during and after light adaptation (**Figures 2-3D** and **2-6E**). Furthermore, compared to photoreceptors, these oscillations were larger and faster, peaking at around 100 Hz (**Figure 2-3E**); thus, the network transferred stimulus energy to higher output frequencies.

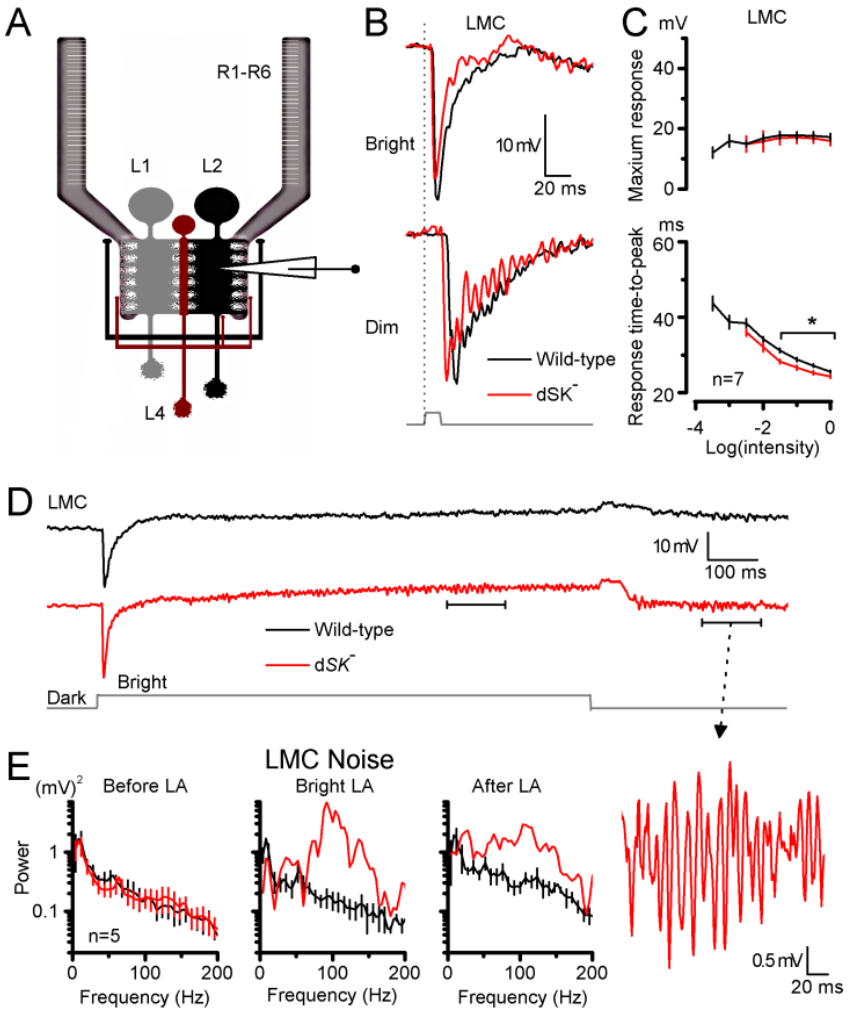

Figure 2-3: dSK fine-tunes synaptic transmission to large monopolar cells (LMCs). (**A**) Recordings from LMCs in intact lamina; feedback connections (L2/AC and L4) to R1-R6 photoreceptor axon terminals highlighted. (**B**) Voltage responses of WT and *dSK⁻* LMCs to a bright and a dim 10 ms pulse in the dark. *dSK⁻* responses fall and rise faster. (**C**) Respond ranges of WT and *dSK⁻* are similar, but time-to-peak to bright pulses is faster in *dSK⁻* ($p < 0.019$; t-test). (**D**) Oscillations in *dSK⁻* LMCs are experience-dependent. Voltage responses of WT and *dSK⁻* before, during and after bright light adaptation. Insert: an oscillating response magnified. (**E**) Noise power spectra of corresponding epochs in **D**. WT and *dSK⁻* LMCs, during and after light adaptation. Oscillations occur at around 100 Hz; at higher frequencies than in *dSK⁻* R1-R6 (Figure 3E). Mean ± SEM shown.

Nonetheless, in both mutant R1-R6s and LMCs, the oscillations varied with the light history (*cf*. oscillations before and after LA in **Figure 2-3E**), showing clear activity-dependency. Thus, these findings provide further evidence that dSK channels oppose intracellular Ca^{2+} increases, which are expected to peak during and immediately after light changes, and by this sensitivity control improve packaging of neural messages within the limited signalling bandwidth of the synapses.

2.3.4 dSK role in photoreceptor adaptation and coding

So far my results have shown that removal of the dSK channel from the synaptic microcircuits between photoreceptors and LMCs leads to activity–dependent oscillations in the lamina network. These perturbations were accompanied with altered response properties of photoreceptors, including decrease in their input resistance, more depolarized resting potentials and faster light-induced voltage responses. Next, I asked to what degree these changes, many of which mimicked electrophysiological effects of light-adaptation (Klocker *et al.*, 2001; Nikolaev *et al.*, 2009b), affected the adapting properties and signalling performance of *dSK*¯ photoreceptors.

My experiments were designed to quantify how well wild-type and *dSK*¯ photoreceptors could encode different light patterns (*i.e*. their intensity resolution) over a wide range of luminances. The photoreceptors were stimulated by repeatedly presenting naturalistic time series of contrasts, collected from natural environments (van Hateren, 1997), while recording their intracellular voltage responses. Consistent with the results of the light pulse experiments, the responses of *dSK*¯ photoreceptor mostly oscillated at dim stimuli (**Figure 2-4A**), during which the gain of feed-forward and feedback synapses is high (Zheng *et al.*, 2006a). However, some recordings lacked oscillations and many oscillated only sporadically; in some cases, oscillations died out during stimulation. All these observations underline the variable dynamic nature of gain regulation in the lamina network.

Interestingly, during the stimulation, the mean output of mutant photoreceptors adapted to the tested stimulus luminances much faster than that of wild-type photoreceptors (**Figure 2-4B**), suggesting that the lamina network was tonically driving them to elevated states of activity, in tune with their lower input resistance (*cf*. **Figure 2-2B**). However, early in the adaptation phase, as a sign of limited gain control, the dynamic range of *dSK*¯ photoreceptors contracted significantly (**Figure 2-4C**). Then, instead of desensitizing to the new stimulus luminance, as wild-type photoreceptors do, most *dSK*¯ photoreceptors sensitized to it (6/8 cells); their responses grew larger as the contrast pattern was repeated, reaching a relative steady-state in about 12 seconds of bright naturalistic stimulation. This recovery rate ($\tau \approx 6$ s) matches the rate of network adaptation in wild-type LMC output (τ = 1-7 s), which improves temporal representation of similar stimuli (Zheng *et al.*, 2009), suggesting that inputs from the lamina network might be amplifying *dSK*¯ photoreceptor output over time. After removing the first 20 responses with clear adapting trends, the photoreceptor signal was estimated by averaging the rest of the responses (**Figure 2-4D**), and the photore-

ceptor noise was taken as the difference between individual traces and the signal. Their power spectra indicated that, apart from the dimmest stimulation (*cf.* **Figure 2-4A**), once steady-state adapted, *dSK*¯ photoreceptors produced larger responses to fast light changes than wild-type cells, allocating more power at higher output frequencies (>50 Hz; **Figure 2-4E**), but that these fast responses were more variable (**Figure 2-4F**).

Because voltage oscillations in *dSK*¯ photoreceptors were sporadic or disappear during repeated stimulation, they contributed relatively little to this analysis (**Figure 2-4D**), which can underestimate their real impact. In fact, it can be expected that the oscillations and reduced gain control of *dSK*¯ photoreceptors, (the latter during light-dark transitions), will blur vision more when a mutant fly locomotes in its natural environment, as this requires even more demanding spatiotemporal gain changes in the lamina network.

Nonetheless, the striking finding was that the variable signal and noise dynamics of wild-type and *dSK*¯ photoreceptors, provided unexpectedly similar information captures of naturalistic stimuli over a large luminance range, saturating at ~300 bits/s during bright stimulation (**Figure 2-4G**). This is mainly because whilst *dSK*¯ photoreceptors show higher power on the high frequencies (**Figure 2-4F**), (due to faster dynamics), this is compromised by the presence of higher noise on the same frequencies (**Figure 2-4F**). Also, information capacity measurements only indicate the average coding ability occurring over a long period of time. Although these results highlight the inherent robustness of encoding in the lamina network after light adaption (Niven *et al.*, 2003; Vähäsöyrinki *et al.*, 2006; Zheng *et al.*, 2006a), it is worth keeping in mind that *dSK*¯ flies still suffer from the sporadic oscillations and defects during dark-to-light transitions.

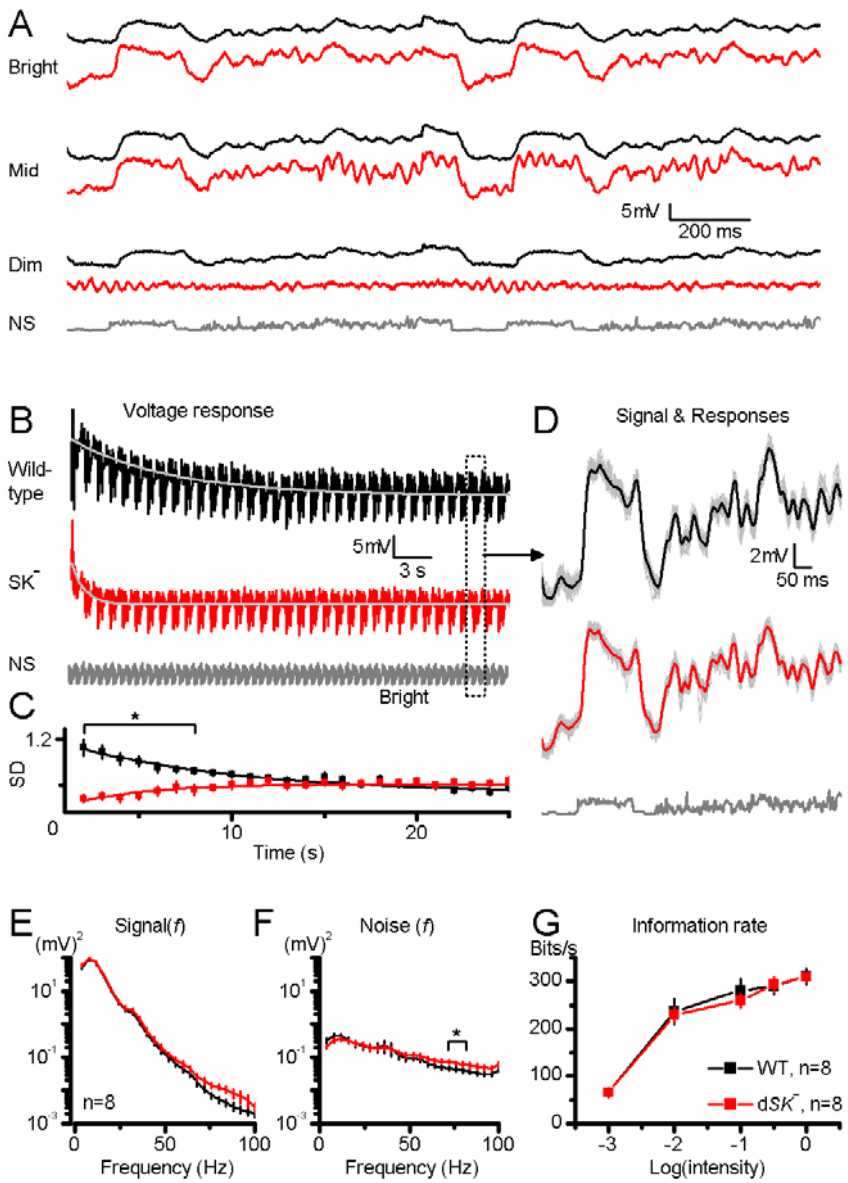

Figure 2-4: *dSK⁻* photoreceptors show fast but inefficient adaptation to dark-light transitions, yet their rate of information transfer appears normal. (**A**) Voltage responses of *dSK⁻* photoreceptors oscillate sporadically during naturalistic stimulation (NS) at dim and middle luminances, but rarely at bright luminances. (**B**) Responses of R1–R6 photoreceptors to a repeated bright naturalistic stimulation. Mean *dSK⁻* photoreceptor output adapted to a steady-state level significantly faster than WT (τSK = 1.2 ± 0.2 s; τWT = 6.2 ± 1.8 s; mean ± SEM; $p < 0.017$, n = 10 cells). Dotted window: repeated 1 s patterns. (**C**) Dynamic range (SD) of *dSK⁻* photoreceptors output was significantly reduced at the dark-light transition ($p < 0.024$, t-test), but recovered (sensitized) to the WT level in ~ 12 s (τSK = 6.3 ± 2.8 s). In contrast, WT photoreceptor output contracted (desensitized) and slower (τWT = 15.4 ± 4.6 s; mean ± SD, n = 6). (**D**) The signals (mean responses: black and red) and individual voltage responses (gray) of 8 photoreceptors after steady-state adaptation (first 20 responses omitted). (**E**) Signal power spectra: *dSK⁻* photoreceptors generate larger responses to fast light changes (70-100 Hz) than WT (mean ± SEM). (**F**) Noise power spectra: *dSK⁻* photoreceptors are noisier at high frequencies (mean ± SEM); i.e. at 72 ± 4 Hz ($p = 0.024$). (**G**) Information transfer rate estimates: *dSK⁻* photoreceptor output shows similar encoding capacities to WT at all tested luminances (mean ± SD).

2.3.5 Cellular localization of dSK functions at the first visual layer

Both light dependent oscillations and light-independent electrophysiological changes in the lamina network indicate suboptimal sensitivity regulation in photoreceptors and/or interneurones in *dSK*¯ flies, suggesting dSK has a direct role in synaptic communication as an adaptive damper. To further map dSK's contribution to the lamina network, I used a mutant with only dominant negative dSK subunit expressed in the R1-R6 cells (see method). Intracellular recordings from photoreceptors expressing a dominant negative dSK subunit showed accelerated response kinetics, approaching those seen in *dSK*¯ photoreceptors (**Figure 2-5**). However, no light-dependent oscillations were detected in such photoreceptors, although their conductance deficits match those of *dSK*¯ photoreceptors (**Figures 2-2**), suggesting that oscillations seen in mutant photoreceptors and LMCs might result from a less adequately tuned network. This view is consistent with the dSK immunostaining results (Abou Tayoun *et al.*, 2011), which suggested that in *dSK*¯ mutants, glutamatergic feedbacks from L2 and AC interneurones to photoreceptor axons should function normally, while some non-glutamatergic contacts in their lamina might not (including those of L4 LMCs). In clear contrast, in flies, where photoreceptor axons express functionally-impaired dominant negative dSK, the lamina is otherwise normal, and so better equipped to compensate this loss in neuronal function (**Figure 2-5**) by tuning its network functions. Thus, oscillations in mutant cells probably arose from improper control of synaptic gain in *dSK*¯ LMCs, and/or possibly in other interneurones.

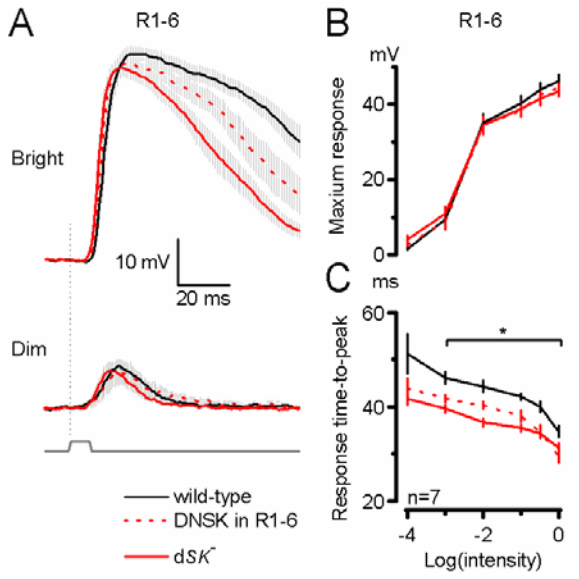

Figure 2-5: Photoreceptors expressing a dominant negative dSK subunit have faster light responses. (**A**) Voltage responses of WT, *dSK*¯ and photoreceptors with specific dSK dominant negative expression (red dashed, DNSK in R1-6) to a bright and a dim 10 ms pulse in the dark.

dSK⁻ and DNSK in R1-6 responses rise and decay significantly faster than WT. (**B**) Voltage ranges of all genotypes are similar. (**C**) Time-to-peak of the responses is as fast in photoreceptors expressing a dominant negative dSK subunit as in *dSK*⁻ photoreceptors when compared to wild-type ($p < 0.0184$, $n = 7$ cells; student's t-test). The genetically altered cells have faster responses over most of the tested light intensities.

2.4 Discussion

The essential characteristic of the *Drosophila* lamina is its massively parallel synaptic connections (Meinertzhagen & O'Neil, 1991b), which, similar to our retina, supposedly evolved to reliably process and redistribute information about environmental regularities to multiple retinotopic pathways (Barlow, 1961). Its robust design can also withstand mutations or damage without losing much of its encoding performance (Zheng *et al.*, 2006a). Indeed, I discovered that many detriments of missing dSK channels appeared to have been compensated homeostatically by network functions; most likely by tuning synaptic currents. Nonetheless, this compensation, which disrupted the photoreceptor membrane properties, accelerating responses and some aspects of their adaptation, was suboptimal. Consequently, it could establish that dSK channels in wild-type mediate activity-dependent inhibition in the lamina network, preventing responses from oscillating while its synapses operate with high gain; presumably to curb the costs of noise (van Hateren, 1992b) and energy (Laughlin *et al.*, 1998). These results concur with the view that dSK current counteracts light-induced Ca^{2+} increases, which drive transmitter release from the photoreceptor axons and interneurones, refining their representations of visual information in changing conditions.

2.4.1 The dSK fly model

Unlike mammals and *C. elegans*, which have three and four *SK* genes, respectively (Kohler *et al.*, 1996; Salkoff *et al.*, 2005), the fruit fly genome contains a single highly conserved *SK* gene (*dSK*) that encodes a remarkably similar current to the mammalian counterpart. To my knowledge, this report is the first to evaluate the impact of SK channel on neuronal and network functions, which affect adaptation and signalling performance of photoreceptors. Because of this new model system, and the new insight it has given about sophisticated network functions, it is now possible to start dissecting the contributions of dSK channel and dSK-expressing cells in circuits, involved in complex behaviours, addiction, and learning and memory.

2.4.2 Homeostatic sensitivity regulation

The photoreceptor output is sign-inverted by LMCs/ACs' histamine-receptors and then partially fed back to photoreceptors through synaptic conductances (**Figure 2-6**). Darkening

hyperpolarizes photoreceptors, reducing their tonic histamine release (Uusitalo *et al.*, 1995a; Zheng *et al.*, 2006a). This in turn depolarizes LMCs/ACs, increasing their feedbacks to photoreceptor axons (Zheng *et al.*, 2006a). These excitatory conductances can explain why in the dark, photoreceptors of the fully functioning network are more depolarized than the dissociated photoreceptors, which lack axons.

At the photoreceptor terminals, the slowly hyperpolarizing K^+ conductances of dSK channels (**Figure 2-2B**) are likely to facilitate local inhibition by offsetting voltage dependent Ca^{2+} increases, as a part of axonal sensitivity control that refines waveforms and patterning of presynaptic signals (**Figure 2-6A**). Here, dSK might be also required in fine-tuning histamine release, whereby any synaptic transmission defect would lead to increased feedback inputs into photoreceptor axons (**Figure 2-6B**). These scenarios (**Figures 2-6A** and **S1B**) are not mutually exclusive and in the absence of dSK would result in increased synaptic feedback conductances from the lamina interneurones, leading to the observed lowered input resistance and the more depolarized resting potential of photoreceptors. They are further supported by our expression data, and the intact morphology and phototransduction machinery in *dSK*¯ photoreceptors.

During and following prolonged light exposure, both *dSK*¯ photoreceptor and LMC voltage responses oscillated in an activity-dependent manner, implying that in wild-type, dSK channels would have a direct role as adaptive dampers in synaptic communication. It is possible that these perturbations resulted from faulty synaptic gain control in dSK-expressing non-glutamatergic interneurones, because inactivation of dSK only in photoreceptors was not sufficient to induce them, and because in mutant, dSK seemed not expressed in glutamatergic interneurones (ACs and L2s), which synapse directly to photoreceptor axons. Furthermore, photoreceptor oscillations were strengthened *after* light adaptation and to dim but not bright luminances. Such stimulus conditions lower presynaptic (photoreceptor) potentials and, therefore, are expected to boost post-synaptic feedbacks from the network. Thus, in dim luminances, mistuned synaptic feedbacks of high gain could transfer energy to wrong stimulus frequencies, oscillating the photoreceptor output. Collectively, these findings hint that oscillations might originate from *dSK*¯ L4 monopolar cell synapses, which feedback to both photoreceptor axons and L2 monopolar cells (**Figure 2-6**) in the same and neighbouring lamina cartridges (Meinertzhagen & O'Neil, 1991b), and thus are ideally placed to mediate adaptive network functions (Strausfeld & Campos-Ortega, 1977).

To optimise visual information, network adaptation to dim environment involves integration over space and time, whereupon functional connectivity increases between cells (redundancy), smoothing low signal-to-noise images. But when adapting to bright environment its cells operate more independently, as lateral and temporal inhibition reduces redundancies to sharpen high signal-to-noise images (van Hateren, 1997). Thus, I speculate that faulty gain control in the lamina branches of *dSK*¯ L4 monopolar cells would hinder such connectivity transitions between dark- and light-adapted network states; affecting the rate of adaptation in photoreceptor and LMC outputs and making them more susceptible to oscillations. This view is further supported by the recording statistics from *dSK*¯ flies: all R1-R6 receive inputs from L4, and correspondingly most photoreceptor outputs showed suboptimal adaptation and oscillated; only L2 monopolar cells receive inputs from L4 and only ~40% of LMC outputs oscillated. These observations highlight how the neuronal functions in the early motion pathways can depend upon adaptive gain control, leading to different behavioural outcomes in different stimulus conditions (Zheng *et al.*, 2006a; Rister *et al.*, 2007; Katsov & Clandinin, 2008; Nikolaev *et al.*, 2009b; Zhu *et al.*, 2009; Joesch *et al.*, 2010).

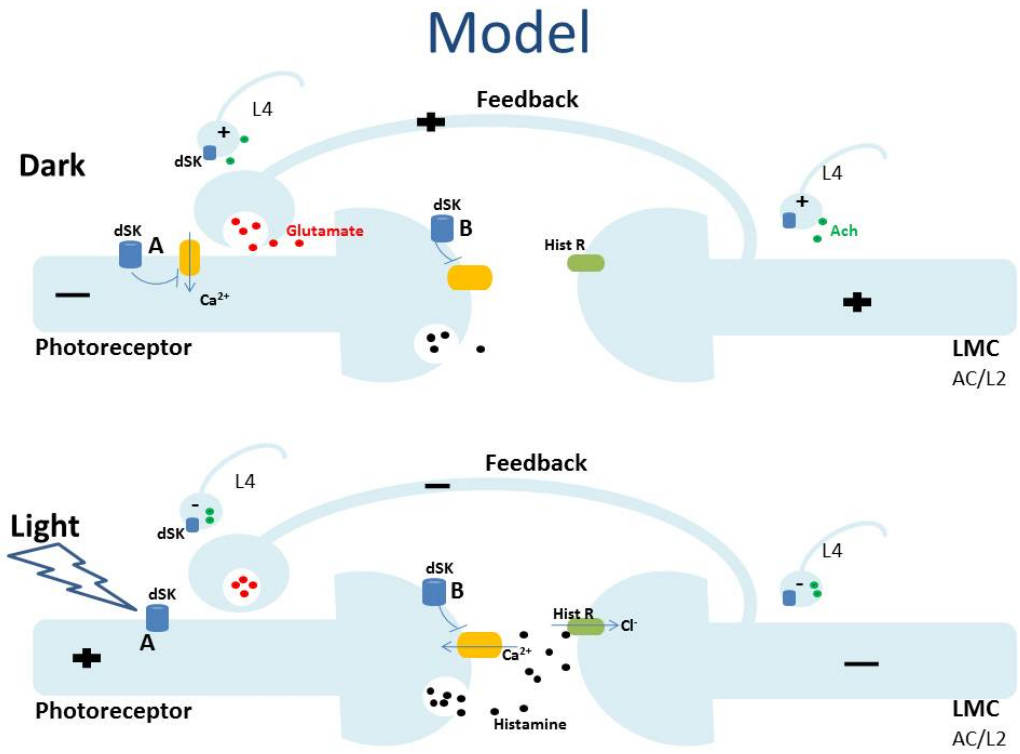

Figure 2-6: dSK contributes to photoreceptor performance by fine-tuning synaptic transmission at the photoreceptor-LMC-photoreceptor network. In this model, dSK is expressed in photoreceptor axons, while glutamatergic AC interneurones and L2 monopolar cells, which form the direct synaptic feedbacks to photoreceptor axons, do not express dSK. In addition, photorecep-

tor axons and AC/L2 receive extra inputs from the lamina network; through functional contacts with non-glutamatergic LMCs that express dSK, including L4s. Within R1-R6 axons, dSK counteracts Ca2+ and fine-tunes neurotransmitter release. In the dark, LMCs receive less feed-forward input from photoreceptors and are, therefore, more depolarized. In the absence of dSK, the observed depolarized resting potential and the lowered input resistance can be attributed to an inability to zero photoreceptor axonal voltages (A) and/or increased feedback synaptic inputs into photoreceptor axons due to misregulated histamine release (B). In the light, photoreceptors are more depolarized and, therefore, the feedback input is reduced (both direct and extra). In the dark/dim conditions, an inability to fine-tune neurotransmitter release from non- glutamatergic LMCs (most likely L4), at least partially, can lead to the observed oscillatory responses in both photoreceptors and LMCs (particularly in L2s) in *dSK*$^{-}$ flies.

2.4.3 Robustness of dynamic coding in *dSK*$^{-}$ mutant photoreceptors

Despite the fast oscillatory responses, *dSK*$^{-}$ photoreceptors revealed a near-normal encoding capacity. The decreased input resistance in *dSK*$^{-}$ photoreceptors is similar to that found in *Shaker* and *Shab* mutant photoreceptors (Niven *et al.*, 2003; Vähäsöyrinki *et al.*, 2006), where it has been argued to compensate for mutant defects and underlie the robustness of encoding. In *Shaker* photoreceptors, the decrease in input resistance partially restores the efficient use of the operating voltage range (Niven *et al.*, 2003). Conversely, *dSK*$^{-}$ photoreceptors, like *Shab*, show remarkable robustness in their light–voltage relationships, sensitivities, and reliability of dynamic encoding (rate of information transfer).

Although it is unclear whether the underlying mechanisms are the same, the lower input resistances in all these mutant photoreceptors are believed to be direct manifestations of compensation. In this study, the lowered input resistance, measured from intact *dSK*$^{-}$ photoreceptors *in vivo*, indicates an increase in conductance at the photoreceptor axon. Here I propose that this compensation results from feedback synaptic inputs from the neighbouring interneurones, because everything else being equal, instead of depolarizing *dSK*$^{-}$ photoreceptors, excess of K^{+} and/or Cl^{-} leak-conductances would work to hyperpolarize the cells toward the reverse potentials of these ions (-80 mV) (Niven et al., 2003). Thus, even if such leaks existed - a possibility that we cannot exclude - they would be masked by the depolarizing synaptic conductances from the network. Furthermore, response dynamics of photoreceptors, with inactivated dSK channels, were closer to wild-type when the network was normal rather than mutated (*cf*. **Figure 2-5A**), implying that extrinsic conductances (from the network) shape photoreceptor output more than intrinsic leak conductances (which, if dominating, should produce identical outputs for the two cases).

The faster kinetics and re-tuned adapting properties of *dSK*$^{-}$ photoreceptors impose a constant high energy cost to maintain both a low input resistance and a depolarized resting

potential in the dark, suggesting that the mutants are at a clear disadvantage. Thus, managing energy costs is a powerful evolutionary objective (de Polavieja, 2002), which together with noise and various behavioural objectives, supposedly refined the molecular constituents of the lamina network to overcome the limitations of its unreliable, slow hardware.

3 Quantal dynamics at photoreceptor-LMC synapse adapt to maximize the rate of information transfer

3.1 Introduction

In the fly eye, outer photoreceptors (R1-R6) transmit information to their neural downstream targets: large monopolar cells (LMCs) and amacrine cell (AC). In R1-R6-LMC synapses, information in presynaptic voltage changes is converted to quantal bursts of histamine (Hardie, 1987a), released from vesicles to the synaptic cleft. Changes in the neurotransmitter concentration are then sampled by specific receptor-complexes in the postsynaptic membrane (Skingsley *et al.*, 1995), thereby channelling information back to voltage changes.

In the classic view, synaptic vesicles are uniform in size, with each carrying similar dozes of neurotransmitter (Sudhof, 2004), enabling transmission of pulsatile messages. However, R1-R6-LMC synapses, like graded potential synapses in mammalian sensory systems, can support much higher rates of information transfer than conventional synapses (Van Steveninck & Laughlin, 1996), having specific structural adaptations to maintain this performance (T-bar ribbon synapses) (Prokop & Meinertzhagen, 2006). The fly eyes have evolved to encode environmental information in various light conditions, from single photon regimes to full daylight. It remains an open question whether the quantal dynamics in graded potential synapses remain constant at all conditions. Study on fly photoreceptors has revealed that their quantum bumps, voltage responses to single photons, adapt to changes in the input signal-to-noise ratio (Juusola & Hardie, 2001a), thereby optimising their sampling to the ongoing visual information capture and representation. Because sampling of neurotransmitter changes faces similar info-max constraints, it is possible that the presynaptic transmitter release and post-synaptic capture would have also evolved mechanisms for adaptive sampling. In addition, some evidence imply that there could be two forms of vesicle retrieval in *Drosophila* photoreceptor terminals (Koenig & Ikeda, 1996), suggesting potential kiss-and-run fusion release mode. Although previous study on the photoreceptors-interneurone synapses has shown that synaptic filtering adapts to the changing light input (Juusola *et al.*, 1995b), no detailed analysis on 'postsynaptic bumps', voltage re-

sponses induced by histamine release from single presynaptic vesicles, has been done so far.

Here I exploit the *in vivo* blowfly preparation (*Calliphora Vicina*) (Juusola *et al.*, 1995b) to investigate light-induced quantal histaminergic transmission from photoreceptors to LMCs. By analyzing the voltage noise of LMCs under different stimulus conditions, I could estimate changes in the corresponding average unitary postsynaptic events (bumps). I recorded voltage responses of photoreceptors and LMCs: (1) during darkness, (2) to different light backgrounds, and (3) to repeated pseudorandomly modulated light contrast patterns. I also recorded (4) voltage noise in LMCs when synaptic output from photoreceptors was silenced by massive Na^+-K^+-exchanger driven hyperpolarisation, following intense light pulsation (Uusitalo *et al.*, 1995a; Uusitalo & Weckstrom, 2000). The signal and noise properties of synaptic throughput at different stimulus conditions were studied in the same neurones.

My data shows that postsynaptic bump waveforms change with the mean light intensity. With low SNR inputs (dim light condition), mean post-synaptic unitary events are large and slow, leading to low-passing responses with high gain. With high SNR inputs (bright light condition), smaller and faster synaptic quanta were found, which sum up band-passing voltage responses with lesser gain. Since the mean postsynaptic membrane impedance and potentials remain relatively constant in all stimulus conditions, these results suggest that the presynaptic quantal vesicle release in photoreceptor-LMC synapses adapts to ongoing light inputs. By dynamically adjusting the size and numbers of the transmitted quanta, photoreceptors-LMC synapses seem to help maximising the flow of visual information within the lamina network.

3.2 Methods

3.2.1 Fly stocks

The majority of experiments were performed in female *Calliphora Vicina,* taken from a culture that originated from the flies caught in wild. Occasionaly, wild specimens were also used and no distinguishable difference was found in comparison to the cultured flies.

3.2.2 *In vivo* Electrophysiology

Intracellular recordings of R1-R6 photoreceptors and LMCs were carried out as described in Chapter 2. To exclude poor data contaminating my analysis, only high quality stable recordings were used. Such photoreceptors had resting potentials in the dark <−70 mV and

maximum responses to saturating bright pulses >50 mV. The corresponding standards for LMCs are <−30 mV resting potential and >35 mV pulse response. Here, I have not identified different LMC subtypes, but as L1 and L2 occupy the largest volume most recordings were probably in them; I may have also infrequently recorded from amacrine cells that share histaminergic input with L2 and L1 cells (Shaw, 1984b; Zheng *et al.*, 2006a; Zheng *et al.*, 2009). Nevertheless, because the recordings in this chapter had rather similar hyperpolarizing characteristics, all LMC data were analysed together.

Cells were stimulated at the center of their receptive fields with a high-intensity white LED (Seoul, model Z-power LED P4, white 240m). The light stimulus was delivered through a fibre optic bundle, mounted on a rotatable Cardan arm, subtending 2.7° as seen by the fly. Its Luminance was controlled by neutral density filters (Kodak Wratten), covering a 4 log unit range. The responsiveness of the cells was tested by repeated presentations of light pulses or white-noise light intensity series (200 intensity values). Since their luminance was adjusted by placing neutral density filters on the light source, the stimulus sequence retained its contrast constant ($c = \Delta I/I$).

Voltage responses were amplified by an SEC-10L single-electrode amplifier (NPI Electronic) in current-clamp mode using 15 kHz switching rate. The stimuli and responses were low-pass filtered at 500 Hz (KemoVBF8), and sampled at 1 or 10 kHz. The data were often re-sampled/processed off-line at 2 kHz for the analysis. Stimulus generation and data acquisition were performed by custom-written Matlab (MathWorks, Natick, MA) programs: BIOSYST (Juusola & Hardie, 2001a; Juusola & de Polavieja, 2003), with an interface package for National Instruments (Austin, TX) boards (MATDAQ; H. P. C. Robinson, 1997–2005).

3.2.3 Data Analysis

All analysis were described in detail in previous studies (Juusola *et al.*, 1995b; Juusola & Hardie, 2001a) and were very similar to those in the last chapter.

3.2.3.1 Processing of Voltage Responses to White-noise in Time Domain

Identical repeated pseudorandom light contrast patterns (gaussian white-noise, WN) were presented to the flies in this chapter (30–60 times). Both 1,000 ms and 5,000 ms long patterns were used as inputs and no obvious differences were found in the resulting output dynamics. All the analyses below are based on the 1,000 ms data. Analysis was done in the same way as in Chapter 2.

3.2.3.2 Signal and Noise Power Spectra and $SNR_V(f)$

The power spectrum of signal,$|\langle\tilde{S}_V(f)\rangle|^2$, and noise, $|\langle\tilde{N}_V(f)\rangle|^2$, was calculated using Matlab's Fast Fourier Transform (FFT) algorithm. Each 1,000ms data gave seven 500-point-long samples. Thus, for 50 repeats of 1,000 ms recording with sampling frequency 2k Hz, I obtained 350 spectral samples for the noise and 7 spectral samples for the signal. These were averaged, respectively, to improve the estimates. Same method was used for noise during static adaptations.

The signal-to-noise ratio in the frequency domain,$SNR_V(f)$, of the given LMC voltage responses was determined by dividing their signal power spectrum, $|\langle\tilde{S}_V(f)\rangle|^2$, by their noise power spectrum, $|\langle\tilde{N}_V(f)\rangle|^2$:

$$SNR_V(f) = \frac{|\langle\tilde{S}_V(f)\rangle|^2}{|\langle\tilde{N}_V(f)\rangle|^2} \tag{3.1}$$

3.2.3.3 Frequency and Impulse Responses

The LMC frequency response, $T_V(f)$, can be calculated from the autospectrum of the corresponding input (contrast, $\langle C(f)\cdot C^*(f)\rangle$) and output (Here, signal, $\langle S_V(f)\cdot C^*(f)\rangle$) and their cross-spectrum $\langle S_V(f)\cdot C^*(f)\rangle$:

$$T_V(f) = \frac{\langle S_V(f)\cdot C^*(f)\rangle}{\langle C(f)\cdot C^*(f)\rangle} \tag{3.2}$$

where * denotes the complex conjugate, and ⟨⟩ is the average over the different stretches of data.

The linear impulse responses, $k_V(t)$, (or first-order Wiener kernel) were then calculated as an inverse FFT of the corresponding frequency responses:

$$k_V(t) = F^{-1}(T_V(f)) \tag{3.3}$$

3.2.3.4 Information Capacity

From the signal-to-noise ratio, the information capacity (*H*) can be calculated (Shannon, 1948; Figs. 1 B and 2 B, f):

$$H = [\int_0^\infty (\log_2[SNR_v(f)+1])df] \tag{3.4}$$

The dimension is bits/s. Because the obtained high frequency components carry little biological signals but noise, the upper frequency limit of the integral was not taken to infinity (∞) but 400 here.

3.3 Results

The results are based on recordings from at least 5 photoreceptors and LMCs in different flies. All findings were robustly repeatable; but for the sake of clarity, single cell data are shown in some of the following figures.

Basic assumption of noise in LMCs

The fundamental assumption in this study is that voltage noise of LMC contains information about the average waveform of discrete voltage events induced by histamine release from single vesicles (Juusola *et al.*, 1995b). To investigate LMC's quantal response dynamic, I recorded postsynaptic LMCs membrane potentials in darkness and when adapting to steady light backgrounds (dim, mid and bright here). Dark- or light-adapted LMC membrane potential fluctuates in time (**Figure 3-1B**); and since the stimulus is not changing these fluctuations constitute voltage noise. Most of LMCs' voltage noise are assumed to originate from feed-forward synaptic inputs at photoreceptor terminals, representing chloride channel openings to the neurotransmitter, histamine (Hardie, 1989b). However, to a much lesser extent this noise must also contain stochastic channels openings, spontaneous intracellular intrinsic/metabolic noise and instrumental noise from the high resistance recording electrodes (Juusola *et al.*, 1995b); (Juusola & Hardie, 2001a), all of which are assumed to be additive. Thus, power spectrum of LMC voltage noise, $|\widetilde{N}_V^{total}(f)|^2$, contains synaptic noise, $|\widetilde{N}_V^{light}(f)|^2$ and instrumental plus intrinsic metabolic noise, $|\widetilde{N}_V^{intri}(f)|^2$:

$$|\widetilde{N}_V^{total}(f)|^2 \cong |\widetilde{N}_V^{light}(f)|^2 + |\widetilde{N}_V^{intri}(f)|^2 \tag{3.5}$$

Although instrumental noise makes only a minor component of total noise, it is more accurate to analyze synaptic quantal histamine dynamics of LMCs after minimising or eliminating the instrumental and intrinsic noise components. However, photoreceptors' transmitter release occurs tonically even in darkness (Uusitalo *et al.*, 1995a). Therefore, to estimate the actual background noise component, $|\widetilde{N}_V^{intri}(f)|^2$, I silenced the tonic histamine release from the local photoreceptors by a very bright prolonged light pulse. This stimulus overactivates photoreceptors' Na^+/K^+-pumps, hyperpolarising them momentarily to such a low voltage-level where their synapses fail to function (Uusitalo *et al.*, 1995a; Uusitalo & Weckstrom, 2000) (**Figure 3-2**).

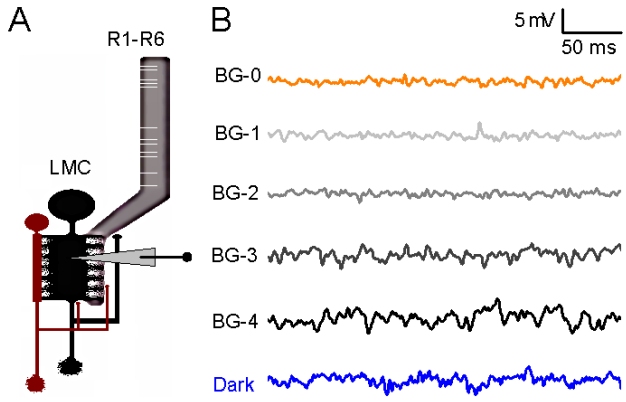

Figure 3-1: Dynamics of LMC voltage noise. (**A**) In vivo recordings from LMCs. Schematic drawing illustrate the R1-R6-LMC synapse and other possible lamina cells in the network. (**B**) Dynamics of LMC voltage noise to static light input under different background.

3.3.1 Hyperpolarisation by Na^+/K^+ exchanger silences photoreceptors' tonic histamine release

A strong light pulse was presented to photoreceptors to silence their synapses (**Figure 3-2B**). First, this prolonged stimulus (6 s in this case) depolarised photoreceptors. But once the light was switched off, photoreceptors were progressively hyperpolarised well below their dark-resting potential by Na^+/K^+-exchanger hyper-activity: trying to recover the diminished ion gradients. As fly photoreceptors hyperpolarise below a certain voltage threshold (~10-20mV below the dark resting potential), their tonic histamine release stops, because the voltage has become too low to activate voltage-dependent calcium-channels, which are needed for histamine exocytosis (Juusola *et al.*, 1996). Consequently, during photoreceptor hyperpolarisation (**Figure 3-2B**), the postsynaptic LMCs depolarised by 2-6 mV (by missing their hyperpolarising histamine-input) and their noise was reduced dramatically (**Figure 3-2B,** pink section). Gradually, the photoreceptor potentials recovered, depolarising to their normal darkness level. But when crossing the voltage threshold of synaptic histamine release, postsynaptic noise suddenly jumped from the near silence to abnormally high level, before finally returning to their normal dark-noise level. Correspondingly, I found a strong correlation between presynaptic voltage level, which drives the histamine release, and postsynaptic voltage noise (**Figure 3-2C**).

This period of photoreceptor hyperpolarisation is called the 'silent period', indicated by $|\widetilde{N}_V^{silence}(f)|^2$ power spectrum. Since LMC voltage noise during the 'silent period' noise is less than that of the dark-adapted photoreceptors (**Figure 3-2B**, also on power spectra, **3-2D**), it seems safe to assume that histamine release is more or less completely ceased dur-

ing the extensive photoreceptor hyperpolarisations. Thus, LMCs' 'silence noise' ($|\tilde{N}_V^{silence}(f)|^2$) is the presumptive minimal noise background, representing instrumental and intrinsic noises.

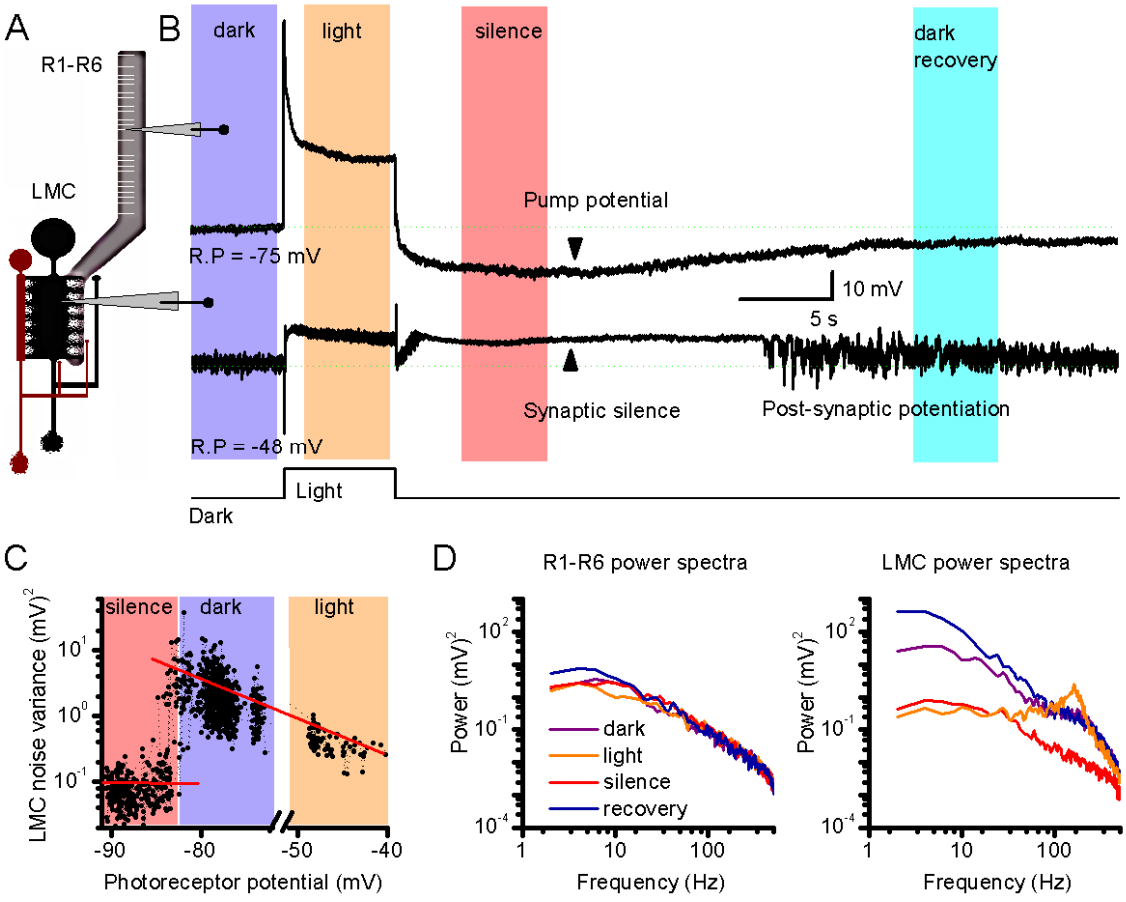

Figure 3-2: Silencing R1-R6-LMC synapse by Na^+/K^+-exchanger induced presynaptic hyperpolarisation. (**A**) Schematic of the R1-R6-LMC synapse and the likely recording sites. (**B**) Following a very bright light pulse, photoreceptor hyperpolarises ~20 mV below its dark resting potential, ceasing its synaptic histamine release. Consequently, without input to histamine-gated Cl^--channels, LMCs depolarise by ~10 mV and their voltage noise diminishes (synaptic silence). R.P stands for the resting potential. (**C**) There is a strong correlation between the presynaptic voltage level, which drives the histamine release and the postsynaptic noise. (**D**) Power spectra of photoreceptors voltage noise remain similar throughout the experiment. Power spectra of LMC voltage noise show large differences between the dark and light periods, and during the synaptic silence and recovery. These results strongly suggest that LMC noise follows dynamic changes in the histamine release rather than photoreceptor voltage noise.

3.3.2 LMC voltage noise reflects mostly histamine release

I then examined how LMC voltage noise correlated with photoreceptor voltage noise during different phases of the experiment. In particular, I wanted to find out to what extent changes in postsynaptic voltage noise reflected changes in presynaptic light-induced voltage noise, rather than changes in the presynaptic histamine release. Photoreceptor and

LMC noise data was analysed on frequency domain, $|\widetilde{N}_{photoreceptor}(f)|^2$ and $|\widetilde{N}_{lmc}(f)|^2$ respectively, or the four different phases of the experiment (**Figure 3-2C**): (1) dark period before the light pulse stimulus (0-5s); (2) during the light pulse (6-11s); (3) at silence period (12-17s); and (4) at the recovery period (30-35s). Power spectra of these four sections are calculated separately for the photoreceptor and LMC data (**Figure 5-2D**) (Details in the Method). Unlike the voltage noise of steady-state adapted photoreceptors, which varies greatly at different light levels (Juusola *et al.*, 1996; Juusola & Hardie, 2001a), here, photoreceptor voltage noise remained relatively constant throughout the experiment, indicating that both darkness and very bright light induce little presynaptic noise. This, in fact, is not very surprising as theoretically photoreceptor noise should approach the minima when most/all light-gated channels are either closed (darkness) or open (bright light). At the same time, however, LMC voltage noise varied significantly. Its power shifted to higher frequencies during the light stimulus and remarkably attenuated during the silence period, when histamine was absent. Noise power recovered to the pre-stimulation (darkness) level in about 35-45 s. The independence of photoreceptor and LMCs voltage noise strongly suggests that LMC noise mostly reflects variations in histamine–release and –sampling, rather than synaptic transmission of photoreceptor voltage noise, as proposed before (Laughlin et al., 1987). Along with the strong correlation between presynaptic voltage level and postsynaptic noise (**Figure 3-3C**), it is reasonable to assume that LMCs noise reflects post-synaptic summation of discrete histamine-gated Cl^--channel openings (bumps), possibly reflecting the quantal histamine release from individual vesicles.

3.3.3 LMC voltage noise suggests that quantal histamine release changes with illumination

By subtracting LMCs noise power during the synaptic silence from that during darkness and different light levels (**Figure 3-3B**):

$$\left|\widetilde{N}_{lmc}^{light}(f)\right|^2 \cong |\widetilde{N}_{lmc}^{total}(f)|^2 - |\widetilde{N}_{lmc}^{silence}(f)|^2 \tag{3.6}$$

The effects of presynaptic voltage (light-induced depolarization) on quantal histamine release dynamics can be investigated in frequency domain (**Figure 3-3C**). Noise was the greatest at the dimmest background (BG-4), but its power dropped and shifted from low to higher frequencies with brightening backgrounds (**Figure 3-3B**).

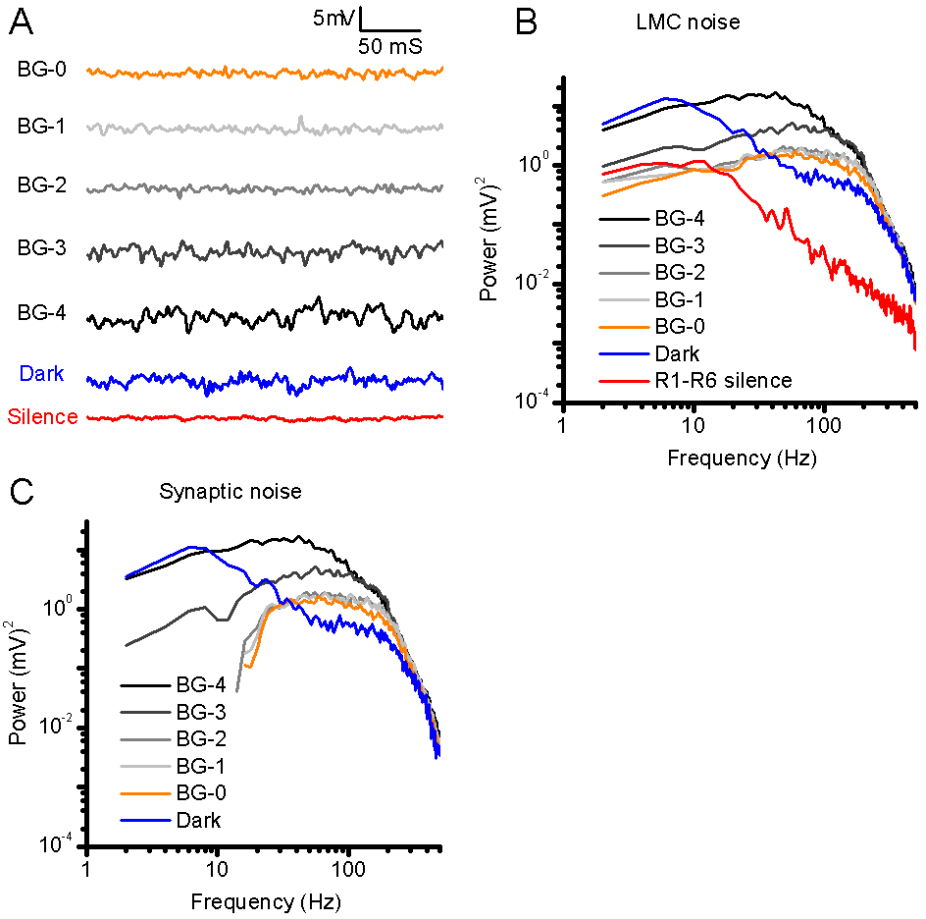

Figure 3-3: Postsynaptic voltage noise profiles. (**A**) LMC voltage noise to different light background and during synaptic silence (**Figure 3-2A**). (**B**) Power spectra of LMC voltage noise in **A**. (**C**) Quantal histamine release dynamics at different light levels were estimated by subtracting the LMC noise power spectra during the period of synaptic silence (red trace in A) from the ones estimated at different light levels.

Similar to what has been shown for quantum-bumps of photoreceptors (Dodge, Knight et al. 1968; Wong and Knight 1980; Juusola and Hardie 2001), I assume that the macroscopic voltage responses of LMCs are composed of unitary responses to histamine bursts (quantal vesicle release), each of which generate on average a similar response waveform, $B_V(t)$ which follows the well-defined Γ-distribution shape. Then, from the histamine-induced LMC noise, the averaged waveform of the elementary postsynaptic voltage response (bump) to the average histamine quanta can be estimated as:

$$B_V(t) = \Gamma(t; n, \tau) = \frac{1}{n!\,\tau}(t/\tau)^n e^{-t/\tau} \tag{3.7}$$

To find the two free parameters *n* and τ, I fitted a single Lorentzian function to the experimental power spectrum of the histamine-induced voltage noise (**Figure 5-4A**):

$$\tilde{B}_V(f)|^2 \propto |\tilde{\Gamma}(f;n,\tau)|^2 = \frac{1}{[1+(2\pi\tau f)^2]^{n+1}} \tag{3.8}$$

Where $\tilde{\Gamma}$ indicates the Fourier transform. The duration, T (i.e., the duration of a square pulse with the same power) of quantal postsynaptic voltage response, is then:

$$T = \frac{2^{2n+1}(n!)^2}{(2n)!} \cdot \tau \tag{3.9}$$

Normalized bump waveforms indicated that released histamine quanta became dramatically briefer with brightening light, as the bump duration shrunk (**Figure 3-4B**).

Notably, the power spectrum of LMC voltage noise in darkness has three components (**Figure 3-3C**), matching the results of previous study (Juusola *et al.*, 1995b). All of these can be fitted with individual Lorentzian functions (**Figure 3-4A**) and be further analysed for their bump waveforms. In **Figure 3-4B**, only two dark bumps are shown, because the third one has a much longer duration from lower end of its power spectrum. Nonetheless, this feature implied different dynamics for histamine release in darkness and in light.

However, previous studies have reported that filtering properties of LMCs adapt to light intensity changes, which probably lead to more complex bump waveforms than the conventional Γ-distribution (Juusola *et al.*, 1995b). To improve the data fitting, I assumed that the bumps actually follow the first derivative of Γ-distribution, $D_V(t)$, which represents a bi-phasic shape that matches well LMCs' biphasic macroscopic response waveforms (**Figure S4**):

$$D_V(t) = B_V{}'(t) \ = \Gamma'(t;n,\tau) \tag{3.10}$$

Then, I tried to find the best fits to the histamine-induced LMC voltage noise (**Figure 3-4C**):

$$|\widetilde{D}_V(f)|^2 \propto \tilde{B}_V{}'(f)|^2 = |\widetilde{\Gamma'}(f;n,\tau)|^2 \tag{3.11}$$

No analytical equations of $D_V(t)$ and $|\widetilde{D}_V(f)|^2$ are given here, as all the data fitting was done with real numbers.

This new fitting gave bi-phasic bump waveforms (**Figure 3-4D**); but similar to the previous results, the bump duration was reduced dramatically with brightening background.

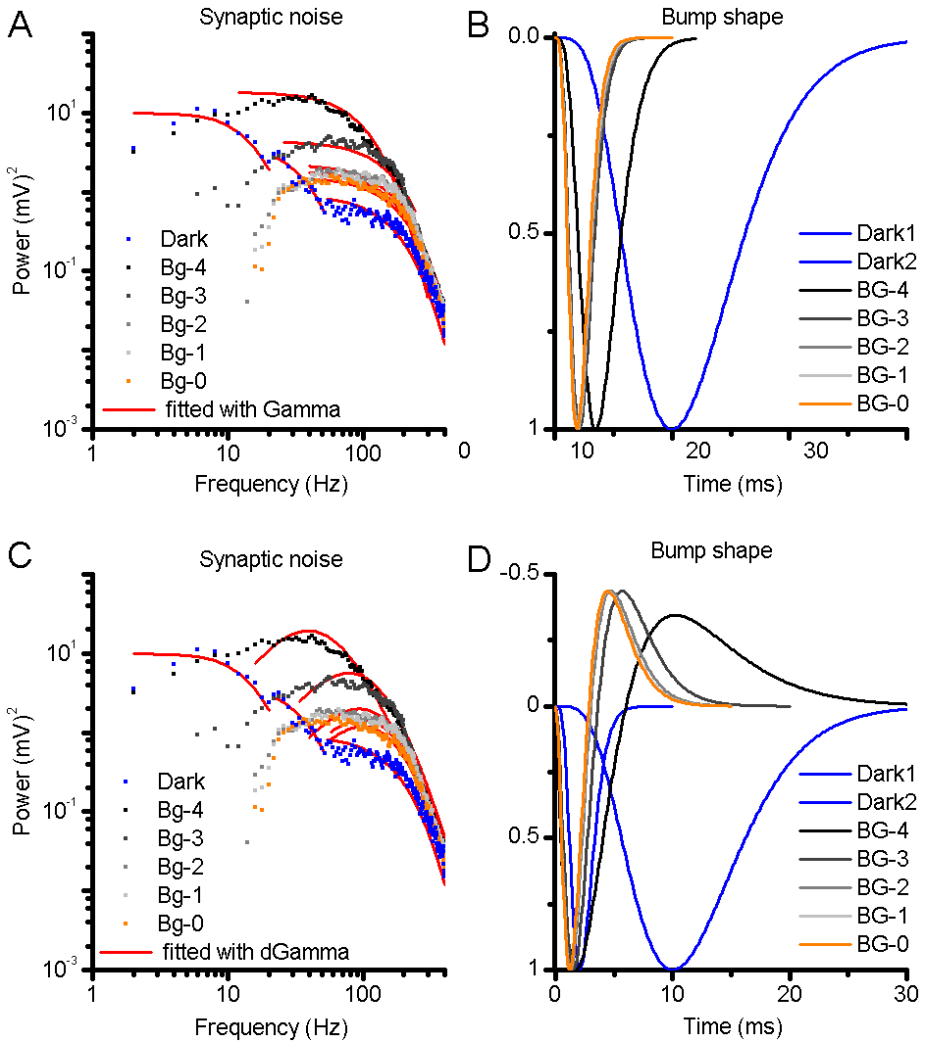

Figure 3-4: Histamine-induced bump shapes under different adapting light backgrounds. (**A**) Power spectra of LMC voltage noise in Figure 3-3B, after subtracting the silence noise (dots), is fitted with single Lorentzian functions (red lines). (**B**) Corresponding histamine bumps with Gamma distribution to **A**. (**C**) Same power spectra of LMC voltage noise were fitted with the FFT power of the first derivative of Gamma distribution (red lines). (**D**) Corresponding histamine bumps with first derivative Gamma distribution to **C**.

Previous studies (Wong & Knight, 1980; Freed, 2000) on quantal photoreceptor responses have applied Campbell's theorem, a classic technique for extracting amplitude and rate information from Poisson shot noise processes, to further analyze mean unitary bump amplitude (h) and bump rate (λ):

$$h = \frac{variance^2(N_{lmc}^{light})}{\Delta mean(N_{lmc}^{light})} \tag{3.12}$$

$$\lambda = \frac{\Delta mean^2(N_{lmc}^{light})}{variance^2(N_{lmc}^{light}) \cdot T} \tag{3.13}$$

Combining with shape, duration and amplitude, a complete estimation of bump waveform in LMC voltage noise could be achieved. Yet, LMC membrane potential has a clear none-linear property to light increment (**Figure S5**). As shown in **Figure S5**, this analysis will lead to unreasonable bump amplitude (h) and rate (λ) estimates. Thus, no further attempt were made to analyze the bump amplitude (h) and bump rate (λ) here.

Instead, I normalized the bump size simply by noise variance under different conditions (after subtracting silence variance) (**Figure 3-5**), because variance more or less reflected bump size under the constant light adaptation. Although this estimation is not accurate, it provided a rough approximation of the postsynaptic bump. In dim light condition, the mean bumps were large and slow. But with brightening light background, the bumps became smaller and faster. Interestingly, in dark adaptation, two underlying components share some features with light-adapted bumps, indicating that adaptation of these components may influence the form of the light-adapted bumps.

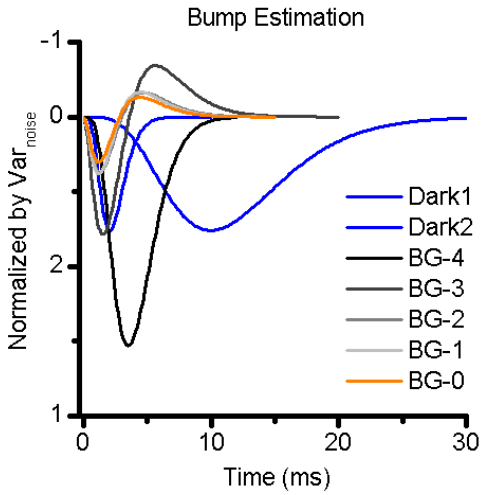

Figure 3-5: Histamine bump normalized by noise variance. Darkness and BG-4 bump are fitted using gamma distribution in figure 4B, and BG-3 to BG-0 are fitted with the first derivative of gamma distribution.

3.3.4 Quantal histamine release adapt to maximise the rate of information transfer

In the previous sections, I analysed LMC voltage noise at different light levels. However, the flies encounter light fluctuation in their natural habitats continuously, caused by both changing environment and self-motion.

To quantify how well LMCs encode dynamic light changes, I recorded their voltage responses to a repeated light contrast pattern (white-noise; see method). Their voltage sig-

nals were then averaged from the individual voltage responses. **Figure 3-6A** shows how the magnitude of LMC signals increased with brightening light backgrounds; this was accompanied with a power shift towards higher frequencies, $|\langle \tilde{S}_V(f) \rangle|^2$ (**Figure 3-6B**). Noise in each response was again determined by subtracting the signal from the individual voltage responses. In contrast to the increasing signal with brighter light, the corresponding voltage noise decreased dramatically, but shifted towards higher frequencies (**Figure 3-6C**). The shape of LMC noise power spectrum, $|\langle \widetilde{N}_V(f) \rangle|^2$, was dominated, as expected, by the frequency characteristics of the average bump waveform. Voltage noise in a single LMC behaves almost identically whether the cell is stimulated by a mean light level (**Figure 3-6C**, dotted lines, only bright and dim conditions are showed for clarity) or by a Gaussian contrast stimulus (white-noise) superimposed on it (**Figure 3-6C** solid lines). This implies that the mean (presynaptic) photoreceptor voltage, but not its dynamic modulation, mostly determines the quantal histamine release dynamics.

Because LMC voltage response to contrast stimulus increases with light intensity while noise decreases, the signal-to-noise ratio, SNR_V, calculated by dividing the signal by the corresponding noise, improves significantly, as reported previously (Juusola *et al.*, 1995b; Van Steveninck & Laughlin, 1996).

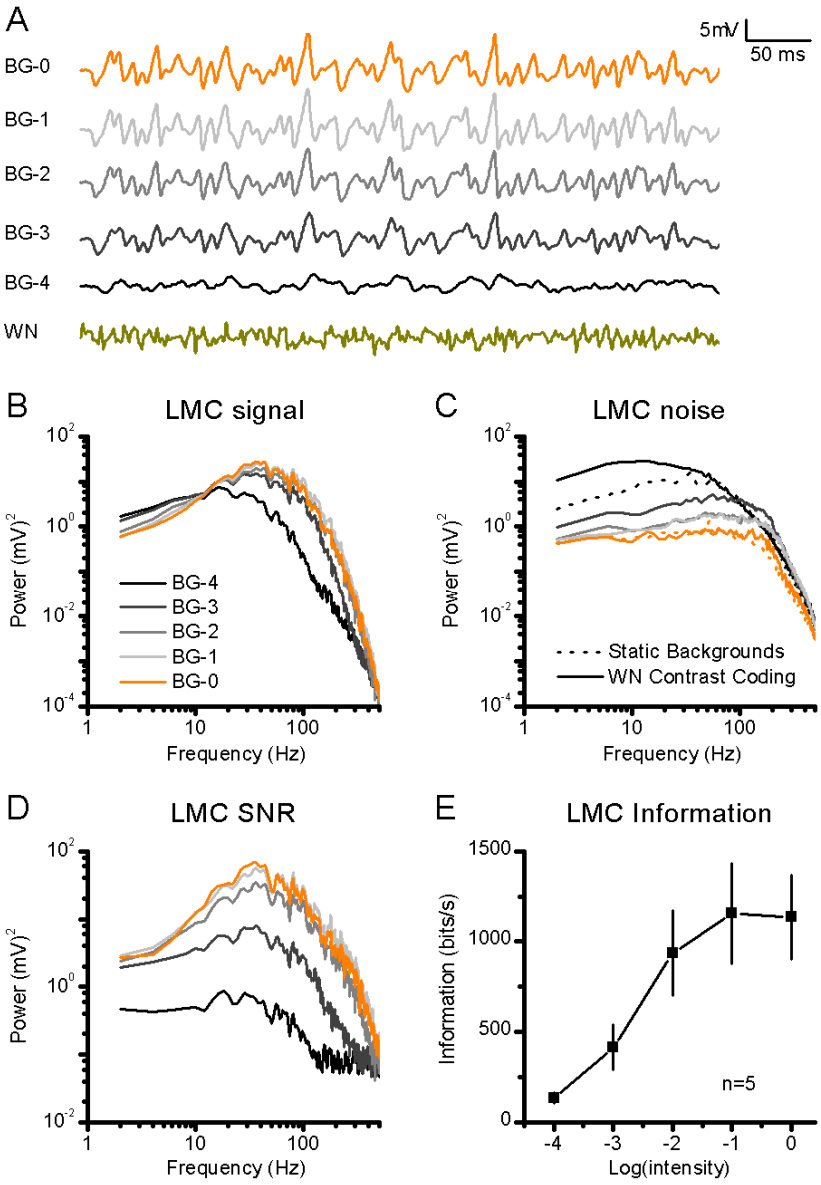

Figure 3-6: LMC voltage responses to a white-noise modulated contrast stimulus at different light levels (adapting backgrounds; BG). (**A**) Average responses (signals). In dim light, slow bumps sum up slow voltage responses, enhancing redundancies in the input. In bright light, fast bumps sum up transient responses, reducing redundancies. (**B**) Power spectra of LMC voltage signals. (**C**) Power spectra of LMC voltage noise. (**D**) LMC signal-to-noise ratio (*SNR(f)*) at different light levels. *SNR(f)* of LMC output increases with brightening light. (**E**) The rate of information transfer under different adaptation backgrounds. BG0, bright; BG–4, dim. Mean ± SD, n=5 cells

In frequency domain, the LMC signal-to-noise ratio, $SNR_V(f)$, was calculated by dividing the signal power spectrum by the noise power spectrum (Figure 5-5D). The signalling performance of LMCs improves with brightening stimulation, with the $SNR_V(f)$ progressively shifting towards high frequencies. As light adaptation expands the bandwidth of reliable

signalling, the average information capacity increases from ~150 bits/s at the background of BG-4 to ~1100 bits/s at BG0 (**Figure 3-6E**).

3.4 Discussion

Neural information transmission at synapses is a fundamental coding process. By using linear signal and noise analysis, I presented a novel postsynaptic bump estimation at fly's photoreceptor-LMC synapse.

3.4.1 Histamine Bump in LMC Coding

Historically, many studies have investigated the possible roles of LMCs in neural information processing (Laughlin & Hardie, 1978; Srinivasan *et al.*, 1990; Nikolaev *et al.*, 2009a; Zheng *et al.*, 2009). It is generally believed that LMCs serve as adaptive filters in which frequency response adjusts to the input statistics (Van Hateren, 1992a; Juusola *et al.*, 1995b): under dim/low-SNR conditions, they act as low-pass filters to enhance the signal reliability; under bright/high-SNR conditions, they perform band-pass filtering to reduce redundancy, on both temporal and spatial domains (Juusola *et al.*, 1996). Interestingly, this filtering property transformation is indeed reflected in the postsynaptic bump analysis of this study.

With low intensity/SNR inputs, the mean postsynaptic unitary events are large and slow, leading to high gain low-passing filtering. As a result, correlation in the input signals is increased, which thereby increases signal redundancy and reliability. This general integration strategy has a clear advantage on enhancing the information transfer (Van Hateren, 1992a).

In contrast, with high intensity/SNR inputs, I found smaller and faster synaptic quanta, which generated band-passing voltage responses with lesser gain (Juusola *et al.*, 1995b) reducing redundancy in neural information (Barlow, 1961). This bump property enables LMC to encode signals in a finer detail when input SNR, or 'richness of input information', is high. These results suggest that the quantal dynamic in photoreceptor-LMC synapses adapts to ongoing light inputs to maximize the flow of visual information.

Nonetheless, the mechanism behind this dynamic is still unclear. Voltage output of fly LMC constitutes a complex convolution of presynaptic input, postsynaptic membrane filtering (Uusitalo *et al.*, 1995a) and feedbacks from their neuronal neighbours (Shaw, 1984b; Weckstrom & Laughlin, 1995; Zheng *et al.*, 2006c). Thus, possibly any or all of these mechanisms could lead to the observed bump dynamic change. However, before going to the dis-

cussion of the underlying mechanism, there are two issues in this study that are worth mentioning.

3.4.2 Presynaptic noise or histamine-induced noise

One issue that might arise from the current study is that, to what extent, presynaptic noise influenced postsynaptic LMC voltage noise, because the fundamental assumption of the current bump analysis is that LMCs noise are postsynaptic. Although there might be some noise components that shared the same feature in both pre- and post synaptic sites (Juusola *et al.*, 1995b), it is very unlikely that these noises have the same source. Because one LMC receive six photoreceptors, which look at the same point in space, asynchronic presynaptic noise in individual photoreceptor will be largely cancelled out in the postsynaptic cells. From my data, it is clear that the photoreceptor voltage noise does not drive the LMC voltage noise (**Figure 5-2 D**). Instead, LMC noise strongly correlate to presynaptic voltage level (**Figure 5-2 C**); since the vesicle fusion is voltage dependent (Juusola *et al.*, 1996), my data strongly suggest that the postsynaptic noise was histamine induced. Thus, it is not unreasonable to assume that LMC voltage noise mostly reflects quantal dynamics in the histamine-gated post-synaptic Cl^--channel openings.

3.4.3 Postsynaptic change: Histamine bump & membrane resistance

Another issue of the present study is that dynamic changes in postsynaptic bumps could result from the changes in LMCs' membrane properties, because generation of voltage noise involves both membrane currents and resistance. Thus, changes in the bump size and speed could result from the altered LMC membrane filter at different adapting light backgrounds. Such scenario could be eliminated by deconvolving the membrane filter from the bump shape under each light condition. However, it has been reported that the LMC membrane resistance reduces with increasing light, and enhances during the silence period when the synaptic input has stopped (Uusitalo *et al.*, 1995b). Such decovolution would only produce even bigger changes in the bump shape as reported here. Thus, no such attempt has been made.

3.4.4 Postsynaptic dynamic: histamine channel dynamics

The potential mechanisms that regulates bump dynamic could occur either or both postsynaptic and presynaptic sites. On the LMC membrane, histamine-gated chloride channels mediate postsynaptic voltage responses (Hardie, 1989b). Postsynaptic bump dynamic could represent histamine-gated Cl^--channel conductances to different transmitter concentrations in the synaptic cleft. Whole-cell currents in dipteran LMCs show similar features to my

in vivo recordings: variance of LMCs noise fluctuation peaks in the low concentration of histamine, and decreases with increasing doses (Skingsley *et al.*, 1995). Thus, increasing histamine release could reduce the open time of the histamine-gated channels through cooperative binding, making the bumps faster and smaller (Skingsley *et al.*, 1995; Pantazis *et al.*, 2008a)

3.4.5 Presynaptic change: vesicle exocytosis

Another possible mechanism, which is not mutually exclusive, is the adaptive presynaptic vesicle exocytosis. With low presynaptic voltage levels (dim light), the mean histamine quantas (vesicles) could be large; with more depolarised presynaptic voltages (bright light), the histamine quantas could be smaller, leading to the corresponding average postsynaptic bumps. As discussed in the general introduction chapter, at the presynaptic release site, the vesicles may fully collapse with the plasma membrane, releasing its neurotransmitter content as a single bolus, or just release part of it though some kind of "kiss-and-run" process (Rohrbough & Broadie, 2005). Because vesicle fusion is voltage-dependent and calcium-induced (Broadie & Richmond, 2002), it is possible that in bright light condition, when photoreceptor voltage potential is high, the "kiss-and-run" mode could dominate the vesicle release, leading to small and fast quantal histamine release.

Meanwhile, recent work has shown activity-dependent compound fusion in Calyx of Held, forming large vesicles of increased quantal size (He *et al.*, 2009). Realistic simulations of changing vesicle size and mEPSC (minor Excitatory Postsynaptic Current) are consistent with my postsynaptic bump data: released boluses of neurotransmitter become smaller and briefer (with smaller vesicle size). EM studies in *Drosophila* neuron-muscular junction suggested similar compound fusion in an experience-dependent manner (Steinert *et al.*, 2006) with some mutants showing considerable vesicle size differences (Zhang *et al.*, 1998). Furthermore, it is not clear why inner (R7-R8) and outer (R1-R6) photoreceptor terminals show different vesicle sizes (44 vs 31 nm (Takemura *et al.*, 2008)) when they both use histamine as neurotransmitter. Based on my current findings, it is possible that UV (ultraviolet)-sensitive R7s undergo dark-adaption, leading to bigger vesicles, while the others are light-adapted as EM preparations are fixated in room light, which lack of UV. All these observation suggest that the large and slow postsynaptic bumps in dim condition may reflect larger quantal histamine boluses.

Preliminary electron microscopy examination of *Drosophila* R1-R6-LMC synapses in our laboratory has found that there is no significant difference in vesicle size, when comparing

preparations produced under differing light conditions, e.g. 'normal' light conditions, or under 'red' light conditions, (which should be similar to darkness, or at least dim light). However, this data was not conclusive, because the red-light preparations were left under normal light prior to fixation. It is very likely that the synapses are still active shortly after optic lobe isolation, leading to normal light-adaptation in the preparation. Also, if the formation and fusion of vesicles have a fast dynamics, it might not be detectable under normal electron microscopy preparation. Finally, 'T-bar' at R1-R6-LMC synapses could serve as a potential vesicle release controller (Parsons & Sterling, 2003) (Singer *et al.*, 2004), involved in the mechanisms above. Due to time constraints, I have not yet obtained direct biological or morphological evidence for changes in the quantal vesicle release size or release dynamics. This study continues.

4 Electrophysiological characterisation of spectral sensitivity in *Drosophila* R1-R6 photoreceptors and large monopolar cells (LMCs)

4.1 Introduction

To better understand colour vision in *Drosophila* requires knowledge of its input channels' spectral transmission properties. In fly compound eyes, visual inputs to each ommatidium are sampled by six outer-photoreceptors (R1-R6) and two inner-photoreceptors (R7 and R8). It is generally believed that R1–R6 feed information to the achromatic motion channels, while R7 and R8 photoreceptors supply inputs for the chromatic channels (Gao *et al.*, 2008). Although morphological studies have reported connectivity details of the achromatic/motion channels and the colour channels (Meinertzhagen & O'Neil, 1991a; Bausenwein *et al.*, 1992), but as for now, the spectral sensitivities of neither *Drosophila* photoreceptors nor their postsynaptic cells have not been characterized physiologically *in vivo*.

Therefore, it remains unclear if and how the colour and motion channels interact. Although motion information appears routed and processed through on- and off-channels (de Polavieja, 2006; Joesch *et al.*, 2010) similar to vertebrate retina (Gollisch & Meister, 2010; Schiller, 2010), these could crosstalk with the colour pathway in the fly early visual system. Ultrastructural studies imply interactions in the medulla, with synapses between R7/R8 photoreceptors and LMCs (Takemura *et al.*, 2008), but possibly also in the lamina where gap-junctions (Shaw, 1984b; Shaw *et al.*, 1989b) and synapses (Zheng *et al.*, 2006b) form complex local processing networks (Meinertzhagen & O'Neil, 1991a).

In this study, I first measured *in vivo* spectral sensitivities of R1-R6 photoreceptors and their primary postsynaptic targets (large monopolar cells; LMCs) in *Drosophila* using conventional sharp microelectrodes. Then, by comparing the wild-type recordings to those of mutants, which had genetically deactivated colour channels, I could examine whether the motion channel receives any inputs from the colour channels in early visual processing.

My results show that *Drosophila* R1-R6 photoreceptors have a dual-peaked spectral sensitivity, which verifies the *in vitro* pigment studies and matches the spectral sensitivity of R1-

R6 photoreceptors in larger dipteran flies. Although postsynaptic LMC outputs follow mostly the presynaptic input, nonlinear synaptic transmission whitens/flattens out their spectral sensitivity. I also discovered that light-adaptation shifted the 'blue peak' towards lower wavelengths in R1-R6s, in accordance with the pupil effect, reported in *Calliphora* and *Musca* (Hardie, 1979a; Vogt *et al.*, 1982). However, I found no significant difference in the spectral sensitivity of R1-R6 photoreceptors and LMCs in the mutant, which had normal WT eye pigmentation but lacked light-sensitive R7s and R8s.

4.2 Methods

4.2.1 Fly stocks

Canton-S (wild-type) fly strain was acquired from the Bloomington Stock Center.

Mutant flies with light-sensitive R7s and R8s, w+ norpA24; +; P {w+, Rh1: norpA}, were generated by expressing norpA under the Rh1 promoter in R1-R6s in norpA24- background flies.

The flies were raised at 18 °C in a 12: 12h dark: light cycle. Flies of both sexes were used in the experiments and no clear differences were found in the spectral sensitivity of their R1-R6 photoreceptors and LMCs.

4.2.2 *In vivo* Electrophysiology

Intracellular recordings from R1-R6 photoreceptors and LMCs were carried out as described in Chapter 2. In this chapter, the head temperature of the flies was kept at 22 ± 1°C by a feedback-controlled Peltier device (Juusola & Hardie, 2001a). Same criteria for data selection was used here as in Chapter 2.

4.2.3 Cell identification

R1-R6 photoreceptors were identified by their depolarizing responses to light and dual-peaked spectral sensitivity, while LMCs were identified by their hyperpolarizing responses to light. Here, I have not identified different LMC subtypes, but no clear differences were found in the spectral sensitivities. So, no further attempts were made for cell type identification and all presumptive LMCs recordings were analyzed together.

4.2.4 Stimulation

Two different light sources were used in the recordings. A high intensity white LED (spectral output from 400- 800 nm, with three peaks at blue, green and red), with a full set of quartz

neutral density filters, covering 4 log unit, were used to test the intensity-response function (V/log I, or time-to-peak/log I) of the cells. Xenon arc lamp (OSRAM, 75w) with OptoScan monochromator (Cairn Research) was used to generate monochromatic light (details below). Light stimuli were delivered through a fiber optic bundle (Oxford Electronic, UK; spectral transmission range: 180-1,200 nm), mounted on a rotatable Cardan arm, subtending <5° as seen by the fly. Thus, spatially, the stimuli fitted well inside a typical receptive field of a R1-R6 photoreceptor (Gonzalez-Bellido *et al.*, 2011). After positioning the light source at the center of a cell's receptive field, its voltage responses to chosen colour stimuli were measured from the same point in space.

4.2.5 Monochromator calibration

For the intracellular spectral sensitivity measurements, I used a custom-designed, programmable (computer controlled by Biosyst) monochromator, which supported wavelengths from 300–700 nm with bandwidths from 0–30 nm, controlling both the mid-wavelength and bandwidth with millisecond-resolution (Cairn OptoScan, UK, with 75w Xenon arc lamp, OSRAM, having spectral output range: 250-1,200 nm) (**Figure S2A**). Monochromators typically generate residual harmonics, or secondary wavelength, which operate on logarithmic intensity scale (for example, 620 nm output comes with a much smaller harmonic at 310 nm) and can be large enough to stimulate photoreceptors. Therefore, the light output of the monochomator system was further sectioned by a steep long-pass edge-filter (LP420 nm, having $<10^{-6}$ throughput <420 nm and 99% throughput 420-640 nm (**Figure S2B**); Beijing Bodian Optical Technology, China) into two spectral ranges: 300-420nm without filter, and 420-640 nm with the filter. This arrangement eliminated major harmonics and minimized spectral irregularities of the narrow-bandwidth colour pulses. Thus, all the measurement value at the wavelength 420nm in this and next chapter is the average of the data with or without this 420nm filter. The monochromator system's light output was measured and calibrated by using a spectrometer (Hamamatsu Mini TM-VIS/NIR C10082CAH; 250 to 1000 nm, Japan) (**Figure S2C**). The energy of each narrow-bandwidth colour pulse (2-5 nm ± center-wavelength) was measured in 1 nm resolution and equalized by changing the software commands for specific driver settings (input slit, output slit, bandwidth) until its energy integral matched the integrals of all the other pulse energies used (**Figure S2D**). The spectral output of the calibrated spectrometer system was retested regularly and found to consistently produce the same range of isoluminant colours, even after lamp changes.

4.2.6 Measurement procedures

I used conventional flash stimuli to determine the spectral sensitivity of R1-R6 photoreceptors and LMCs. Short (10 ms) flashes of 16 monochromatic wavelengths (300-620 nm, with 20nm interval) were presented to the cells at the centre of their receptive fields. To ensure that their spectral sensitivity was not affected by rhodopsin/metarhodopsin ratio (Tsukahara & Horridge, 1977), each cell adapted 2 minutes with 590nm light before dark-adaptation. As metarhodopsin isomerizes back to rhodopsin by red-light, this method reset the rhodopsin/metarhodopsin equilibrium for accurate tests. Similarly, in light adaptation experiments, static 590nm light, which can evoke ~40% Vmax response (~45mv), was presented to the cells 30 seconds before the spectral scan. In both dark and light adaptation tests, I used 3-5 seconds flash intervals to recover the cells' sensitivity.

Similar to the previous studies (Hardie, 1979a; Vogt *et al.*, 1982), I readjusted the spectral sensitivity of photoreceptors' by their V/log I functions. This function was obtained by eight light intensity steps with different neutral density filters (0.5 log units each), then fitted with a sigmoid Hill function (**Figure S3C**):

$$\mathrm{V_n} = \mathrm{V_{max}} \frac{\mathrm{Intensity^a}}{\mathrm{k^a} + \mathrm{Intensity^a}} \tag{4.1}$$

Every cell was tested with sub-saturating stimuli, which kept the voltage responses within the linear range of their V/log I functions (~8-35mv, **Figure S3C**). After changing the intensity to linear scale, the relative spectral sensitivity was calculated as:

$$\text{Sensitivity \%}_{\text{at spectrum (n)}} = 100 * (\text{intensity}_n / \text{Intensity}_{\text{max across spectrum}}) \tag{4.2}$$

LMCs in *Drosophila*, as in larger flies, responded to photoreceptors' depolarisations with graded hyperpolarisations (**Figure S3B**). With increasing stimulus intensities, the speed and amplitude of the presynaptic responses increased (**Figure S3C**) and the postsynaptic LMC output became increasingly transient, saturating at very low intensities (**Figure S3C**). Thus, instead of normalising the spectral sensitivities of LMCs by their maximum voltage amplitudes, I used the time-to-peak of the responses, which remains linear over a large intensity range (**Figure S3C**):

$$\mathrm{T_n} = \mathrm{d} * \mathrm{Instensity} + \mathrm{b} \tag{4.3}$$

Then the relative spectral sensitivity was calculated as in 4.2.

4.3 Result

4.3.1 Spectral sensitivity of wild-type *Drosophila* R1-R6 photoreceptors and large monopolar cells (LMCs)

The spectral characteristic of R1-R6 photoreceptors and their postsynaptic targets, the LMCs, were measured from their voltage responses to monochromatic light flashes of different wavelengths. Spectral sensitivity of the photoreceptors and LMCs were normalized.

Spectral sensitivities of dark-adapted *Drosophila* R1-R6 photoreceptors are shown in **Figure 4-1C**. Comparable to the results obtained from larger flies, *Drosophila* R1-R6 photoreceptors have similar spectral sensitivities, characterised by two main peaks at ~360 nm and ~480 nm. The first peak is caused by the sensitising pigment that transfers the absorbed photon energy to the Rh1 rhodopsin, inducing its pigment activation (Kirschfeld & Franceschini, 1977; Minke & Kirschfeld, 1979), while the second peak (Kirschfeld & Franceschini, 1977) can be well fitted by Rh1 rhodopsin nomogram with absorption maximum at 478 nm (Salcedo *et al.*, 1999). My recordings also showed broader peak half-widths with significantly longer tails at both UV- and red-ends of the spectrum.

Drosophila LMCs receive input directly from R1-R6 and, accordingly, show similar dual-peaked sensitivity curves. (**Figure 4-1D**) However, their spectral sensitivity curves are much flatter than those of R1-R6s; presumably owing to nonlinear synaptic transmission (Juusola *et al.*, 1996).

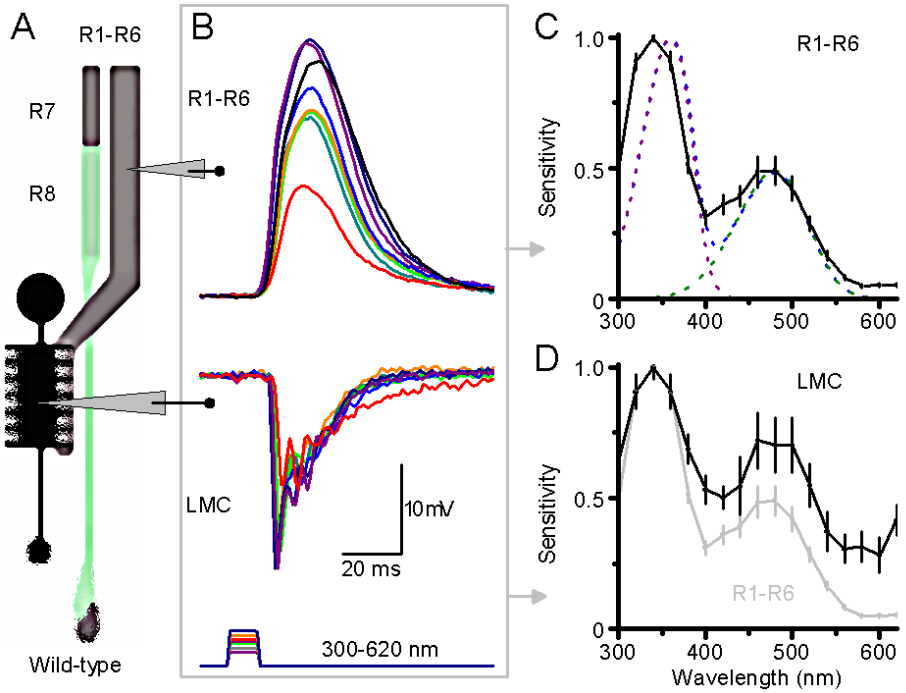

Figure 4-1: Voltage responses of R1-R6 Photoreceptors and LMC to monochromatic (narrow-band) impulses. (**A**) A greatly simplified wiring diagram of the first visual synapse, with R7 and R8 photoreceptors by passing it. R1-R6 photoreceptors transmit their signals to postsynaptic LMCs (L1-L3); electrodes indicate possible recording sites. (**B**) Responses of R1–R6s and LMCs to light impulse (10ms) of different wavelengths. (**C**) Normalized peak responses of R1–R6 photoreceptors to different wavelengths; purple and green dotted lines show the predicted spectra of the sensitizing pigment and Rh1, black dotted line is their sum. (**D**) Normalized time-to-peak of the corresponding responses in LMCs; R1-R6s' spectral sensitivity shown in grey. (R1–R6 photoreceptors, n = 14; LMCs, n = 15). Mean ± SEM shown.

Although I recorded from more than 40 LMCs, I included the data from only the best 15 cells, which satisfied the criteria set in the Method for the final analysis. Given the larger size of L1 and L2 in comparison to the other lamina cells, most recordings can be expected to be from them; rather than from the much smaller histaminergic processes of amacrine cells (Shaw, 1984b; Zheng *et al.*, 2006a; Zheng *et al.*, 2009). However, since all the recordings showed similar dynamics, no further attempt was made to identify them.

4.3.2 Spectral sensitivity of R1-R6 photoreceptors under light-adaptation

I also tested the spectral sensitivities of R1-R6 photoreceptors under light adaptation. To minimise rhodopsin/metarhodopsin ratio affecting these results, the cells were adapted prior the experiments with steady 590 nm light, which efficiently converts metarhodopsin back to rhodopsin (Hardie, 1979a). This procedure was expected to generate high rhodopsin/metarhodopsin ratios in both dark- and light-adaptation conditions, ensuring their fair comparisons.

My data revealed a slight shift in the long wavelengths (440-540 nm) peak sensitivities towards the UV-end during light-adaptation (**Figure 4-2**). This selective reduction in the green range, while the region below 420 nm remained unchanged, coincides with the 'blue-shift' reported in larger dipteran flies (Hardie, 1979a; Vogt *et al.*, 1982). Its cause is believed to be the intracellular pupil mechanism, whereupon migration of screening pigment granules, inside photoreceptors, changes the spectral content of the light input, and thus shifts its spectral sensitivity (Roebroek & Stavenga, 1990).

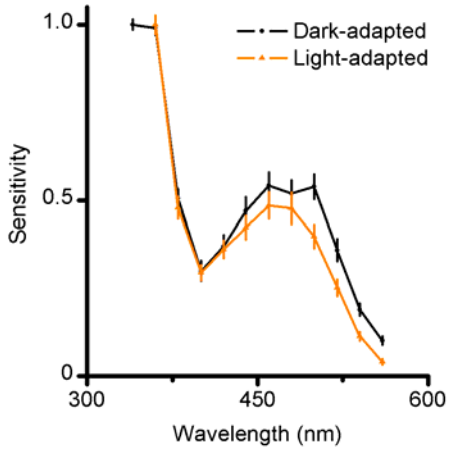

Figure 4-2: Spectral sensitivity of R1-R6 photoreceptors under light-adaptation. Only 320-560nm range is shown here; 590 nm was used to adapt the cells. (n = 7 photoreceptors) Mean ± SEM shown.

4.3.3 Spectral sensitivity of R1-R6 in mutant flies without R7 and R8

It has been shown that R6 and R1 photoreceptors form gap-junctions with R7 and R8 photoreceptors in larger dipteran flies (Shaw, 1984; Shaw et al., 1989). To investigate whether R1-R6 photoreceptors receive additional inputs from R7 or R8 photoreceptors, I examined the spectral sensitivity of R1-R6s in a mutant fly strain, which had normal WT eye pigmentation but light-insensitive R7 and R8 photoreceptors. To generate these flies, I used the *norpA* mutation as the host strain, in which the *norpA*-encoded phospholipase-C, a necessary component for signal transduction in all photoreceptor cells, was abolished genetically (Bloomquist *et al.*, 1988). Then, this activity was restored only in R1–R6 cells by expressing the *norpA* cDNA under the control of the *ninaE* (Rh1) promoter (Pearn *et al.*, 1996), leaving the R7 and R8 light-insensitive. R1-R6 photoreceptors and LMCs in this strain were examined under dark-adaption. I found that their mean spectral sensitivity was practically indistinguishable from that of wild-type flies (**Figure 4-3**).

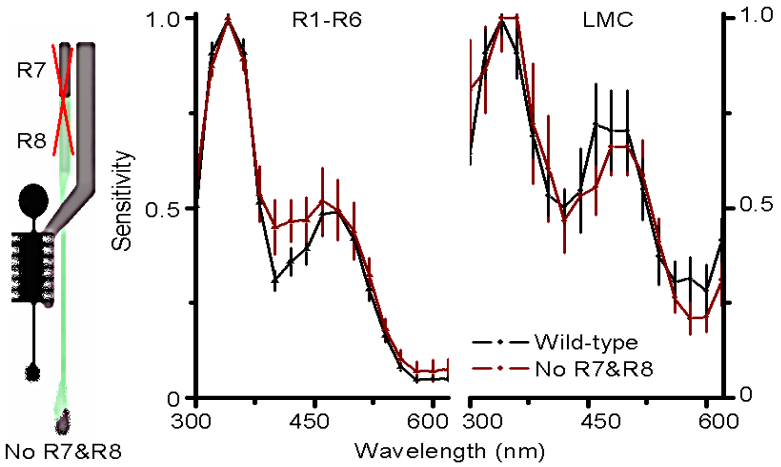

Figure 4-3: Spectral sensitivity of R1-R6 photoreceptors and LMCs in mutant flies flies (dark red traces) with light-insensitive R7 and R8 photoreceptors, compared to the corresponding WT data (black traces). Spectral sensitivity of R1–R6 photoreceptors is normalized by their maximum voltage responses, while that of LMCs is normalized by the minimum time-to-peak of the responses to different wavelengths. (Mutant: R1–R6 photoreceptors, n = 8; LMCs, n = 8).

4.4 Discussion

This study was aimed at characterising the spectral sensitivity of *Drosophila* early motion and colour channels, but owing to the small size of R7 and R8 photoreceptors, no stable recordings were achieved from them. I have described the spectral sensitivity of *Drosophila* R1-R6 photoreceptors and large monopolar cells (LMCs) in both wild-type flies and in a transgenetic fly strain, which has light-insensitive R7 and R8 photoreceptors. To my knowledge, this is the first study to report such intracellular characterisations *in vivo*.

4.4.1 Spectral sensitivity for wild-type *Drosophila* R1-R6 photoreceptors

Many studies have reported the dual-peaked spectral sensitivity of R1-R6 photoreceptors in large dipteran flies (Kirschfeld & Franceschini, 1977; Hardie, 1979a; Vogt *et al.*, 1982). The absorption spectrum of blowfly Rh1 visual pigment consists of two components; a band with a peak at 490 nm, due to the spectral absorption properties of the rhodopsin proper, and an additional UV-band, due to the energy transfer from the sensitizing pigment, which is sometimes also called the antenna pigment. Here, my recordings demonstrated highly similar spectral properties in *Drosophila* R1-R6 photoreceptors. Conversly, my *in vivo* recordings show these peaks with broader half-widths (**Figure 4-1C**) and longer tails.

4.4.2 Spectral sensitivity for *Drosophila* large monopolar cells (LMCs) in wild-type

The spectral sensitivity of fly monopolar neurons has not been studied as extensively before. It has been generally assumed that LMCs would share the same dual-peaked spectral sensitivity of their presynaptic inputs, R1-R6 photoreceptors. One study has reported that the spectral sensitivities of LMCs in *Calliphora* come in two groups: one with dual-peaked sensitivity maxima, at 353 and 486 nm, the other with a clear UV-sensitivity peak at 353 nm; both of these groups contained L1 and L2 cells (Moring, 1978). However, no such subtypes of spectral sensitivities were found in this study.

In my recordings, all LMCs showed dual-peaked spectral sensitivity, with much flattened distribution. This 'whitening' effect is likely to be caused by the nonlinear synaptic signal transfer (Juusola *et al.*, 1995b), which works towards providing each monochromatic band an equal likelihood to be transmitted. This coding procedure may maximise the rate of information transfer of environmental reflectances.

4.4.3 *Drosophila* pupil effect

Visual systems of animals have evolved sophisticated light-adaptation mechanisms to cope with vastly varying environmental light patterns, ranging over 10 log intensity units. Pupil-mechanism in fly photoreceptors is one of these adaptation mechanisms. Under bright illumination, the screening pigment granules, which are scattered inside photoreceptors migrate to face their rhabdomere (Kirschfe.K & Francesc.N, 1969). The pigment granules attenuate light propagation along the rhabdomeres, changing their waveguide properties. Thus, the pigment migrations provides a similar functional role as the mammalian pupil (Minke & Katz, 2009). Activation of pupil helps to prevent saturation, expanding the intensity range in which photoreceptors can operate (Howard *et al.*, 1987). Simultaneously, the intracellular pupil both narrows a photoreceptor's angular sensitivity function (Stavenga, 2004), and causes a 'blue shift' in the spectral sensitivity function (Hardie, 1979a; Vogt *et al.*, 1982).

As predicted, I discovered the 'blue-shift' in the spectral sensitivity of *Drosophila* R1-R6 photoreceptors under light adaptation. Given the small size of its eye and fewer transduction units, the impact of saturation on vision and visual behaviour may be more severe in *Drosophila* than in larger dipteran flies (Jonson *et al.*, 1998). This intracellular characterisation complements the previous study on *Drosophila* pupil mechanism (Hardie, 1979a; Vogt *et al.*, 1982).

4.4.4 Interaction of motion and colour channels in Drosophila retina

Linking colour to object motion neutrally may improve perceptual discrimination of moving coloured objects, but little is known if and how colour and motion pathways interact in the early visual system. In large dipteran flies, R1 and R6 make gap-junctions with R7 and R8, which can at the level of the lamina circuits influence the spectral sensitivity of transmitted signals (Shaw, 1984b; Shaw *et al.*, 1989c). In the present study, my recordings showed that in transgenetic flies with light-insensitive R7 and R8, R1-R6 photoreceptors and LMCs on average have WT-like spectral sensitivities. This result suggests that R7 and R8 does not influence R1-R6-LMC pathway significantly. However, this data is only suggestive, because:

1) In this study, the method for comparing the spectral sensitivity might not be sufficiently sensitive for detecting crosstalk between the two pathways. This is because the spectral sensitivity was calculated by normalizing the maximum response (here, response to 360 nm). This arbitrary normalization disregards the possibility that the same cell could also receive inputs from R7 and R8 at the same time. Ideally, responses at particular wavelength should be used for fair comparison. However, the variance among individual cells is quite large (the error bar in **Figure 4-3**). As there is no clear threshold for separating the contributions of different cells and the sample size of photoreceptors is relatively small, thus, any network contribution is easily diluted by the population mean.

2) In addition, probably not every photoreceptor or LMC receive input from R7/R8. In the simple circuit model, R7 and R8 photoreceptors feed information to R1-R6 terminals through gap-junctions (Shaw, 1984b; Shaw *et al.*, 1989c), while R1-R6 are also coupled by gap junction (Ribi, 1978). In fact, only R6 is expected to consistently make gap-junctions with R8y, which have an extended long-wavelength range; thus, only ~12% of R1-R6 photoreceptors are thought to do so. If so, the extra input might not be easily distinguished from the variance of individual recordings.

3) Furthermore, the interactions between photoreceptors might be communicated by small voltage responses via their gap-junctions close to their terminals. Since intracellular recordings were performed at the level of photoreceptor and LMC somata, as such, these signals could be easily missed. In the next chapter, to overcome these problems I used transgenically produced UV-sensitive flies, which enabled the activation of one pathway without activating the other. Therefore, even very small crosstalk between the channels could be now seen in the recordings.

5 Colour pathway improves motion discrimination through functional contacts in the early visual system of *Drosophila*

5.1 Introduction

In the previous chapter, I intended to identify possible signal transfer between colour (R7, R8) and motion channels (R1-R6-LMC) by using mutant flies with normal R1-R6 photoreceptors, but light-insensitive R7 and R8. However, no significant spectral sensitivity differences were detected in their R1-R6 photoreceptors and LMCs. It was recognised that such interactions are hard to investigate because the spectral sensitivities of the colour and motion channels overlap, thereby weaker parallel inputs could easily be masked by the cells' direct responses. In this chapter, to overcome this problem, I used variants of UV-sensitive flies (**Figure S6**), which enabled activation of one pathway without activating the other.

In these UV-flies, which were generated in the Juusola laboratory by Dr. Trevor Wardill and Dr. Olivier List, the blue-green opsin of R1-R6 photoreceptors (Rh1) was removed and genetically substituted with the ultraviolet opsin (Rh3), eliminating the dominant spectral sensitivity overlap between the motion and R8-colour channels. Thus, R8s could now be independently excited by long-wavelength light (≥460 nm), while R1-R6s should only respond to short-wavelength light (<460 nm). Whole cell patch-clamp recordings of dissociated R1-R6 photoreceptors indicated that, besides the expected UV-sensitivity of Rh3-opsin (**Figure S6B**), their phototransduction dynamics (**Figure S6B**) approximated those of the wild-type photoreceptors (Hardie & Postma, 2008). Furthermore, the normal-like retina ultrastructure (**Figure S6E**), *in vivo* response dynamics (**Figure S6C, D, Figure S7**), and electroretinograms (**Figure S6F**) indicated undistorted signal transmission from R1-R6 to LMCs, suggesting that the underlying circuit computations would be genuine. Therefore, by using green-amber stimulation, which is invisible to the UV-sensitive R1-R6 but visible to R8 photoreceptors, we could examine whether the early motion and colour channels crosstalk between each other.

Here, I tested the spectral sensitivity and visual information processing of R1-R6 photoreceptors and LMCs in different UV-flies. In UV-flies with normal R7 and R8, I discovered an

extra long-wavelength (440-620nm) spectral sensitivity peak in R1-R6 and LMC output that matches the spectral sensitivity of R8 photoreceptors. Previous physiological and morphological studies in photoreceptors of large dipteran flies (Shaw, 1984a; b; Shaw *et al.*, 1989c) indicated that this input arrives most likely via gap junctions between R8 and R6 photoreceptors. Intracellular recordings from R1-R6 photoreceptors and LMCs of *ninaE*-mutant, having light-insensitive R1-R6s but light-sensitive R7s and R8s, supported the conclusion that the motion pathway received inputs from the colour pathway in the early visual system of *Drosophila*. This input refined and extended the chromatic range of motion vision as verified by the flies' optomotor behaviour. Together with the results from the behavioural and optical imaging experiments in our laboratory, these results clarify how the retinal wiring and its circuit computations improve visual perception and the robustness of behaviour.

5.2 Methods

5.2.1 *In vivo* Electrophysiology and Monochromatic Stimulation

Details are given in Chapter 3

5.2.2 Drosophila Genetics

5.2.2.1 Fly stocks

The fly stocks in this chapter were generated by Drs. Trevor Wardill and Olivier List. Original *Drosophila* mutants and transgenic stocks were obtained from the following sources; *ninaE*^{r8} with ebony^{sooty} stocks from Bloomington Stock Centre; *norpA*^{36} (aka. *norpA*^{P24}), and *ort*^{5} from Roger Hardie (*ort*^{5} was then recombined with wild type Canton-S to remove the *scarlet* marker); Rhodopsin3 (UV sensitive) rescue constructs, labeled as *"[Rh1+3]"* in this paper, were a gift from Charles Zuker (Columbia University). P-element inserts of *[Rh1+3]* on different chromosomes were tested, and all contained a Rhodopsin1 promotor that drove the expression of Rh3 in photoreceptors R1-R6 exclusively (Feiler *et al.*, 1992). A P-element rescue for the *norpA* mutants, labeled as "[Rh1+*norpA*]" in this paper, was a gift from Steve Britt (University of Colorado). The [Rh1+*norpA*] rescue used the Rhodopsin1 promotor that drove the expression of *norpA*-cDNA in photoreceptors R1-R6 exclusively (Salcedo *et al.*, 1999).

5.2.2.2 Optimization of genotype

Optimization of genotype was performed by Drs. Trevor Wardill and Olivier List. Many genetic manipulations have unwanted side effects that can potentially invalidate results

(Gonzalez-Bellido *et al.*, 2009). To minimize these unwanted effects, we attempted to find a rhodopsin1 mutant that was completely non-functional for phototransduction, rather than being a traditional null allele that prevented protein production. It was important that rhodopsin1 was expressed, but non-functional for phototransduction, because *ninaE* is required for the structural formation of rhabdomeres (Kumar & Ready, 1995; Ahmad *et al.*, 2007). To confirm whether phototransduction and neurotransmission machinery operated similar to wild type, we rescued various *ninaE* mutants with a *[Rh1+3]* P-element (Feiler *et al.*, 1992) and used electroretinograms (ERGs) to validate the response properties of *ninaE* and *[Rh1+3]* rescued *ninaE* mutants. To ultimately confirm the response properties, we recorded intracellularly and also patched dissociated photoreceptors in controlled conditions to determine their spectral sensitivity; these patch-clamp recordings were performed by Prof. Roger Hardie, University of Cambridge. Furthermore we checked the structural formation of the rhabdomeres using transmission electron microscopy.

To generate *Drosophila* with effectively non-functional but intact R7/R8 photoreceptors, we combined the $norpA^{36}$ mutant, with a P-element *[Rh1+norpA-cDNA]* rescue. The $norpA^{36}$ mutant is a strong hypomorph, requiring immense light to activate phototransduction (Hardie *et al.*, 2003), which equates to lighting conditions well above normal experimental conditions used in this paper. Furthermore, $norpA^{36}$ has been shown to have intact R7 photoreceptors, 6 weeks post-eclosion (Pearn *et al.*, 1996) and shown here. These lines were also used to generate UV-flies with non-functional, but intact R7/R8 photoreceptors.

To ensure that background genetic affects were minimized, we replaced all chromosomes without P-element insertions, with chromosomes from a single wildtype Canton-S stock. To do this most efficiently, we created a temporary triple balancer stock; FM6/FM7; If/CyO; MKRS/TM6b. This stock produced very few offspring and so to obtain sufficient offspring, we intercrossed two stocks (FM6/FM7; If/CyO; + [CantonS]/TM6b and FM6/FM7; If/CyO; + [CantonS]/MKRS).

5.2.2.3 Data analysis

See details in Chapter 2

5.3 Result

5.3.1 Spectral sensitivity of R1-R6 photoreceptors and LMCs in UV-flies

First, I tested the spectral sensitivities of R1-R6 photoreceptors and LMCs in UV-flies using intracellular recordings. Interestingly, apart from their predicted UV-blue sensitivity (**Figure 5-1B**), the recordings also show relatively small, brief and slightly delayed responses to longer wavelength impulses (**Figure 5-1C**). Thus, the spectral sensitivity of many R1-R6s (12/36 of somatic recordings) and every tested LMC were selectively boosted at 460-600 nm range.

Further analysis revealed three types of intracellular responses from R1-R6 photoreceptors, which were appropriately reflected by the opposing LMC outputs. R1-R6s of the first type (**Figure 5-1, i**) contained Rh3-opsin induced short-wavelength (300-420 nm) sensitivity peak with a secondary long-wavelength (420-620 nm) peak/bulge (**Figure 5-1D**), which matched the spectral sensitivity of Rh6-opsin (R8y-photoreceptors) (**Figure 5-1D**). R1-R6 of the second type also had the extra Rh6-like sensitivity peak, but interestingly these cells responded to the long-wavelength (420-620 nm) stimuli with hyperpolarizations, while some LMCs depolarised correspondingly (**Figure 5-1C, ii**). R1-R6s of the third type shared the same short-wavelength (300-420 nm) sensitivity peak (**Figure 5-1, iii**), but had a long-wavelength (420-620 nm) peak/bulge, which matched the spectral sensitivity of Rh5-opsin (R8p-photoreceptors) (**Figure 5-1D**).

All together, ~30% of R1-R6 photoreceptors (12/36) and all LMCs (28/28) responded clearly to longer wavelength impulses, either by brief depolarizations (7% LMCs) (**Figure 5-1**C) or hyperpolarizations (93% LMCs). Variable sensitivity and resistance changes in R1-R6 photoreceptors of UV-flies confirmed that these signals were neither recording artefacts nor field potentials (data not showed here). These findings, along with their relatively small and slightly delayed response dynamic, implied an extra R7s/R8s input at R1-R6 photoreceptor terminals, which back-propagated toward photoreceptor soma and transmitted to every LMC.

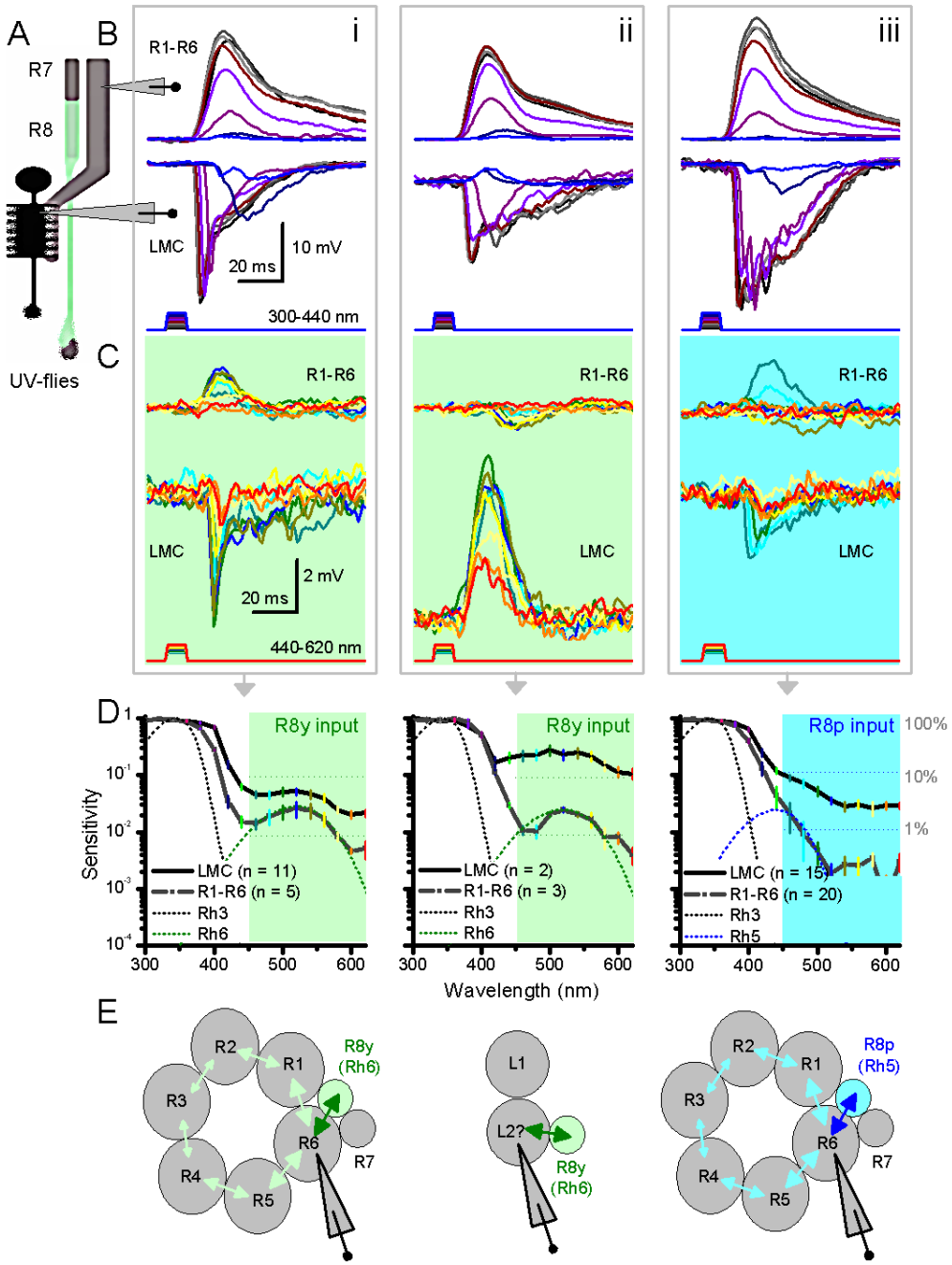

Figure 5-1: Spectral sensitivity of R1-R6 photoreceptors and large monopolar cells (LMCs) in UV-flies. (**A**) A greatly simplified wiring diagram of the first visual synapse, with R7 and R8 photoreceptors by passing it. Electrodes indicate possible recording sites. (**B**) Three types of intracellular responses from R1-R6 and LMCs to sub-saturating short-wavelength (300-420 nm) pulses (10ms) of equal energy and (**C**) to long-wavelength (420-620 nm). (**D**) Spectral sensitivities of corresponding R1-R6 and LMC outputs show a 2nd peak/bulge, which matches the sensitivity of Rh6-opsin (R8y-photoreceptors) (**i**, **ii**) or Rh5-opsin (R8p-photoreceptors) (**iii**), in colour pathway. Black, green and blue dotted lines show, respectively, the predicted spectra of the sensitizing pigment Rh3 Rh6 and Rh5. Mean ± SEM shown. (**E**). Results suggest a model (Shaw, 1984b), in which information spreads via gap-junctions from R8 axon to R6 axon, and further to other photoreceptors in the same cartridge, before transmission to LMCs. Depolarizing responses (420-620 nm) in some LMCs suggest gap-junctions between L2 and R8 axons.

These results were in concordance with the results from the previous micro-stimulation experiments and electron microscopy in larger dipteran flies **(Figure S8)**, which showed efficient R7/R8 input to R6 photoreceptors and gap-junctions between their axons (Shaw, 1984b; Shaw *et al.*, 1989a). All these results support a wiring model (**Figure 5-1E**), in which gap-junctions between R6 or R1 and R8y or R8p photorceptors, producing two groups of R1-R6 cells with unique spectral sensitivities (**Figure S8**). Only some of the recorded R1-R6 (12/36) showed clearly these extra R8 inputs, possible owing to signal gradation from R6s to R1-R5s through gap junctions. Since every R1-R6 forms synapses with every L1-L3 (Meinertzhagen & O'Neil, 1991a), LMCs in different cartridges (input from R8y or R8p) should come with the corresponding two flavours. Furthermore, these synapses should mostly amplify changes in inputs (Zheng *et al.*, 2006b; Zheng *et al.*, 2009). Accordingly, all recorded LMCs of UV-flies responded to green-yellow stimuli, having higher sensitivities than those recorded from R1-R6s (**Figure 5-1D**). LMCs' sensitivity to long wavelengths (460-620 nm) was ~10-times less (9.5% $\pm$ 7.0, SD; n = 28; range: 2.8-34.4%) than that to UV-light (100%; 300-440 nm), consistent with the model that they receive green-yellow inputs mainly from one R6, instead of the normal R1-R6.

5.3.2 Spectral sensitivity of R1-R6 photoreceptors and LMCs in UV-flies with light-insensitive R7s and R8s

To further verify the model, we produced UV-flies, which had structurally intact but light-insensitive R7/R8 photoreceptors by selectively expressing Rh3-opsins in R1-R6 photoreceptors of blind norpA *(no-receptor potential A)* flies. The *norpA gene encodes* the phospholipase C protein, which in null mutant leads to a complete block of phototransduction cascade in all photoreceptors (Hardie & Minke, 1995). Here, only R1-R6 photoreceptors were rescued with Rh3-opsin expression instead of Rh1-opsin, leaving R7 and R8 photo-insensitive. Because this manipulation prevented dynamic interactions between the early colour and motion channels, I could compare the spectral sensitivities of their R1-R6 and LMCs to those of UV-flies with light-sensitive R7s and R8s.

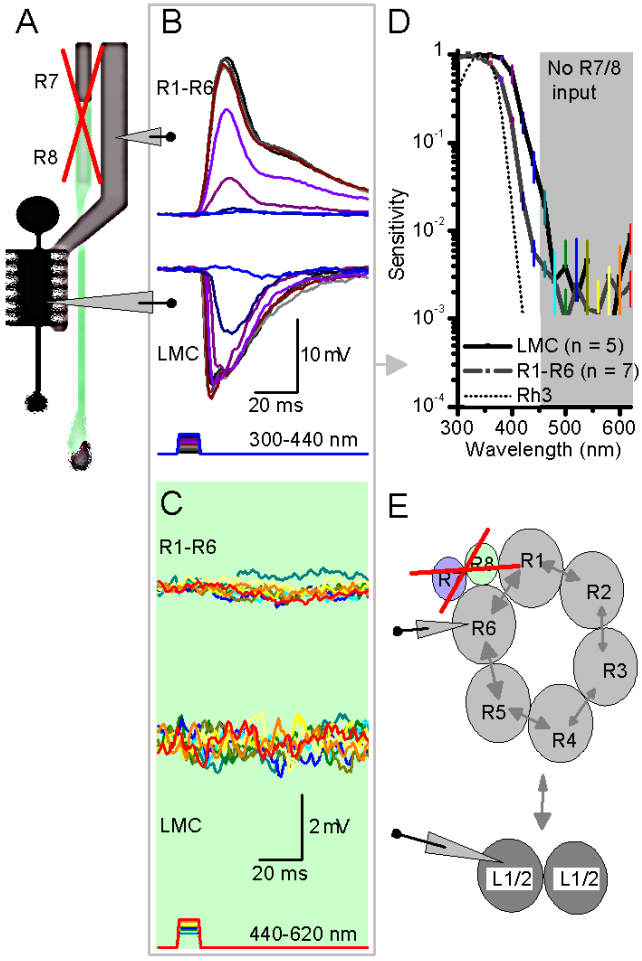

Figure 5-2: Spectral sensitivity of R1-R6 photoreceptors and large monopolar cells (LMCs) in UV-flies with light-insensitive R7s and R8s. (**A**) A greatly simplified wiring diagram of the first visual synapse, with R7 and R8 photoreceptors by-passing it. (**B**) Responses of R1–R6s and LMCs to short wavelengths (300-440nm) impulses. (**C**) R1–R6s and LMCs failed to respond to long wavelength impulses (440-620nm). (**D**) Spectral sensitivities of the corresponding R1-R6 and LMC outputs follow Rh3 sensitivity peak. (**E**) Schematic highlighting the missing gap-junctional inputs from light-insensitive R7s and R8s to R1-R6 photoreceptors (R1–R6 photoreceptors, n = 7; LMCs, n = 5). Mean ± SEM shown.

As expected, I found that without R7/R8 inputs, R1-R6s and LMCs from UV flies could respond only to 300-440 nm stimuli (**Figure 5-2BC**), closely following the spectral sensitivity of the Rh3-opsin pigment absorbance (**Figure 5-2D**). In addition, R1-R6 photoreceptors' spectral sensitivity, but not that of LMCs', was significantly narrower in the UV range (300-340 nm) than the spectral sensitivity of R1-R6s in the UV-flies with light-sensitive R7s and R8s; although their electrical properties were unchanged (**Figure S4**). Furthermore, when R7/R8 cells were not participating in the circuit, the responses of R1-R6s typically appeared briefer (the response half-widths in **Figure 5-1B** and **Figure 5-2B**), even to UV-stimuli invisible to R8 photoreceptors (300-340 nm). Thus, these observations suggested that, as well as R8 input,

the UV-sensitive R7y/R7p photoreceptors might further refine processing in the motion pathway.

5.3.3 Signalling performance of R1-R6 photoreceptors and LMC in UV-flies with/without R7/R8s

To further quantify how the colour pathway refines motion processing, I compared impulse responses of R1-R6s and LMCs when R7/R8 cells were light-sensitive to those when they were light-insensitive. Here, a saturating UV-impulse (340 ± 20 nm), which maximally excites R1-R6s and R7s but less so R8 photoreceptors, ensured that the sensitivity differences between the two UV-fly phenotypes would not bias the results. The means of their normalized responses are shown in Figure 3A. Both R1-R6 and LMC outputs clearly lacked some components when R7/R8 cells were light-insensitive. Interestingly, these missing components (thick lines) shared similar features of the respective cell types to green-yellow impulses (**Figure 5-1C**), but their waveforms were less pronounced, hinting a weaker dynamic connectivity.

Nevertheless, the briefer responses of R1-R6s (**Figure 5-3A**; half-width: $P = 0.012$, one-way ANOVA) and LMCs (**Figure 5-3A**; hyperpolarization: $P = 0.021$) probably reflected the absent R7/R8 inputs in their processing. These results are in accordance with the spectral sensitivity recordings, where the R1-R6s', but not LMCs', had significantly narrower UV ranges (300-340 nm). Together, these findings suggested that both R7 and R8 inputs would exert effects on R1-R6 outputs; but less so on LMC outputs, probably resulting from the non-linear synaptic transmission (Juusola *et al.*, 1995b).

Previous investigations have showed extra inputs to R1-R6s from the network feedbacks, which play an important role in shaping the temporal structure of the transmitted signals (Zheng *et al.*, 2006b; Zheng *et al.*, 2009). Motivated by the possibility that colour pathway input could also influence motion pathway coding, I next quantified the role of R7/R8 inputs in refining the signalling performance of R1-R6s (**Figure 5-3B**) to changing information. These cells were repeatedly stimulated with a naturalistic intensity pattern of UV-light (390 nm) in preparations where R7/R8s either functioned normally or were light-insensitive. I found that on average, input from R7 and R8 photoreceptors increased the signal-to-noise ratio (SNR) of a R1-R6 photoreceptor for low-frequency stimuli (<10 Hz) by ~100% (**Figure 5-3C**; $P < 0.05$, one-way ANOVA). This coding improvement translated to 10-20 bit/s of new information (**Figure 5-3C**, inset), increasing the rate of information transfer of an average

R1-R6 photoreceptor by ~5%. Together these findings imply that R7/R8 photoreceptors participate in refining the early neural output in the motion pathway.

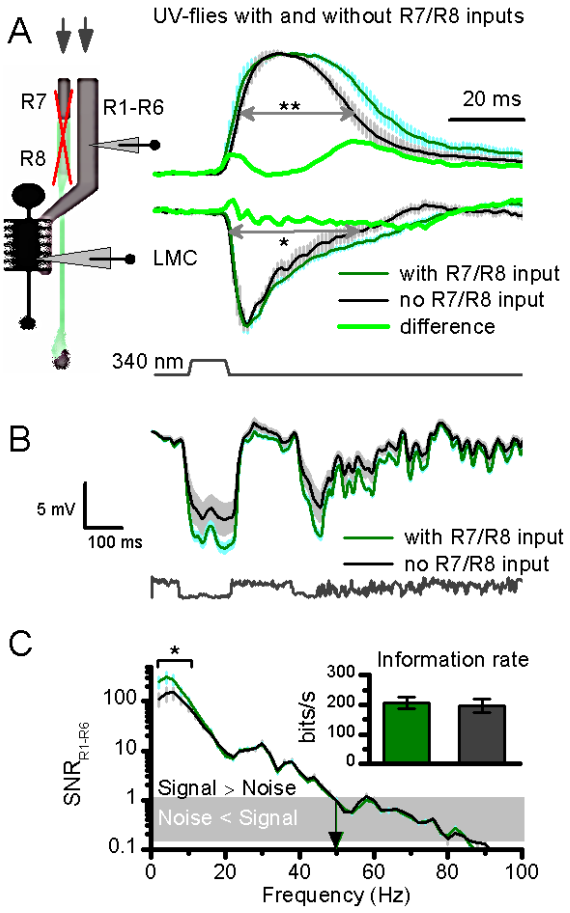

Figure 5-3: R7/R8 photoreceptors shape R1-R6 and LMC outputs. (**A**) Normalized R1-R6 and LMC outputs to a saturating UV-impulse in UV-flies with/without light-sensitive R7/R8s. Wider responses suggest extra R7 inputs (mean ± SEM; n = 6-19). Differences (green) share similar features of R1-R6 and LMC outputs to longer wavelength impulses, probably mediated by R8s (**Figure 1C**), implying that R7 inputs also shape motion pathway output. (**B**) R1-R6 outputs to naturalistic UV-intensity series, NS, with/without normal R7/R8s (mean ± SD; n = 5). (**C**) Corresponding signal-to-noise ratios (SNRs) and information transfers (inset). Significance: * < 0.05; ** < 0.01, one-way ANOVA.

5.3.4 Output of *ninaE*^{8} R1-R6 terminals and LMCs follow R7/R8s' sensitivity

I then asked whether R7/R8 input alone is sufficient to drive LMC output. For these experiments, I used specific *ninaE*-mutants (*neither inactivation nor afterpotential E)*, in which R1-R6 photoreceptors were structurally intact (Kumar & Ready, 1995) but blinded by mutated Rh1-opsin (*ninaE*^{8}), whilst their R7/R8 photoreceptors functioned normally. Here, I only used *ninaE*^{8}-flies because many other *ninaE*-lines carry additional mutations (**See method**), including a faulty *ort* histamine-receptor in LMCs, which may blind them (Gengs *et al.*,

2002a). *In vitro* patch-clamp experiments (data from Prof. Roger Hardie) showed no macroscopic light responses in their R1-R6s (**Figure 5-4G**) but ample K^+ conductances (not shown here) and only moderately reduced capacitance, indicating proper plasma-membrane integrity, as further supported by their normal-like ultra-structure (Kumar & Ready, 1995). However *in vivo* (**Figure 5-4D**), photoreceptor terminals in *ninaE*^{8}-flies responded to a broad spectral range of light pulses with small biphasic polarizations, consistent with the model in which they receive information from R7/R8s (Shaw, 1984b; Shaw *et al.*, 1989a) and LMCs through functional contacts, as in UV-flies (**Figure 5-1C**). Importantly, the responses of the postsynaptic LMCs (**Figure 5-3B**) matched the spectral sensitivity of R7/R8 pairs (**Figure 5-3C**) (Hardie, 1979b; Britt *et al.*, 1993; Chou *et al.*, 1996). We conclude that R7 and R8 inputs alone in *ninaE*^{8}- and UV-flies can drive the synaptic output of R1-R6 terminals (**Figure 5-3B**), passing enough information to activate the colour-independent on- and off-channels (L1 and L2 monopolar cells, respectively (Joesch *et al.*, 2010)), as the allied inputs for motion detection. To further differentiate (and delay) responses in the colour-independent off-channel (Joesch *et al.*, 2010), R7/R8 axons may form depolarizing contacts with L2 cells closer to/in the medulla; either through gap-junctions or synapses, as suggested by **Figure 5-1C** (middle).

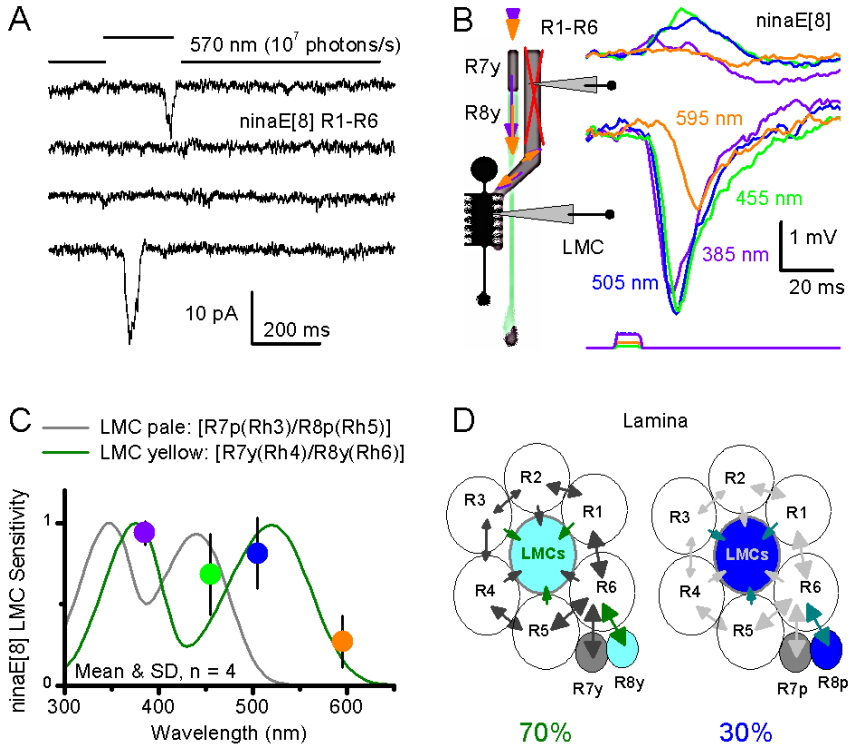

Figure 5-4: ninaE8 R1-R6 terminals and LMCs follow R7/R8s' spectral sensitivity. (**A**) Mutant ninaE8 R1-R6s are profoundly light-insensitive. In patch-clamp data (from Prof. Roger Hardie), dissociated R1-R6s lack macroscopic light-induced current; intense green-yellow light rarely evokes single-photon responses (two shown). (**B**) In vivo, ninaE8 R1-R6 terminals and LMCs follow R7/R8s' sensitivity, here R7y/R8y. Response dynamic again share similar features of R1-R6 and LMC outputs to longer wavelength impulses (**Figure 5-1B, C**). (**C**) Four ninaE8 LMCs had spectral sensitivity of R7y/R8y-pairs. (**D**) The proposed model: input to each lamina-cartridge come from a R7 or R8, or from R7y/R8y- or R7p/R8p-pairs through gap-junctions to R6 axons to drive synaptic output to LMCs.

5.4 Discussion

Here, I have shown conclusive evidence that in the early visual system of *Drosophila* R7 and R8 photoreceptors feed information to motion pathway through functional contacts . These findings refute the long-standing belief that in the dipteran visual systems colour and motion pathways function independently (Yamaguchi *et al.*, 2008; Zhu *et al.*, 2009).

5.4.1 New wiring model explains early interactions between the colour and motion pathways in *Drosophila*

Together with previous micro-stimulation experiments and electron microscopy in larger dipteran flies, my findings support a wiring model in which one photoreceptor (R6 or neighbouring R1) receives information either from one R8y or R8p cell (**Figure S8**). Efficient R7/R8 input then feeds into R6 photoreceptors and further spreads to R1-R5 through gap-

junctions between their axons (Shaw, 1984b; Shaw *et al.*, 1989a). Gap-junctions between R1-R6 terminals (Shaw, 1984b; van Hateren, 1986) produced diminishing green-yellow sensitivity in the somatic recordings from the photoreceptors, which presumably were the furthest away from the R6 in the cartridge (**Figure S8**). Since every R1-R6 forms synapses with every L1-L3 (Meinertzhagen & O'Neil, 1991a) and these synapses can amplify small signals (Zheng *et al.*, 2006b; Zheng *et al.*, 2009), all LMCs in the same cartridge receive extra input from the colour pathway with higher sensitivities than those recorded from R1-R6s (**Figure 5-1D**). Furthermore, in type 3 pairs, R1-R6 and LMC showed reversed polarities, implying that the lamina connectivity is more complex than previously proposed models. The speed and size of LMCs depolarisations to green-yellow stimuli (**Figure 5-1C** and **E**, middle-panels) implied that the R8 axon may form gap-junctions with one LMC, and that such signals may feed back to selected R1-R6s, inhibiting their output.

Given the rich connectivity in the complex lamina and medulla wiring, it is also possible that our finding of R7/R8 input into R1-R6-LMC results from the feed-back propagation of R7/R8 signals, through the centrifugal cells C2 and C3 from the medulla (Meinertzhagen and Oneil, 1991b). This scenario might not be mutually exclusive to the gap junction model, as we observed different response dynamics from R1-R6 and LMCs to long wavelength stimulus. It might be possible to completely prove the gap-junction model by genetically 'sliencing' the gap junction proteins, or prove the feedback model by using *shibire*^{ts1} mutants to silence the feedback. However, both methods could be problematic, because previous study showed that mutation to gap junction genes, i.e. *innexin*s, *shakingB*, and *ogre,* leads to defective responses in LMCs of the lamina (Kathryn D. Curtin, 2002) and it has been reported that UAS-*shibire*^{ts1} over-expression in *Drosophila* photoreceptors might irreversibly distort neural function at previously reported permissive temperatures (Gonzalez-Bellido, P.T., 2009). Also, further modification of transgenic UV flies might result in even worse side-effects and thus it will not be able to provide a fair comparison. Thus, no further attempts have been made to discriminate/prove these two models.

5.4.2 R7 and R8 inputs help motion detection

L1 and L2 pathways have been considered as the on- and off-channels for the fly motion detection system (Rister *et al.*, 2007; Reiff *et al.*, 2010). My data showed that R7 and R8 inputs changed the coding properties of R1-R6s and LMC's output, which has direct impact on the temporal characteristics of the on-and-off signalling for motion detection. To provide the best confidence in my results, colleagues in our laboratory performed experiments on

many different *Drosophila* strains with genetic backgrounds more similar to wild-type, using other direct methods from calcium imaging and quantitative behavioural tests (paper submitted) which show that this information is sufficient for motion perception. All the evidence agrees with the simple circuit model in which R7 and R8 photoreceptors feed information to R1-R6 terminals through gap-junctions (Shaw, 1984b; Shaw *et al.*, 1989a), boosting the responses of LMCs in the motion pathway. Furthermore, some of our results suggest that the R7/R8s may also help to refine the light-off responses of the off-motion channel (L2) directly (**Figure 5-1E,** middle). Thus, we can safely conclude that functional contacts from the colour pathway extend the spectral range of the on- and off-channels, improving the fly's motion perception. Importantly, the visual behaviour of flies matches the predictions of the proposed scheme. In particular, we find that *Drosophila*, which have their R7/R8 photoreceptors inactivated, generate weakened optomotor responses to rotating optic flow, because their on- and off-channel outputs have less well-defined temporal structure (data not showed).

5.4.3 Possible reason for the random distribution of R7/R8 photoreceptor pairs in the fly retina

When observed from the new point of view that R7 and R8 photoreceptors contribute to motion detection, these results suggest a fresh answer to the old, open question: why are R7y/R8y and R7p/R8p pairs randomly distributed across the retina? Although a colour-blind movement detector can be optimal in many a sense (Srinivasan, 1985), it cannot perceive movement of two-colour patterns, when their intensities produce no contrast to the input channels (Kaiser, 1975). Furthermore, in the spatial domain, the receptive fields of on- and off-channels, of an optimal motion detector, should be maximally correlated, *i.e.* identical, for the two channels to filter the scene in the same way (Srinivasan, 1985). We have shown here that by deriving its inputs from combinations of different spectral receptors, whose overlapping receptive fields gather information from the same point in space, and by using different combinations of spectral receptors, in the on- and off-channels for the neighbouring points in space (Hardie, 1979b; Britt *et al.*, 1993; Chou *et al.*, 1996), motion detection circuits of *Drosophila* have evolved to overcome such shortcomings. Thus, these circuits provide simultaneous and robust encoding of multiple visual attributes from the ever-changing external world with limited wiring costs.

Nevertheless, results in this chapter are derived solely from transgenic flies. Due to time constraints, no direct evidence for this mechanism in wild-type *Drosophila* has been found

in this study. One possibility worth mentioning here, is that the gap-junctions themselves could be 'left-overs' from a previous developmental stage, given their vital roles in cell-cell communication and neuronal differentiation during development (Cecilia W. Lo, 1996). Temporary gap junctions have been found between adjacent neurons before synapse formation (Allen and Warner, 1991, Chang and Balice-Gordon, 2000). In this scenario, if the gap junctions are those remaining from the cohort present during development, they might not serve vital function in adult, wild-type flies. To further clarify the existence and potential benefits of this mechanism in wild-type flies, I propose the following experiments: 1) Further characterization of R1-R6 photoreceptors' spectral sensitivity and receptive fields with dye injection to identify their cell type. If our wiring model is correct, we should be able to see R8 inputs (higher sensitivity on amber-light range) most significantly in R6 cell recordings, in comparison to R1-R5. 2) Characterization of wild-type R1-R6 photoreceptor receptive fields with dye injection to identify their cell type. R7/R8 input into R1-R6 will lead to different receptive fields, which depend on their distance to input receptors (R1/R6). As proposed earlier, if occurring in wild-type flies, this organisation of photoreceptors could provide potential benefits for visual sampling and motion detection.

Supplement Figures

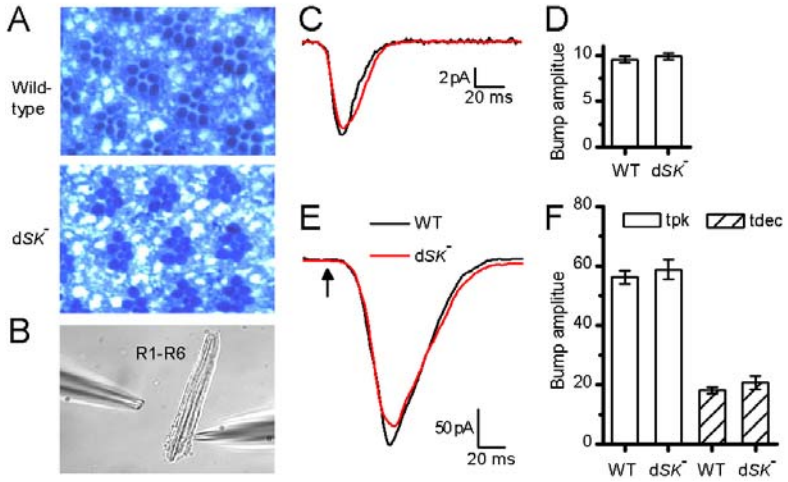

Figure S1: Normal photoreceptor morphology and phototransduction in *dSK*⁻ flies. (**A**) Retinal cross sections (1 µm) of WT and *dSK*⁻ flies show intact morphology. (**B**) Whole-cell recordings from dissociated photoreceptors. (**C**) WT and *dSK*⁻ quantum bumps (average of >30; aligned by rising phase) are indistinguishable. (**D**) Bump amplitude from C: n = 4-9 cells. (**E**) Macroscopic responses to brief flashes (5 ms; arrow) containing ~75 effective photons were similar in *dSK*⁻ and WT. (**F**) Macroscopic response (in **E**) kinetics; time-to-peak (tpk) and time to 50% decay (tdec) were similar in WT and dSK- . n = 8-11 cells.Mean ± SEM shown.

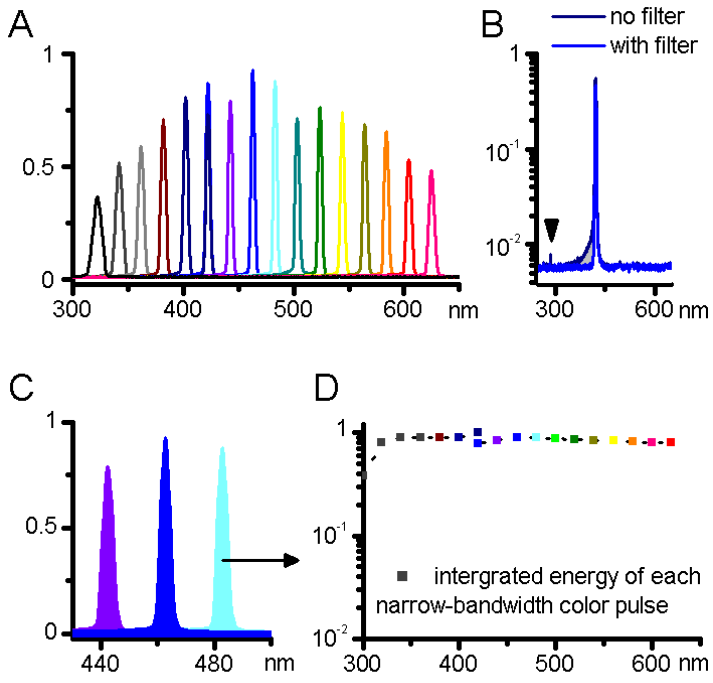

Figure S2: Monochromator calibration. (**A**) Monochromatic light generated by Cairn OptoScan monochromator, measured by Hamamatsu spectrometer. (**B**) Property of steep long-pass edge-filter (LP420 nm), eliminating the short wavelength "light leakage" (indicated by the arrow, and the difference is in grey shadow). (**C**) Individual narrow-bandwidth colour pulses. (**D**) The monochromator system's light output was measured and calibrated to ensure that the difference in individual energy integration was less than 5%.

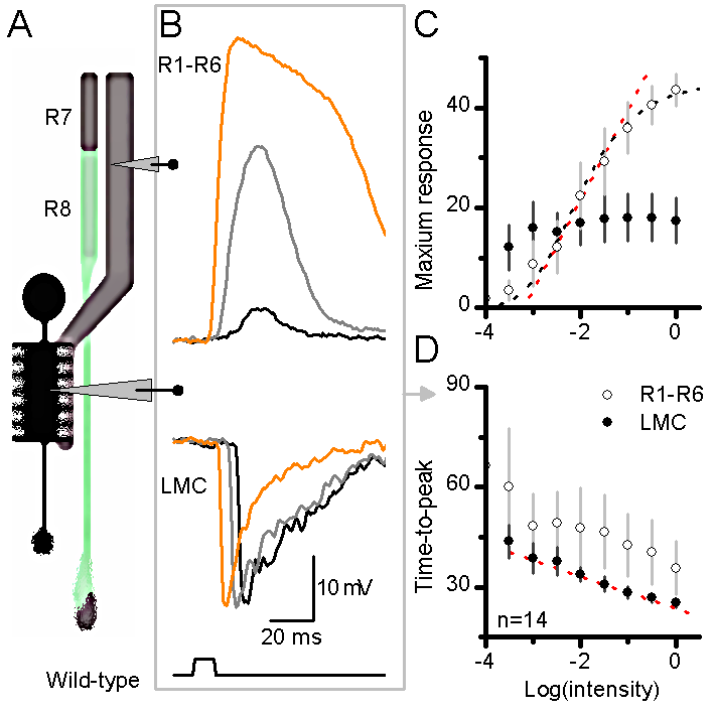

Figure S3: Volatge responses of R1-R6 photoreceptors and LMC to light impulses. (**A**) Greatly simplified wiring diagram of the first visual synapse, with R7 and R8 photoreceptors passing by it. Electrodes indicate hypothetical recording sites. (**B**) Responses of R1–R6 photoreceptors and LMCs to bright, mid and dim 10 ms pulse in the dark. (**C**) Maximum responses of cells. (**D**) Time-to-peak of the responses. (R1–R6 photoreceptors, n = 14; LMCs, n = 14). Mean ± SD shown.

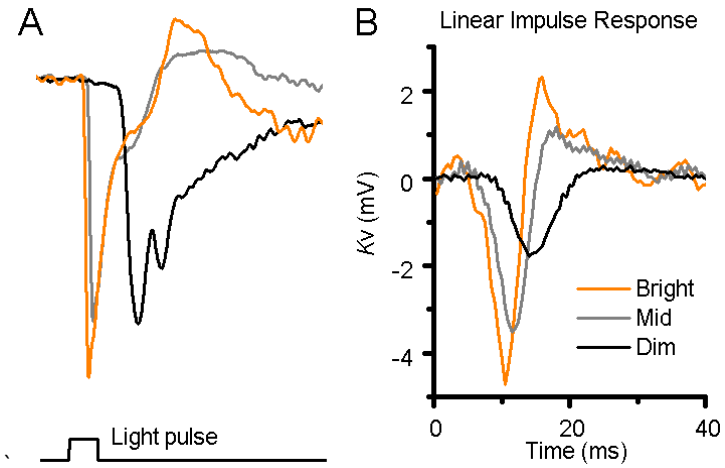

Figure S4: LMC filter properties under different intensity light stimulus. (**A**) LMC voltage response to 10 ms light pulses, showing clear bi-phase shape under bright light. (**B**) Linear impulse responses calculated from LMC response to white-noise contrast.

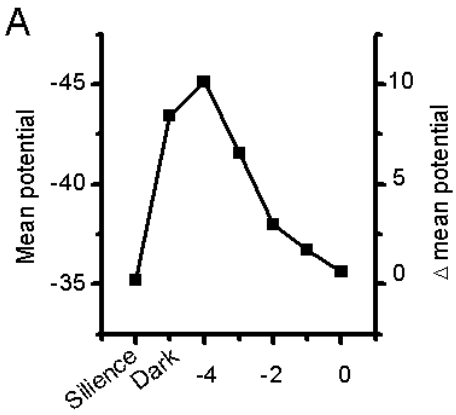

Figure S5: none-linearity of LMC hyperpolarisation. Mean potential of the same recorded LMC in the main paper. The level of hyperpolarisation (from silence period level) is on the right axis

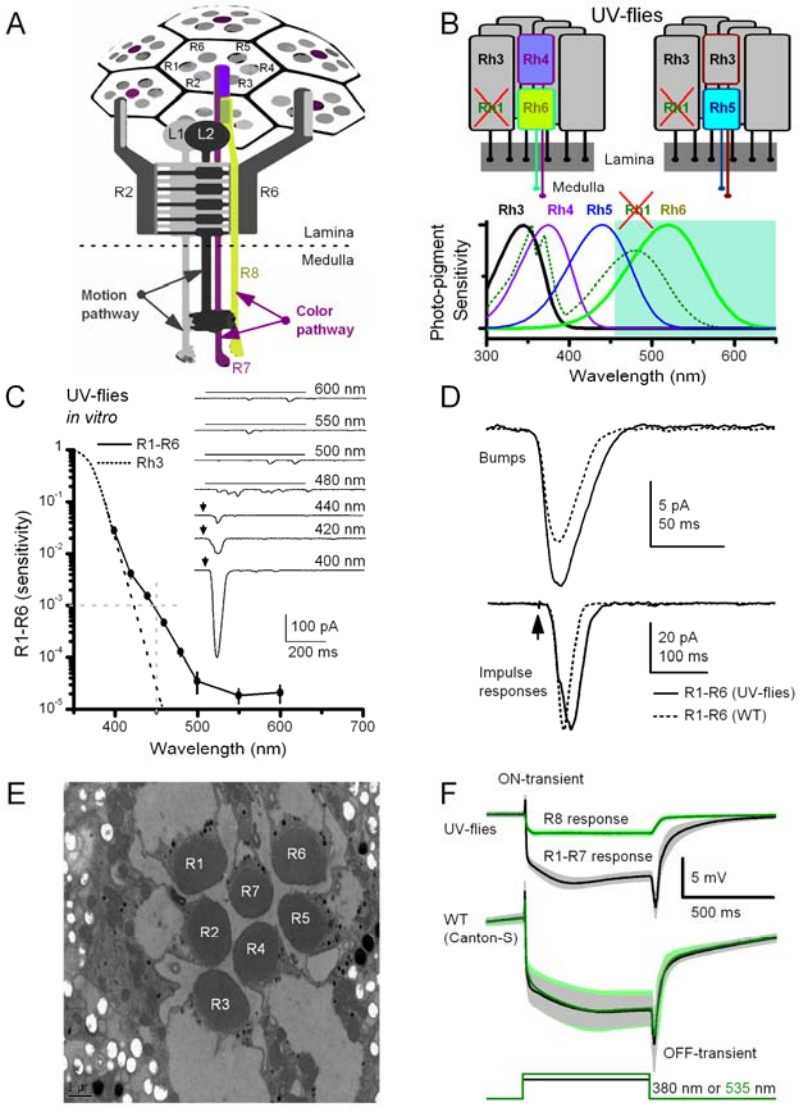

Figure S6: Manipulating spectral sensitivity of the motion pathway to elucidate circuit computations. (**A**) Schematic of fly photoreceptors innervating motion and colour pathways. Light-point is sampled by six outer photoreceptors (R1-R6) in neighboring ommatidia and by central R7/R8 photoreceptors. R1-R6 innervate large monopolar cells (L1 and L2) in 1st optic neuropile, lamina, while R7/R8 synapse in 2nd neuropile, medulla. (**B**) In UV-flies, UV-sensitive Rh3-opsin is expressed in R1-R6s, which contain non-functional Rh1-opsin (ninaE8). This circumvents the spectral overlap between motion and R8 pathways, allowing independent assessment of their individual parts. (**C**) Spectral sensitivity of light-induced currents (inset) in dissociated R1-R6s of UV-flies traces Rh3-opsin's sensitivity, diminishing <1/1,000th at ≥450 nm (mean ± SEM; 4 photoreceptors). Inset shows example responses to brief flashes (5-20 ms: arrows) or 1s stimulus (bars). (**D**) Although single photon responses (bumps) can be larger than those of wild-type (Canton-S) and impulse responses last slightly longer, their responses accelerate and adapt as WT counterparts, indicating normal-like photo-transduction (Liu *et al.*, 2008). (**E**) Photoreceptors of UV-flies have normal-like ultra-structure. (**F**) Electroretinograms (ERGs) show comparable dynamics to those of WT-flies: preferred colours evoke large receptor components, and On- and Off-transients, indicating normal synaptic transmission from R1-R6 to LMCs (Means ± SD; 6 flies). Importantly with UV-flies, one can separate the responses for green (R8s) and UV (R1-R7s).C-D: data by Roger Hardie.

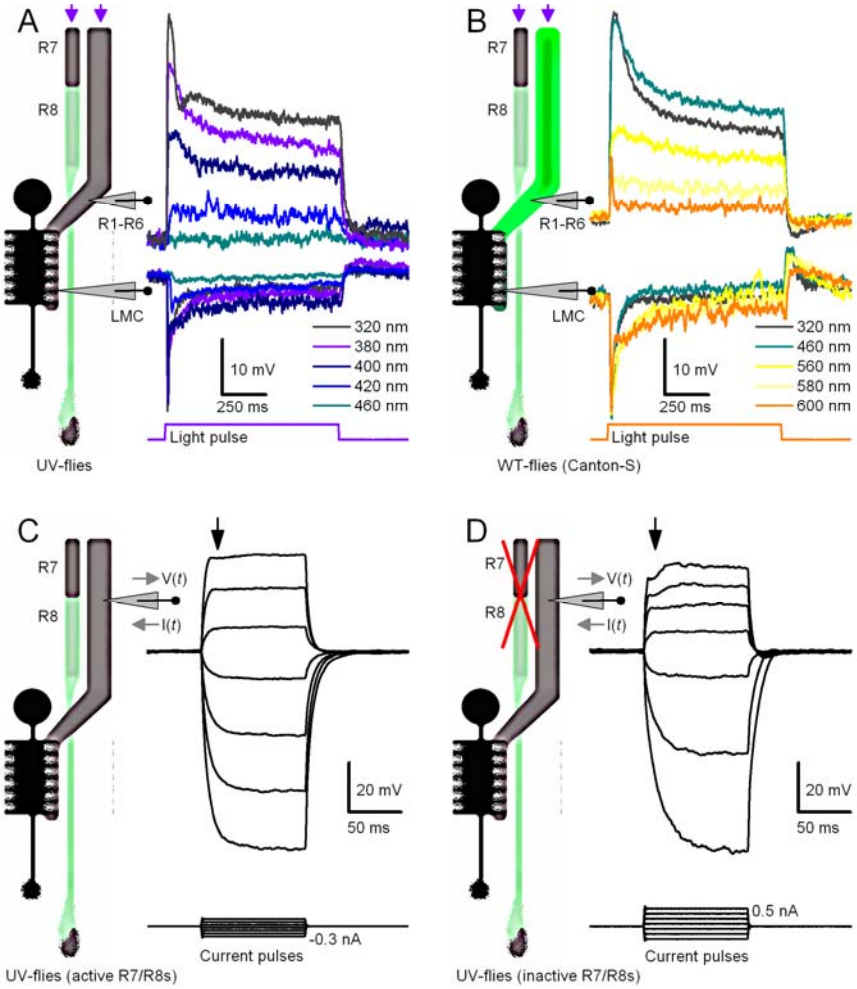

Figure S7: Pre- and postsynaptic response dynamics in UV-fly retina/lamina *in vivo* are WT-like. (**A**) Intracellular voltage responses of a R1-R6 photoreceptor and a LMC to 700-ms colour pulses, recorded from two UV-flies, respectively. Typically post-synaptic recordings show variable degrees of off-response, possibly attributable to different LMCs: L1 (on-channel) or L2 (off-channels) (Joesch *et al.*, 2010). Responses illustrate how sensitivity and speed of adaptation diminish with increasing stimulus wavelength. (**B**) Similar recordings as in (**A**), but to different colours from two WT-flies. Comparable response dynamics in UV- and WT-flies indicate preserved circuit computations in the lamina. (**C**) Representative voltage responses of a R1-R6 to current pulses in a dark-adapted UV-fly. (**D**) Similar responses in an UV-fly, whose R7/R8s were light-insensitive (using a norpA36 mutant and a norpA rescue in R1-R6). In both cases (**C** and **D**), depolarizing current pulses caused outward rectification (black arrows) of the membrane; owing to activation of shaker and delayed rectifier K+-channels, analogous to WT R1-R6s (Juusola & Hardie, 2001b; Niven *et al.*, 2003; Vähäsöyrinki *et al.*, 2006). Their characteristic dynamics and impedances (254 and 133 MΩ, respectively) are within the normal variation of WT recordings (Juusola & Hardie, 2001b; Niven *et al.*, 2003; Vähäsöyrinki *et al.*, 2006), indicating normal R1-R6 plasma-membranes. C-D data by Mikko Juusola.

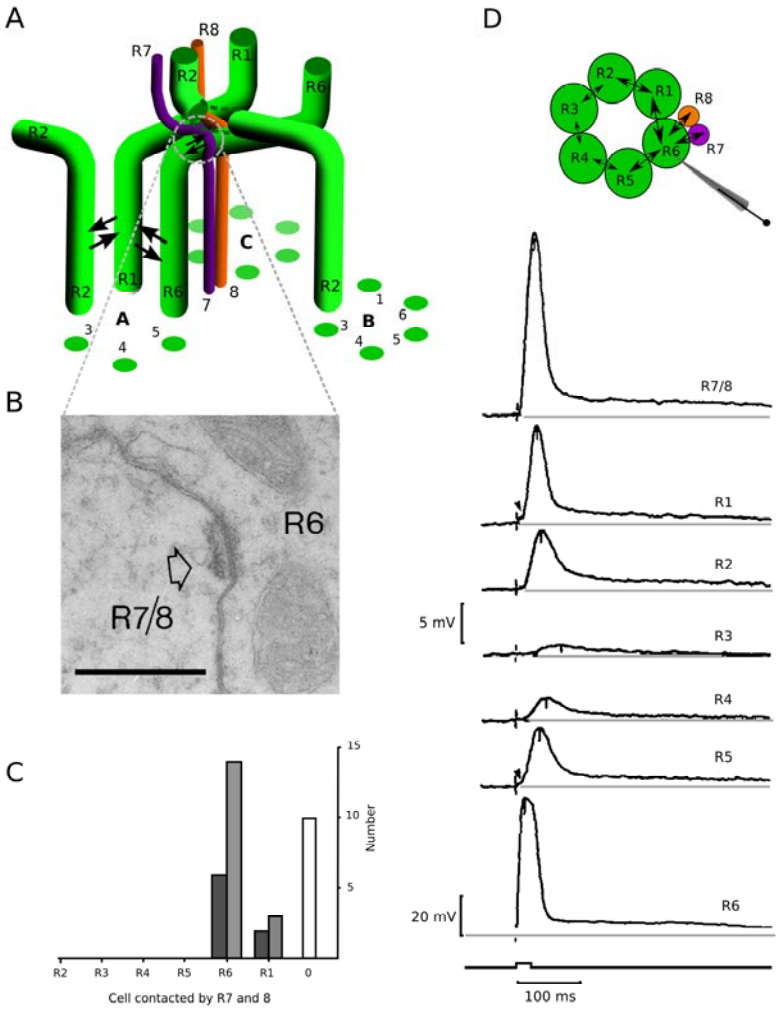

Figure S8: Summary of results by Shaw, Fröhlich and Meinertzhagen, indicating functional contacts between R6 and R7/R8 photoreceptors in lateral eye region of *Lucilia*. (**A**) Diagram showing the receptor contacts in the lamina. [A, B, C: R1-R6 terminals in three cartridges]. Arrows indicate local gap junction coupling between neighbours. R7 and R8 axons travel as a pair on either side of the R2, originating in their own ommatidium, and leaving R6 axon between them. This pattern is repeated in all axon bundles entering the lamina. (**B**) A putative gap junction showing obvious but asymmetrically distributed densities, more prominent in R7/R8 (arrow) than in R6. x36,500, scale bar: 0.5 µm. (**C**) Frequency count for photoreceptor terminals of R1-R6 contacting R7 and R8 axon pairs. Counts have been scored from a photomontage in which the identities of R7 (dark gray) and R8 (light gray) have been inferred from their relative positions only. Blank bar indicates cartridges in which neither profile happened to be found in contact with a R1-R6 terminal. (**D**) Averaged responses traces from the soma of a photoreceptor R6, identified from the position of its own facet in the map of electrically interacting responses plotted around it, using a roving fibre optic probe. Responses R1-R5 illustrate the progressive reduction in the size of the response and the lengthening of time-to-peak, going away from R6 in both directions around the ring of terminals. The largest coupled response in this map came from the R7/R8 input to this cartridge. Figures and legends adapted from Shaw (Shaw, 1984b) and Shaw, Fröhlich and Meinertzhagen (Shaw *et al.*, 1989a) with permission.

Bibliography

Abou Tayoun, A.N., Li, X.F., Chu, B., Hardie, R.C., Juusola, M. & Dolph, P.J. (2011) The Drosophila SK Channel (dSK) Contributes to Photoreceptor Performance by Mediating Sensitivity Control at the First Visual Network. *Journal of Neuroscience*, **31**, 13897-13910.

Ahmad, S.T., Natochin, M., Artemyev, N.O. & O'Tousa, J.E. (2007) The Drosophila rhodopsin cytoplasmic tail domain is required for maintenance of rhabdomere structure. *Faseb J*, **21**, 449-455.

Barlow, H. (1961) Possible principles underlying the transformations of sensory messages . Chapter 13. In Sensory Communication. *Ed W.A. Rosenblith, MIT Press*, 217-234.

Barlow, H.B. (2001) The exploitation of regularities in the environment by the brain. *Behav Brain Sci*, **24**, 602-607; discussion 652-671.

Bausenwein, B., Dittrich, A.P. & Fischbach, K.F. (1992) The optic lobe of Drosophila melanogaster. II. Sorting of retinotopic pathways in the medulla. *Cell Tissue Res*, **267**, 17-28.

Bausenwein, B., Wolf, R. & Heisenberg, M. (1986) Genetic dissection of optomotor behavior in Drosophila melanogaster. Studies on wild-type and the mutant optomotor-blindH31. *J Neurogenet*, **3**, 87-109.

Becker, M.N., Brenner, R. & Atkinson, N.S. (1995a) Tissue-Specific Expression of a Drosophila Calcium-Activated Potassium Channel. *Journal of Neuroscience*, **15**, 6250-6259.

Becker, M.N., Brenner, R. & Atkinson, N.S. (1995b) Tissue-specific expression of a Drosophila calcium-activated potassium channel. *J Neurosci*, **15**, 6250-6259.

Bloomquist, B.T., Shortridge, R.D., Schneuwly, S., Perdew, M., Montell, C., Steller, H., Rubin, G. & Pak, W.L. (1988) Isolation of a putative phospholipase C gene of Drosophila, norpA, and its role in phototransduction. *Cell*, **54**, 723-733.

Borst, A. (2009) Drosophila's View on Insect Vision. *Current Biology*, **19**, R36-R47.

Brenner, R. & Atkinson, N. (1996) Developmental- and eye-specific transcriptional control elements in an intronic region of a Ca(2+)-activated K+ channel gene. *Dev Biol*, **177**, 536-543.

Brenner, R., Thomas, T.O., Becker, M.N. & Atkinson, N.S. (1996) Tissue-specific expression of a Ca(2+)-activated K+ channel is controlled by multiple upstream regulatory elements. *J Neurosci*, **16**, 1827-1835.

Briscoe, A.D. & Chittka, L. (2001) The evolution of color vision in insects. *Annual Review of Entomology*, **46**, 471-510.

Britt, S.G., Feiler, R., Kirschfeld, K. & Zuker, C.S. (1993) Spectral tuning of rhodopsin and metarhodopsin in vivo. *Neuron*, **11**, 29-39.

Broadie, K.S. & Richmond, J.E. (2002) Establishing and sculpting the synapse in Drosophila and C-elegans. *Current Opinion in Neurobiology*, **12**, 491-498.

Chou, W.H., Hall, K.J., Wilson, D.B., Wideman, C.L., Townson, S.M., Chadwell, L.V. & Britt, S.G. (1996) Identification of a novel Drosophila opsin reveals specific patterning of the R7 and R8 photoreceptor cells. *Neuron*, **17**, 1101-1115.

Clark, B.D., Kurth-Nelson, Z.L. & Newman, E.A. (2009) Adenosine-evoked hyperpolarization of retinal ganglion cells is mediated by G-protein-coupled inwardly rectifying K+ and small conductance Ca2+-activated K+ channel activation. *J Neurosci*, **29**, 11237-11245.

Cropper, S.J. & Wuerger, S.M. (2005) The perception of motion in chromatic stimuli. *Behav Cogn Neurosci Rev*, **4**, 192-217.

de Polavieja, G.G. (2002) Errors drive the evolution of biological signalling to costly codes. *J Theor Biol*, **214**, 657-664.

de Polavieja, G.G. (2004) Reliable biological communication with realistic constraints. *Phys Rev E Stat Nonlin Soft Matter Phys*, **70**, 061910.

de Polavieja, G.G. (2006) Neuronal algorithms that detect the temporal order of events. *Neural Comput*, **18**, 2102-2121.

Derrington, A.M. (2000) Vision: can colour contribute to motion? *Curr Biol*, **10**, R268-270.

Dieck, S.T. & Brandstatter, J.H. (2006) Ribbon synapses of the retina. *Cell and Tissue Research*, **326**, 339-346.

Faber, E.S., Delaney, A.J. & Sah, P. (2005) SK channels regulate excitatory synaptic transmission and plasticity in the lateral amygdala. *Nat Neurosci*, **8**, 635-641.

Feiler, R., Bjornson, R., Kirschfeld, K., Mismer, D., Rubin, G.M., Smith, D.P., Socolich, M. & Zuker, C.S. (1992) Ectopic expression of ultraviolet-rhodopsins in the blue photoreceptor cells of Drosophila: visual physiology and photochemistry of transgenic animals. *J Neurosci*, **12**, 3862-3868.

Freed, M.A. (2000) Rate of quantal excitation to a retinal ganglion cell evoked by sensory input. *J Neurophysiol*, **83**, 2956-2966.

Gao, S., Takemura, S.Y., Ting, C.Y., Huang, S., Lu, Z., Luan, H., Rister, J., Thum, A.S., Yang, M., Hong, S.T., Wang, J.W., Odenwald, W.F., White, B.H., Meinertzhagen, I.A. & Lee, C.H. (2008) The neural substrate of spectral preference in Drosophila. *Neuron*, **60**, 328-342.

Gengs, C., Leung, H.T., Skingsley, D.R., Iovchev, M.I., Yin, Z., Semenov, E.P., Burg, M.G., Hardie, R.C. & Pak, W.L. (2002a) The target of Drosophila photoreceptor synaptic transmission is a histamine-gated chloride channel encoded by ort (hclA). *J Biol Chem*, **277**, 42113-42120.

Gengs, C.X., Leung, H.T., Skingsley, D.R., Iovchev, M.I., Yin, Z., Semenov, E.P., Burg, M.G., Hardie, R.C. & Pak, W.L. (2002b) The target of Drosophila photoreceptor synaptic transmission is a histamine-gated chloride channel encoded by ort (hclA). *Journal of Biological Chemistry*, **277**, 42113-42120.

Gollisch, T. & Meister, M. (2010) Eye smarter than scientists believed: neural computations in circuits of the retina. *Neuron*, **65**, 150-164.

Gonzalez-Bellido, P.T., Wardill, T.J. & Juusola, M. (2011) Compound eyes and retinal information processing in miniature dipteran species match their specific ecological demands. *Proc Natl Acad Sci U S A*, **108**, 4224-4229.

Gonzalez-Bellido, P.T., Wardill, T.J., Kostyleva, R., Meinertzhagen, I.A. & Juusola, M. (2009) Overexpressing temperature-sensitive dynamin decelerates phototransduction and bundles microtubules in Drosophila photoreceptors. *J Neurosci*, **29**, 14199-14210.

Hallworth, N.E., Wilson, C.J. & Bevan, M.D. (2003) Apamin-sensitive small conductance calcium-activated potassium channels, through their selective coupling to voltage-gated calcium channels, are critical determinants of the precision, pace, and pattern of action potential generation in rat subthalamic nucleus neurons in vitro. *J Neurosci*, **23**, 7525-7542.

Hardie, R.C. (1979a) Electrophysiological analysis of fly retina. I . Comparative properties of R1-6 and R7 and 8. *Journal of Comparative Physiology A.*, **129**, 19-33.

Hardie, R.C. (1979b) Electrophysiological analysis of fly retina. I: Comparative properties of R1-6 and R7 and 8. *J Comp Physiol A*, **129**, 19-33.

Hardie, R.C. (1987a) Is Histamine a Neurotransmitter in Insect Photoreceptors. *Journal of Comparative Physiology a-Sensory Neural and Behavioral Physiology*, **161**, 201-213.

Hardie, R.C. (1987b) Is histamine a neurotransmitter in insect photoreceptors? *J Comp Physiol A*, **161**, 201-213.

Hardie, R.C. (1989a) A histamine-activated chloride channel involved in neurotransmission at a photoreceptor synapse. *Nature*, **339**, 704-706.

Hardie, R.C. (1989b) A histamine-activated chloride channel involved in neurotransmission at a photoreceptor synapse. *Nature*, **339(6227)**, 704-706.

Hardie, R.C. (1991) Voltage-Sensitive Potassium Channels in Drosophila Photoreceptors. *Journal of Neuroscience*, **11**, 3079-3095.

Hardie, R.C. (1995) Photolysis of caged Ca2+ facilitates and inactivates but does not directly excite light-sensitive channels in Drosophila photoreceptors. *J Neurosci*, **15**, 889-902.

Hardie, R.C. (2001) Phototransduction in Drosophila melanogaster. *Journal of Experimental Biology*, **204**, 3403-3409.

Hardie, R.C., Martin, F., Chyb, S. & Raghu, P. (2003) Rescue of light responses in the Drosophila "null" phospholipase C mutant, norpAP24, by the diacylglycerol kinase mutant, rdgA, and by metabolic inhibition. *J Biol Chem*, **278**, 18851-18858.

Hardie, R.C. & Minke, B. (1995) Phosphoinositide-Mediated Phototransduction in Drosophila Photoreceptors - the Role of Ca2+ and Trp. *Cell Calcium*, **18**, 256-274.

Hardie, R.C. & Postma, M. (2008) Phototransduction in microvillar photoreceptors of *Drosophila* and other invertebrates. In Albright, T.D., Masland, R. (eds) *The Senses: A Comprehensive Reference*. Academic Press, San Diego, pp. 77-130.

Hardie, R.C. & Raghu, P. (2001a) Visual transduction in Drosophila. *Nature*, **413**, 186-193.

Hardie, R.C. & Raghu, P. (2001b) Visual transduction in Drosophila. *Nature*, **413**, 186-193.

Hardie, R.C., Voss, D., Pongs, O. & Laughlin, S.B. (1991) Novel Potassium Channels Encoded by the Shaker Locus in Drosophila Photoreceptors. *Neuron*, **6**, 477-486.

Hardie, R.C. & Weckstrom, M. (1990) 3 Classes of Potassium Channels in Large Monopolar Cells of the Blowfly Calliphora-Vicina. *Journal of Comparative Physiology a-Sensory Neural and Behavioral Physiology*, **167**, 723-736.

He, L.M., Wu, X.S., Mohan, R. & Wu, L.G. (2006) Two modes of fusion pore opening revealed by cell-attached recordings at a synapse. *Nature*, **444**, 102-105.

He, L.M., Xue, L., Xu, J.H., McNeil, B.D., Bai, L., Melicoff, E., Adachi, R. & Wu, L.G. (2009) Compound vesicle fusion increases quantal size and potentiates synaptic transmission. *Nature*, **459**, 93-U99.

Heisenberg, M. & Buchner, E. (1977a) The role of retinula cell types in visual behavior of *Drosophila melanogaster J Comp Physiol*, **177**, 127-162.

Heisenberg, M. & Buchner, E. (1977b) The role of retinula cell types in visual behavior of *Drosophila melanogaster J Comp Physiol*, **177**, 127-162.

Hopf, F.W., Bowers, M.S., Chang, S.J., Chen, B.T., Martin, M., Seif, T., Cho, S.L., Tye, K. & Bonci, A. (2010) Reduced Nucleus Accumbens SK Channel Activity Enhances Alcohol Seeking during Abstinence. *Neuron*, **65**, 682-694.

Howard, J., Blakeslee, B. & Laughlin, S.B. (1987) The Intracellular Pupil Mechanism and Photoreceptor Signal - Noise Ratios in the Fly Lucilia-Cuprina. *Proceedings of the Royal Society of London Series B-Biological Sciences*, **231**, 415-435.

Joesch, M., Schnell, B., Raghu, S.V., Reiff, D.F. & Borst, A. (2010) ON and OFF pathways in Drosophila motion vision. *Nature*, **468**, 300-304.

Jonson, A.C.J., Land, M.F., Osorio, D.C. & Nilsson, D.E. (1998) Relationships between pupil working range and habitat luminance in flies and butterflies. *Journal of Comparative Physiology a-Sensory Neural and Behavioral Physiology*, **182**, 1-9.

Juusola, M. & de Polavieja, G.G. (2003) The rate of information transfer of naturalistic stimulation by graded potentials. *J Gen Physiol*, **122**, 191-206.

Juusola, M., French, A.S., Uusitalo, R.O. & Weckstrom, M. (1996) Information processing by graded-potential transmission through tonically active synapses. *Trends in Neurosciences*, **19**, 292-297.

Juusola, M. & Hardie, R.C. (2001a) Light adaptation in Drosophila photoreceptors: I. Response dynamics and signaling efficiency at 25 degrees C. *J Gen Physiol*, **117**, 3-25.

Juusola, M. & Hardie, R.C. (2001b) Light adaptation in *Drosophila* photoreceptors: I. Response dynamics and signaling efficiency at 25°C. *J Gen Physiol*, **117**, 3-25.

Juusola, M., Uusitalo, R.O. & Weckström, M. (1995a) Transfer of graded potentials at the photoreceptor-interneuron synapse. *J Gen Physiol*, **105**, 117-148.

Juusola, M., Uusitalo, R.O. & Weckstrom, M. (1995b) Transfer of Graded Potentials at the Photoreceptor Interneuron Synapse. *Journal of General Physiology*, **105**, 117-148.

Kaiser, W. (1975) The relationship between movement detection and colour vision in insects *The Compound Eye and Vision of Insects*. Clarendon Press, Oxford, pp. 359-377.

Kaiser, W. & Liske, E. (1974) Die optomotorischen Reaktionen von fixiert fliegenden Bienen bei Reizung mit Spektrallichtern. *J Comp Physiol*, **89**, 391-408.

Katsov, A.Y. & Clandinin, T.R. (2008) Motion processing streams in Drosophila are behaviorally specialized. *Neuron*, **59**, 322-335.

Kawasaki, F., Zou, B.Y., Xu, X. & Ordway, R.W. (2004) Active zone localization of presynaptic calcium channels encoded by the cacophony locus of Drosophila. *Journal of Neuroscience*, **24**, 282-285.

Kirschfe.K & Francesc.N (1969) A Mechanism for Directing Flow of Light in Rhabdomeres of Complex Eyes in Musca. *Kybernetik*, **6**, 13-&.

Kirschfeld, K. & Franceschini, N. (1977) Evidence for a sensitising pigment in fly photoreceptors. *Nature*, **269**, 386-390.

Klocker, N., Oliver, D., Ruppersberg, J.P., Knaus, H.G. & Fakler, B. (2001) Developmental expression of the small-conductance Ca(2+)-activated potassium channel SK2 in the rat retina. *Mol Cell Neurosci*, **17**, 514-520.

Koenig, J.H. & Ikeda, K. (1996) Synaptic vesicles have two distinct recycling pathways. *Journal of Cell Biology*, **135**, 797-808.

Kohler, M., Hirschberg, B., Bond, C.T., Kinzie, J.M., Marrion, N.V., Maylie, J. & Adelman, J.P. (1996) Small-conductance, calcium-activated potassium channels from mammalian brain. *Science*, **273**, 1709-1714.

Kolodziejczyk, A., Sun, X., Meinertzhagen, I.A. & Nassel, D.R. (2008) Glutamate, GABA and acetylcholine signaling components in the lamina of the Drosophila visual system. *PLoS One*, **3**, e2110.

Krause, Y., Krause, S., Huang, J., Liu, C.H., Hardie, R.C. & Weckstrom, M. (2008) Light-dependent modulation of Shab channels via phosphoinositide depletion in Drosophila photoreceptors. *Neuron*, **59**, 596-607.

Kumar, J.P. & Ready, D.F. (1995) Rhodopsin plays an essential structural role in Drosophila photoreceptor development. *Development*, **121**, 4359-4370.

Laughlin, S.B., de Ruyter van Steveninck, R.R. & Anderson, J.C. (1998) The metabolic cost of neural information. *Nat Neurosci*, **1**, 36-41.

Laughlin, S.B. & Hardie, R.C. (1978) Common Strategies for Light Adaptation in the Peripheral Visual Systems of Fly and Dragonfly. *Journal of Comparative Physiology*, **128**, 319-340.

Littleton, J.T. & Ganetzky, B. (2000) Ion channels and synaptic organization: Analysis of the Drosophila genome. *Neuron*, **26**, 35-43.

Liu, C.H., Satoh, A.K., Postma, M., Huang, J., Ready, D.F. & Hardie, R.C. (2008) Ca2+-dependent metarhodopsin inactivation mediated by calmodulin and NINAC myosin III. *Neuron*, **59**, 778-789.

Livingstone, M. & Hubel, D. (1988) Segregation of Form, Color, Movement, and Depth - Anatomy, Physiology, and Perception. *Science*, **240**, 740-749.

Meinertzhagen, I.A. & O'Neil, S.D. (1991a) Synaptic organization of columnar elements in the lamina of the wild type in *Drosophila melanogaster*. *J Comp Neurol*, **305**, 232-263.

Meinertzhagen, I.A. & O'Neil, S.D. (1991b) Synaptic organization of columnar elements in the lamina of the wild type in Drosophila melanogaster. *J Comp Neurol*, **305**, 232-263.

Meinertzhagen, I.A. & Sorra, K.E. (2001) Synaptic organization in the fly's optic lamina: few cells, many synapses and divergent microcircuits. *Prog Brain Res*, **131**, 53-69.

Miller, M.J., Rauer, H., Tomita, H., Rauer, H., Gargus, J.J., Gutman, G.A., Cahalan, M.D. & Chandy, K.G. (2001) Nuclear localization and dominant-negative suppression by a mutant SKCa3 N-terminal channel fragment identified in a patient with schizophrenia. *J Biol Chem*, **276**, 27753-27756.

Minke, B. & Katz, B. (2009) Drosophila photoreceptors and signaling mechanisms. *Frontiers in Cellular Neuroscience*, **3**.

Minke, B. & Kirschfeld, K. (1979) The contribution of a sensitizing pigment to the photosensitivity spectra of fly rhodopsin and metarhodopsin. *J Gen Physiol*, **73**, 517-540.

Moring, J. (1978) Spectral sensitivity of monopolar neurons in the eye of Calliphora. *Journal of Comparative Physiology A: Neuroethology, Sensory, Neural, and Behavioral Physiology*, **123**, 335-338.

Ngo-Anh, T.J., Bloodgood, B.L., Lin, M., Sabatini, B.L., Maylie, J. & Adelman, J.P. (2005) SK channels and NMDA receptors form a Ca2+-mediated feedback loop in dendritic spines. *Nat Neurosci*, **8**, 642-649.

Nikolaev, A., Zheng, L., Wardill, T.J., O'Kane, C.J., de Polavieja, G.G. & Juusola, M. (2009a) Network Adaptation Improves Temporal Representation of Naturalistic Stimuli in Drosophila Eye: II Mechanisms. *Plos One*, **4**.

Nikolaev, A., Zheng, L., Wardill, T.J., O'Kane, C.J., de Polavieja, G.G. & Juusola, M. (2009b) Network adaptation improves temporal representation of naturalistic stimuli in Drosophila eye: II mechanisms. *PLoS One*, **4**, e4306.

Nishida, S., Watanabe, J., Kuriki, I. & Tokimoto, T. (2007) Human visual system integrates color signals along a motion trajectory. *Curr Biol*, **17**, 366-372.

Niven, J.E., Vähäsöyrinki, M., Kauranen, M., Hardie, R.C., Juusola, M. & Weckström, M. (2003) The contribution of Shaker K+ channels to the information capacity of Drosophila photoreceptors. *Nature*, **421**, 630-634.

O'Tousa, J.E., Baehr, W., Martin, R.L., Hirsh, J., Pak, W.L. & Applebury, M.L. (1985) The Drosophila ninaE gene encodes an opsin. *Cell*, **40**, 839-850.

Oberwinkler, J. (2000) Calcium influx, diffusion and extrusion in fly photoreceptor cells. Rijkuniversiteit Groningen, Groningen.

Pantazis, A., Segaran, A., Liu, C.H., Nikolaev, A., Rister, J., Thum, A.S., Roeder, T., Semenov, E., Juusola, M. & Hardie, R.C. (2008a) Distinct roles for two histamine receptors (hclA and hclB) at the Drosophila photoreceptor synapse. *Journal of Neuroscience*, **28**, 7250-7259.

Pantazis, A., Segaran, A., Liu, C.H., Nikolaev, A., Rister, J., Thum, A.S., Roeder, T., Semenov, E., Juusola, M. & Hardie, R.C. (2008b) Distinct roles for two histamine receptors (hclA and hclB) at the Drosophila photoreceptor synapse. *J Neurosci*, **28**, 7250-7259.

Parsons, T.D. & Sterling, P. (2003) Synaptic ribbon: a conveyor belt or safety belt? *Neuron*, **37**.

Pearn, M.T., Randall, L.L., Shortridge, R.D., Burg, M.G. & Pak, W.L. (1996) Molecular, biochemical, and electrophysiological characterization of Drosophila norpA mutants. *J Biol Chem*, **271**, 4937-4945.

Prokop, A. & Meinertzhagen, I.A. (2006) Development and structure of synaptic contacts in Drosophila. *Seminars in Cell & Developmental Biology*, **17**, 20-30.

Pyle, J.L., Kavalali, E.T., Piedras-Renteria, E.S. & Tsien, R.W. (2000) Rapid reuse of readily releasable pool vesicles at hippocampal synapses. *Neuron*, **28**, 221-231.

Ready, D.F., Hanson, T.E. & Benzer, S. (1976) Development of Drosophila Retina, a Neurocrystalline Lattice. *Developmental Biology*, **53**, 217-240.

Reiff, D.F., Plett, J., Mank, M., Griesbeck, O. & Borst, A. (2010) Visualizing retinotopic half-wave rectified input to the motion detection circuitry of Drosophila. *Nature Neuroscience*, **13**, 973-U992.

Ribi, W.A. (1978) Gap junctions coupling photoreceptor axons in the first optic ganglion of the fly. *Cell Tissue Res*, **195**, 299-308.

Richards, D.A., Guatimosim, C. & Betz, W.J. (2000) Two endocytic recycling routes selectively fill two vesicle pools in frog motor nerve terminals. *Neuron*, **27**, 551-559.

Richmond, J.E. & Broadie, K.S. (2002) The synaptic vesicle cycle: exocytosis and endocytosis in Drosophila and C-elegans. *Current Opinion in Neurobiology*, **12**, 499-507.

Rister, J., Pauls, D., Schnell, B., Ting, C.Y., Lee, C.H., Sinakevitch, I., Morante, J., Strausfeld, N.J., Ito, K. & Heisenberg, M. (2007) Dissection of the peripheral motion channel in the visual system of Drosophila melanogaster. *Neuron*, **56**, 155-170.

Rivera-Alba, M., Vitaladevuni, S.N., Mischenko, Y., Lu, Z.S., Takemura, Scheffer, L., Meinertzhagen, I.A., Chklovskii, D.B. & De Polavieja, G.G. (2011) Wiring economy and volume exclusion determine neuronal placement in the Drosophila brain. *Current Biology* **21**.

Roebroek, J.G.H. & Stavenga, D.G. (1990) Insect Pupil Mechanisms .4. Spectral Characteristics and Light-Intensity Dependence in the Blowfly, Calliphora-Erythrocephala. *Journal of Comparative Physiology a-Sensory Neural and Behavioral Physiology*, **166**, 537-543.

Rohrbough, J. & Broadie, K. (2005) Lipid regulation of the synaptic vesicle cycle. *Nature Reviews Neuroscience*, **6**, 139-150.

Saintmarie, R.L. & Carlson, S.D. (1982) Synaptic Vesicle Activity in Stimulated and Unstimulated Photoreceptor Axons in the Housefly - a Freeze-Fracture Study. *Journal of Neurocytology*, **11**, 747-761.

Salcedo, E., Huber, A., Henrich, S., Chadwell, L.V., Chou, W.H., Paulsen, R. & Britt, S.G. (1999) Blue- and green-absorbing visual pigments of Drosophila: ectopic expression and physiological characterization of the R8 photoreceptor cell-specific Rh5 and Rh6 rhodopsins. *J Neurosci*, **19**, 10716-10726.

Salkoff, L., Wei, A.D., Baban, B., Butler, A., Fawcett, G., Ferreira, G. & Santi, C.M. (2005) Potassium channels in C. elegans. *WormBook*, 1-15.

Sanes, J.R. & Zipursky, S.L. (2010) Design Principles of Insect and Vertebrate Visual Systems. *Neuron*, **66**, 15-36.

Schiller, P.H. (2010) Parallel information processing channels created in the retina. *Proc Natl Acad Sci U S A*, **107**, 17087-17094.

Schmitz, F. (2009) The Making of Synaptic Ribbons: How They Are Built and What They Do. *Neuroscientist*, **15**, 611-624.

Shannon, C.E. (1948) A mathematical theory of communication. *Bell Syst. Tech. J*, **27**, 379-423.

Shatz, C.J. (1990) Impulse activity and the patterning of connections during CNS development. *Neuron*, **5**, 745-756.

Shaw, S.R. (1984a) Asymmetric distribution of gap junctions amongst identified photoreceptor axons of Lucilia cuprina (Diptera). *J Cell Sci*, **66**, 65-80.

Shaw, S.R. (1984b) Early visual processing in insects. *J Exp Biol*, **112**, 225-251.

Shaw, S.R., Fröhlich, A. & Meinertzhagen, I.A. (1989a) Direct connections between the R7/8 and R1-6 photoreceptor subsystems in the dipteran visual system. *Cell Tissue Res*, **257**, 295-302.

Shaw, S.R., Fr??hlich, A. & Meinertzhagen, I.A. (1989b) Direct connections between the R7/8 and R1-6 photoreceptor subsystems in the dipteran visual system. *Cell Tissue Res*, **257**, 295-302.

Shaw, S.R., Frohlich, A. & Meinertzhagen, I.A. (1989c) Direct connections between the R7/8 and R1-6 photoreceptor subsystems in the dipteran visual system. *Cell Tissue Res*, **257**, 295-302.

Sinakevitch, I. & Strausfeld, N.J. (2004) Chemical neuroanatomy of the fly's movement detection pathway. *J Comp Neurol*, **468**, 6-23.

Singer, J.H., Lassova, L., Vardi, N. & Diamond, J.S. (2004) Coordinated multivesicular release at a mammalian ribbon synapse. *Nature Neuroscience*, **7**, 826-833.

Skingsley, D.R., Laughlin, S.B. & Hardie, R.C. (1995) Properties of Histamine-Activated Chloride Channels in the Large Monopolar Cells of the Dipteran Compound Eye - a Comparative-Study. *Journal of Comparative Physiology a-Sensory Neural and Behavioral Physiology*, **176**, 611-623.

Srinivasan, M.V. (1985) Shouldn't directional movement detection necessarily be "colour-blind"? *Vision Res*, **25**, 997-1000.

Srinivasan, M.V., Pinter, R.B. & Osorio, D. (1990) Matched Filtering in the Visual-System of the Fly - Large Monopolar Cells of the Lamina Are Optimized to Detect Moving Edges and Blobs. *Proceedings of the Royal Society of London Series B-Biological Sciences*, **240**, 279-293.

Stackman, R.W., Hammond, R.S., Linardatos, E., Gerlach, A., Maylie, J., Adelman, J.P. & Tzounopoulos, T. (2002) Small conductance Ca2+-activated K+ channels modulate synaptic plasticity and memory encoding. *J Neurosci*, **22**, 10163-10171.

Stackman, R.W., Jr., Bond, C.T. & Adelman, J.P. (2008) Contextual memory deficits observed in mice overexpressing small conductance Ca2+-activated K+ type 2 (KCa2.2, SK2) channels are caused by an encoding deficit. *Learn Mem*, **15**, 208-213.

Stavenga, D.G. (2004) Angular and spectral sensitivity of fly photoreceptors. III. Dependence on the pupil mechanism in the blowfly Calliphora. *Journal of Comparative Physiology a-Neuroethology Sensory Neural and Behavioral Physiology*, **190**, 115-129.

Steinert, J.R., Kuromi, H., Hellwig, A., Knirr, M., Wyatt, A.W., Kidokoro, Y. & Schuster, C.M. (2006) Experience-dependent formation and recruitment of large vesicles from reserve pool. *Neuron*, **50**, 723-733.

Sterling, P. & Matthews, G. (2005) Structure and function of ribbon synapses. *Trends in Neurosciences*, **28**, 20-29.

Stocker, M. (2004) Ca(2+)-activated K+ channels: molecular determinants and function of the SK family. *Nat Rev Neurosci*, **5**, 758-770.

Strausfeld, N.J. & Campos-Ortega, J.A. (1977) Vision in insects: pathways possibly underlying neural adaptation and lateral inhibition. *Science*, **195**, 894-897.

Sudhof, T.C. (2004) The synaptic vesicle cycle. *Annual Review of Neuroscience*, **27**, 509-547.

Takemura, S.Y., Lu, Z. & Meinertzhagen, I.A. (2008) Synaptic circuits of the Drosophila optic lobe: the input terminals to the medulla. *J Comp Neurol*, **509**, 493-513.

Takeuchi, T., De Valois, K.K. & Hardy, J.L. (2003) The influence of color on the perception of luminance motion. *Vision Res*, **43**, 1159-1175.

Tomita, H., Shakkottai, V.G., Gutman, G.A., Sun, G., Bunney, W.E., Cahalan, M.D., Chandy, K.G. & Gargus, J.J. (2003) Novel truncated isoform of SK3 potassium channel is a potent dominant-negative regulator of SK currents: implications in schizophrenia. *Mol Psychiatry*, **8**, 524-535, 460.

Tsukahara, Y. & Horridge, G.A. (1977) Visual Pigment Spectra from Sensitivity Measurements after Chromatic Adaptation of Single Dronefly Retinula Cells. *Journal of Comparative Physiology*, **114**, 233-251.

Ugarte, G., Delgado, R., O'Day, P.M., Farjah, F., Cid, L.P., Vergara, C. & Bacigalupo, J. (2005) Putative ClC-2 chloride channel mediates inward rectification in Drosophila retinal photoreceptors. *Journal of Membrane Biology*, **207**, 151-160.

Uusitalo, R.O., Juusola, M., Kouvalainen, E. & Weckström, M. (1995a) Tonic transmitter release in a graded potential synapse. *J Neurophysiol*, **74**, 470-473.

Uusitalo, R.O., Juusola, M., Kouvalainen, E. & Weckstrom, M. (1995b) Tonic Transmitter Release in a Graded Potential Synapse. *Journal of Neurophysiology*, **74**, 470-473.

Uusitalo, R.O., Juusola, M. & Weckström, M. (1995c) Graded responses and spiking properties of identified first-order visual interneurons of the fly compound eye. *J Neurophysiol*, **73**, 1782-1792.

Uusitalo, R.O. & Weckstrom, M. (2000) Potentiation in the first visual synapse of the fly compound eye. *Journal of Neurophysiology*, **83**, 2103-2112.

Vähäsöyrinki, M., Niven, J.E., Hardie, R.C., Weckström, M. & Juusola, M. (2006) Robustness of neural coding in Drosophila photoreceptors in the absence of slow delayed rectifier K+ channels. *J Neurosci*, **26**, 2652-2660.

van Hateren, J.H. (1986) Electrical coupling of neuro-ommatidial photoreceptor cells in the blowfly. *J Comp Physiol A*, **158**, 795-811.

Van Hateren, J.H. (1992a) Theoretical Predictions of Spatiotemporal Receptive-Fields of Fly Lmcs, and Experimental Validation. *Journal of Comparative Physiology a-Sensory Neural and Behavioral Physiology*, **171**, 157-170.

van Hateren, J.H. (1992b) A theory of maximizing sensory information. *Biol Cybern*, **68**, 23-29.

van Hateren, J.H. (1997) Processing of natural time series of intensities by the visual system of the blowfly. *Vision Res*, **37**, 3407-3416.

Van Steveninck, R.R.D. & Laughlin, S.B. (1996) The rate of information transfer at graded-potential synapses. *Nature*, **379**, 642-645.

Verstreken, P., Kjaerulff, O., Lloyd, T.E., Atkinson, R., Zhou, Y., Meinertzhagen, I.A. & Bellen, H.J. (2002) Endophilin mutations block clathrin-mediated endocytosis but not neurotransmitter release. *Cell*, **109**, 101-112.

Vogt, K., Kirschfeld, K. & Stavenga, D.G. (1982) Spectral Effects of the Pupil in Fly Photoreceptors. *Journal of Comparative Physiology*, **146**, 145-152.

Wang, C.T., Lu, J.C., Bai, J.H., Chang, P.Y., Martin, T.F.J., Chapman, E.R. & Jackson, M.B. (2003) Different domains of synaptotagmin control the choice between kiss-and-run and full fusion. *Nature*, **424**, 943-947.

Wang, G.Y., Olshausen, B.A. & Chalupa, L.M. (1999) Differential effects of apamin- and charybdotoxin-sensitive K+ conductances on spontaneous discharge patterns of developing retinal ganglion cells. *J Neurosci*, **19**, 2609-2618.

Weckström, M. & Laughlin, S.B. (1995) Visual ecology and voltage-gated ion channels in insect photoreceptors. *Trends Neurosci*, **18**, 17-21.

Weckstrom, M. & Laughlin, S.B. (1995) Visual Ecology and Voltage-Gated Ion Channels in Insect Photoreceptors. *Trends in Neurosciences*, **18**, 17-21.

Wicher, D., Walther, C. & Wicher, C. (2001) Non-synaptic ion channels in insects - basic properties of currents and their modulation in neurons and skeletal muscles. *Progress in Neurobiology*, **64**, 431-525.

Wolfart, J., Neuhoff, H., Franz, O. & Roeper, J. (2001) Differential expression of the small-conductance, calcium-activated potassium channel SK3 is critical for pacemaker control in dopaminergic midbrain neurons. *J Neurosci*, **21**, 3443-3456.

Wolfram, V. (2001) A small conductance calcium-activated potassium channel in flies: Sequencing and expression studies *Department of Biochemistry*. University of Oulu, Oulu.

Wong, F. & Knight, B.W. (1980) Adapting-Bump Model for Eccentric Cells of Limulus. *Journal of General Physiology*, **76**, 539-557.

Xia, X.M., Fakler, B., Rivard, A., Wayman, G., Johnson-Pais, T., Keen, J.E., Ishii, T., Hirschberg, B., Bond, C.T., Lutsenko, S., Maylie, J. & Adelman, J.P. (1998) Mechanism of calcium

gating in small-conductance calcium-activated potassium channels. *Nature*, **395**, 503-507.

Yamaguchi, S., Wolf, R., Desplan, C. & Heisenberg, M. (2008) Motion vision is independent of color in Drosophila. *Proc Natl Acad Sci U S A*, **105**, 4910-4915.

Yasuhara, J.C., Baumann, O. & Takeyasu, K. (2000) Localization of Na/K-ATPase in developing and adult Drosophila melanogaster photoreceptor. *Cell and Tissue Research*, **300**, 239-249.

Zhang, B., Koh, Y.H., Beckstead, R.B., Budnik, V., Ganetzky, B. & Bellen, H.J. (1998) Synaptic vesicle size and number are regulated by a clathrin adaptor protein required for endocytosis. *Neuron*, **21**, 1465-1475.

Zheng, L., de Polavieja, G.G., Wolfram, V., Asyali, M.H., Hardie, R.C. & Juusola, M. (2006a) Feedback network controls photoreceptor output at the layer of first visual synapses in Drosophila. *J Gen Physiol*, **127**, 495-510.

Zheng, L., de Polavieja, G.G., Wolfram, V., Asyali, M.H., Hardie, R.C. & Juusola, M. (2006b) Feedback network controls photoreceptor output at the layer of first visual synapses in *Drosophila*. *J Gen Physiol*, **127**, 495-510.

Zheng, L., Nikolaev, A., Wardill, T.J., O'Kane, C.J., de Polavieja, G.G. & Juusola, M. (2009) Network adaptation improves temporal representation of naturalistic stimuli in Drosophila eye: I dynamics. *PLoS One*, **4**, e4307.

Zheng, L., Polavieja, G.G., Wolfram, V., Asyali, M.H., Hardie, R.C. & Juusola, M. (2006c) Feedback network controls photoreceptor output at the layer of first visual synapses in Drosophila. *Journal of General Physiology*, **127**, 495-510.

Zhu, Y., Nern, A., Zipursky, S.L. & Frye, M.A. (2009) Peripheral visual circuits functionally segregate motion and phototaxis behaviors in the fly. *Curr Biol*, **19**, 613-619.

Appendix: Published Manuscripts

Abou Tayoun, A.N., Li, X., Chu, B., Hardie, R.C., Juusola, M. & Dolph, P.J. (2011), (Co-first author).

The *Drosophila* SK channel (dSK) contributes to photoreceptor performance by mediating sensitivity control at the first visual network.

Journal of Neuroscience. 31: 13897-13910.